Aus dem Experimental and Clinical Research Center
der Medizinischen Fakultät Charité – Universitätsmedizin Berlin

DISSERTATION

Der Einfluss des Transkriptionsfaktors MAF auf die Physiologie und maligne Transformation in der terminalen B Zell Differenzierung

The impact of the transcription factor MAF on physiology and malignant transformation in terminal B cell differentiation

zur Erlangung des akademischen Grades
Doctor medicinae (Dr. med.)

vorgelegt der Medizinischen Fakultät
Charité – Universitätsmedizin Berlin

von

Marvin Werner

Datum der Promotion: 23.03.2024

Table of contents

List of figures

List of tables

List of abbreviations

+1q	Gain of the long arm of chromosome 1
40LB	NIH3T3 stably transduced with CD40L and BAFF
AID	Activation-induced cytosine deaminase
AP1	Activator protein 1
APC	Allophycocyanin
APS	Ammonium persulfate
ASC	Antibody-secreting cell
ATAC-seq	Assay for Transposase-Accessible Chromatin using sequencing
BCR	B cell receptor
BCM	B cell medium
BFP	Blue fluorescent protein
BM	Bone marrow
BMPC	Bone marrow plasma cell
bp	Base pair(s)
BPB	Bromophenol blue
BSA	Bovine serum albumin
BTZ	Bortezomib
BV	Brilliant violet
CAG	Cytomegalovirus early enhancer element, chicken beta-actin promoter, rabbit beta-globin splice acceptor
CCND1	Cyclin D1
CD	Cluster of differentiation
cDNA	Complementary DNA
Cγ1	Immunoglobulin heavy-chain constant gamma 1
CGG	Chicken gamma globulin
CHIP-seq	Chromatin immunoprecipitation sequencing
COO	Cell of origin
CRE	cAMP-responsive element
Cre	cyclization recombinase from phage P1
CRISPR	Clustered regularly interspaced short palindromic repeats
CSR	Class-switch recombination
D	Diverse region of immunoglobulin heavy-chain
dCTP	Deoxycytidine triphosphate
DMSO	Dimethyl sulfoxide
DNA	Deoxyribonucleic acid
DZ	Dark zone of GC
Eμ	IGH enhancer element
ERT2	Human estrogen receptor ligand-binding domain mutations
eYFP	Enhanced yellow fluorescent protein
FACS	Fluorescence-activated cell sorting
FCS	Fetal calf serum
FITC	Fluorescein isothiocyanate
GC	Germinal center
GFP	Green fluorescent protein
hCD2	Human CD2
HEPES	N-2-hydroxyethylpiperazine-N-2-ethane sulfonic acid
HMCL	Human MM cell line
HRP	Horseradish peroxidase

HSL	High-salt lysis
Ig	Immunoglobulin
IG	Immunoglobulin
IGH	Immunoglobulin heavy-chain
IGL	Immunoglobulin light-chain
IL	Interleukin
IRES	Internal ribosomal entry site
J	Joining region of immunoglobulin (heavy) chains
kb	Kilo base pair
KEGG	Kyoto Encyclopedia of Genes and Genomes
loxP	Locus of crossover (x) in P1 bacteriophage
LPS	Lipopolysaccharide
LZ	Light zone of GC
MACS	Magnetic activated cell sorting
MAF	Musculoaponeurotic fibrosarcoma
MARE	MAF recognition element
MGUS	Monoclonal gammopathy of undetermined significance
MIE	Myeloma-initiating event
MIG	MSCV-IRES-GFP
MM	Multiple myeloma
MMSET	Multiple myeloma SET domain
mRIPA	Modified Radioimmunoprecipitation assay
M-spike	Monoclonal spike
MS	Mass spectrometry
NFκB	Nuclear factor kappa B
NHEJ	Non-homologous end joining
NIP	(4-hydroxy-3-iodo-5-nitrophenyl) acetyl
NP	(4-hydroxy-3-nitrophenyl) acetyl
PB	Plasma blast
PC	Plasma cell
PCL	Plasma cell leukemia
p.i.	Post immunization
PRR	Pattern recognition receptor
RNA	Ribonucleic acid
RNA-seq	RNA sequencing
SHM	Somatic hypermutation
SNV	Single nucleotide variant
t(14;16)	Reciprocal translocation between chromosome 14 and 16
TD	Thymus-dependent
TF	Transcription factor
TI	Thymus independent
TRE	2-O-tetradecanoyl phorbol 13-acetate- responsive element
V	Variable region of immunoglobulin (heavy) chains
WGS	Whole genome sequencing

Abstract

Multiple myeloma is a tumor of terminally differentiated B cells, i.e., plasma cells (PCs), and arises in the bone marrow (BM). Initial genetic events are acquired during the germinal center (GC) reaction of B cells. In approx. 50 % of cases, translocations that juxtapose oncogenes to the immunoglobulin heavy-chain enhancers lead to their respective overexpression and initiate transformation. Next to cyclin D members and MMSET, overexpression of three MAF transcription factors is found, most commonly c-MAF due to the translocation t(14;16).

Previous work by our group therefore aimed to overexpress *Maf* in mouse GC B cells to model myeloma initiation in Cγ1-cre; R26 MafstopF mice. Unexpectedly, B cell-specific overexpression of *Maf* led to a dramatic reduction and counter-selection of *Maf*-expressing GC B cells upon immunization with a thymus-dependent antigen, whereas IgM-expressing antigen-specific PC accumulated in the BM.

To characterize the altered GC reaction upon *Maf* overexpression, the present work examined the proliferation, T cell support, and immunosurveillance of *Maf*-transgenic GC B cells by BrdU incorporation and flow cytometry of splenic cell populations, respectively. The timing-dependent impact of *Maf* overexpression on early, peak, late GC B cells and their progeny was investigated in Cγ1-creERT2; R26 MafstopF mice, which allowed for specific *Maf* transgene expression at distinct time points following immunization. The protein interactome of MAF was assessed by immunoprecipitation and mass spectrometric analysis of coprecipitated proteins in human t(14;16)$^{+}$ multiple myeloma cell lines.

The Cγ1creERT2; R26 MafstopF allele used here, allowed for the overexpression of *Maf* at different stages of terminal B cell differentiation and the study of the corresponding effects in mice. Delayed transgene expression in peak GC B cells mitigated the counter-selection of *Maf*-expressing GC B cells and was compatible with class switch recombination and differentiation into BMPCs. A reduction of *Maf*-expressing B cell populations was observed regardless of the timepoint of *Maf* overexpression. Impaired proliferation of GC B cells, limited T cell support, or immune surveillance were not causative factors. Proteomic analyses showed that oncogenic MAF interacts with a variety of transcription factors, in particular with members of the NFKB and RUNX families. For the future investigation of the cooperation between MAF and putative interactors, an in vitro screening system was

established based on retroviral overexpression of candidate interaction partners in *Maf*-transgenic mouse B cells, using expression analysis of the MAF target gene *Itgb7* as read-out for transcriptional activity. Taken together, the results obtained in this work will contribute to the improvement of future mouse models for the t(14;16) translocation, with the goal of developing new therapies.

Zusammenfassung

Das Multiple Myelom ist ein Tumor maligner Plasmazellen und tritt im Knochenmark auf. Initiale genetische Ereignisse entstehen in B-Zellen während der Keimzentrumsreaktion. In ca. 50 % der Fälle führen Translokationen zur Überexpression spezifischer Onkogene durch die Anlagerung jeweiliger Loci an die Enhancerregion der schweren Immunglobulinkette. Neben Cyclin-D-Mitgliedern und MMSET findet sich die Überexpression dreier MAF-Transkriptionsfaktoren, am häufigsten von c-MAF als Folge der Translokation t(14;16).

Frühere Arbeiten unserer Gruppe beabsichtigen, *Maf* in Keimzentrums-B-Zellen der Maus zu überexprimieren, um die Myelom-Entstehung in Cγ1-cre; R26 MafstopF-Mäusen zu modellieren. Die B-Zell-spezifische Überexpression führte jedoch zu einer dramatischen Gegenselektion *Maf*-exprimierender Keimzentrums-B-Zellen nach Immunisierung, während IgM-exprimierende antigenspezifische Plasmazellen im Knochenmark akkumulierten.

Um die veränderte Keimzentrumsreaktion bei *Maf*-Überexpression zu charakterisieren, wurden in der vorliegenden Arbeit Proliferation, T-Zell-Unterstützung und Immunüberwachung *Maf*-transgener Keimzentrums-B-Zellen durch BrdU-Inkorporation und Durchflusszytometrie entsprechender Zellpopulationen untersucht. Die Auswirkung der *Maf*-Überexpression auf frühe, mittlere und späte Keimzentrums-B-Zellen und ihre Nachkommen wurden durch gezielte Transgenaktivierung in Cγ1-creERT2; R26 MafstopF-Mäusen untersucht. Weiterhin wurde das Protein-Interaktom von MAF durch Immunpräzipitation und Massenspektrometrie in humanen t(14;16)$^{+}$ Myelom-Zelllinien untersucht.

Das hier verwendete Cγ1creERT2; R26 MafstopF-System ermöglichte die Überexpression von *Maf* in verschiedenen Stadien der terminalen B-Zell-Differenzierung der Maus und die Untersuchung entsprechender Auswirkungen. Eine verzögerte *Maf*-expression in Keimzentrums-B-Zellen verringerte die Gegenselektion *Maf*-exprimierender Keimzentrums-

B-Zellen und war mit dem Klassenwechsel und der Differenzierung zu Knochenmark-Plasmazellen vereinbar. Unabhängig vom Zeitpunkt der *Maf*-Überexpression wurde eine Verringerung *Maf*-exprimierender B-Zellpopulationen beobachtet. Eine beeinträchtigte Proliferation von Keimzentrums-B-Zellen, eingeschränkte T-Zell-Unterstützung oder Immunüberwachung waren nicht ursächlich. Proteomanalysen zeigten, dass MAF mit einer Vielzahl von Transkriptionsfaktoren interagiert, vor allem mit Mitgliedern der NFKB und RUNX Familie. Um die Kooperation zwischen MAF und potenziellen Interaktoren zu untersuchen, wurde ein Screening etabliert, das auf der retroviralen Überexpression von Kandidatengenen in *Maf*-transgenen Maus-B-Zellen basiert und die transkriptionelle Induktion des MAF-Zielgens *Itgb7* als Parameter verwendet.

Die in dieser Arbeit gewonnenen Erkenntnisse werden zur Verbesserung künftiger Mausmodelle für die Translokation t(14;16) beitragen, mit dem Ziel der Entwicklung neuer Therapien.

1. Introduction

Antibodies constitute one of the most important effector molecules of the immune system[1]. During the germinal center (GC) reaction, B cells optimize the affinity and functionality of their antigen receptor[2], leading to their terminal differentiation into plasma cells (PC)[3] specialized in the secretion of high amount of antibody. Multiple myeloma (MM) represents the malignant counterpart of PCs[4]. MM cells arise in and are reliant on the bone marrow (BM) and its microenvironment[5]. They disturb normal bone metabolism resulting in pathological fractures and excessively secrete monoclonal antibodies leading to damaging depositions in various organs. Monoclonal immunoglobulin light-chains in the urine of patients were initially described by Henry Bence Jones in 1851[6]. They were found to form homologous electrophoretic bands by Leonhard Korngold and Rose Lipari in 1956[7] and are nowadays designated as kappa and lambda after their discoverers[8]. As can be seen from this, studying MM pathology is crucial for the understanding of B cell biology. However, to this day, MM pathology still poses challenges to investigators[8]. It remains a central burden to correlate different myeloma-initiating events (MIE) with the dysregulations that lead to malignancy. A possible approach to gain insight to this transformation process is the generation and analysis of suitable mouse models. One of the known MIEs is the overexpression of the transcription factor (TF) MAF associated with a high-risk disease course[9]. The present work therefore explores how MAF affects terminal B cell differentiation and malignant transformation.

1.1 Clinical aspects of multiple myeloma

Multiple myeloma is the second most common hematologic malignancy in western countries and is predominantly diagnosed in elderly people with a medium age of 70[10]. It is more often seen in people of African ancestry than in caucasians[11]. First-degree relatives of patients have a 2.1-fold higher risk of developing MM than the reference population[12].

In almost all cases, MM is preceded by a premalignant precursor phase, called MGUS (monoclonal gammopathy of undetermined significance)[9]. In this disease stage, premalignant PCs accumulate in the BM and extensively secrete monoclonal antibodies that form a sharp distinctive band in the γ-globulin fraction of a serum electrophoresis, called M-spike[13]. In this disease stage no secondary end organ damage can be detected. MGUS,

found in approximately 3 % of people aged 45 to 75, rarely becomes clinically relevant, but can progress towards MM with a frequency of 1 % per year[14]. Fully malignant MM is then defined by serum immunoglobulin levels >30 g/l, >10 % PCs in the BM and detectable end organ damage[15]. Of these, the kidney damage can be prognostically relevant and comprises e.g., classical CAST nephropathy due to tubular deposits as well as degeneration of the glomerular filter by AL-amyloidosis or light-chain deposition disease. The impaired hematopoiesis leads to anemia, susceptibility to infections, and bleeding tendency. Hypercalcemia and pathological fractures are further classical symptoms of MM. The disease can eventually progress towards extramedullary tumors and plasma cell leukemia (PCL)[16].

MM is considered an incurable disease. Patients in a good general condition usually undergo high-dose chemotherapy with melphalan after induction therapy, followed by autologous stem cell transplantation[13]. Newer agents, such as proteasome inhibitors (e.g., Bortezomib BTZ) or lenalidomide are considered as maintenance therapy. If patients are not suitable for such an intensive therapy, a triple combination of melphalan, a glucocorticoid and a newer substance is used[13]. Supportive radiation can be given to extramedullary and medullary solitary tumors, e.g., osteolysis with fracture risk. Additionally, risk of fractures can be reduced with substances that modulate bone metabolism (e.g., Denosumab)[17].

1.2 Terminal B cell differentiation and malignant transformation towards multiple myeloma

1.2.1 The germinal center reaction as origin of malignant transformation

To counter a variety of antigens with only a limited genetic repertoire, B cell development is characterized by mechanisms that vary the immunoglobulin (Ig) locus. During somatic recombination at the pro-B cell stage in the BM, V (variable), D (diverse) and J (joining) segments of the Ig locus are linked together by excision of intervening DNA regions through the activity of RAG1, RAG2 and enzymes of the non-homologous end-joining machinery (NHEJ)[18]. This process requires the generation of DNA double strand breaks (DSB). Followed by the respective rearrangement of the light-chains at the pre-B cell stage, the antigen receptors of developing B cells are controlled for self-tolerance, which can be improved by receptor editing[19].

Mature, naïve B cells are recruited to B cell zones of secondary lymphoid organs[20] where they receive necessary survival signals like BAFF[21,22]. Until activation by antigen, naïve B cells stay in a senescence-like state[21], but are epigenetically and transcriptionally primed for rapid activation[23–25]. Encounter with a T cell-dependent (TD) antigen[A] activates the NFκB and IRF4 pathways[26]. Costimulatory signals provided by T follicular helper cells (Tfh) lead to the final activation of the B cell, which is characterized by high expression of *MYC*, *CCND2*, and components of the oxidative phosphorylation pathway[27], leading to global chromatin remodeling[25], a state of high transcriptional activity[23,24], and class switch recombination (CSR)[28]. AID, UNG and APE1 specifically insert DSBs at switch-regions, which are repaired by enzymes of the NHEJ machinery thereby replacing the constant-region of the B cell receptor (BCR)[28]. Afterwards, activated B cells either directly differentiate into short-lived plasmablasts (PB), referred to as extrafollicular PBs[29,30], or upregulate *BCL6*[31] and *FOXO1*[27] and consequently form the dark zone (DZ) of the newly initiated germinal center (GC). Highly proliferative DZ B cells undergo somatic hypermutation (SHM). In this process, AID deaminates cytosine residues of the hypervariable regions of the Ig loci leading to point mutations, intended to enhance BCR affinity[18]. In terms of a selection process, multiple rounds of SHM alternate with the verification of BCR affinity by Tfh cells in the light zone (LZ). While the exact mechanism of GC exit remains elusive, LZ B cells can either differentiate into memory B cells or into PCs[2,3]. The output of pre-memory B cells occurs early[27,32]. LZ B cells differentiating towards PB receive costimulatory signals such as CD40L and IL21 activating the NFκB, IRF4 and STAT3 pathways and downregulate *BCL6* and *PAX5*[33]. Among others, the activation program is re-silenced by repressive epigenetic marks mediated by EZH2[34,35]. After migration to the medullary chords, in the presence of CXCL12, APRIL, and IL6[36], PBs differentiate further while only a subset can leave secondary lymphoid organs and home to the BM, requiring activation of S1PR1[37] and integrin $\alpha_4\beta_7$[38], respectively. The PC transcriptional program is initially mediated by IRF4, PRDM1 and XBP1s[2], while the final maturation is characterized by expression of the transcription factors KLF2[38], ZBTB20[39], IKZF1[40] and IKZF3[41] as well as the markers CD28[42], VLA4[43] and CD93 (AA4.1)[44]. In close contact to BM stromal cells[45] and hematopoietic cells

[A] In contrast to TD antigens, T cell-independent antigens (TI) can directly activate B cells by binding to pattern-recognition receptors (PRR) like toll-like receptors (TLR) (type-I TI) or to the BCR (type-II) without the need of T cell support[218].

like eosinophils[46], PCs form niches in which the preconditions for longevity are only provided for selected PCs by IL6 and APRIL, activating antiapoptotic MCL1[47–49].

In conclusion, the activation of B cells and differentiation into PCs is determined by a temporary highly proliferative and transcriptionally active state as well as processes that can form DSBs rendering GC B cells prone for malignant transformation[18,50]. Incorrectly repaired DSBs induced by RAG1/2 or AID-activity frequently lead to translocations[9] and can constitute oncogenic drivers, often seen in the pathology of lymphomas and MM[9,18,50].

1.2.2 The cell of origin of multiple myeloma

MM represents the malignant counterpart of terminally differentiated B cells[4], but the malignant transformation is initiated earlier during B cell development[51]. Multiple lines of evidence argue for a (post-) GC B cell as the cell of origin (COO). The V_H loci of MM cells are somatically hypermutated arguing for a preceded AID-activity[52,53]. The predominant absence of the V_H4.21 variant in MM cells, which is associated with autoreactivity[9], is another indicator that a counter selecting GC reaction has taken place[54]. Many patients harbor translocations that most likely occur due to aberrant SHM and CSR during a GC reaction[55]. Other findings suggest that disease initiation can happen even earlier during B cell differentiation. Some aberrations, especially the translocation t(11;14) can result from dysfunctional VDJ-recombination in pro-B cells[55]. Furthermore, genetically modified mice expressing *Mafb* (a typical MIE) in lineage negative stem cells or *Maf* in naïve B cells develop features of human MM with age[56,57].

It is assumed that a primary genetic hit confers a proliferative advantage to a (post-) GC B cell giving rise to an initial clone[51]. This clone preserves the ability to terminally differentiate into PCs[51], including trafficking to the BM and interaction with the local microenvironment[5], and accumulates further genetic abnormalities[58]. Rising titers of secreted monoclonal antibodies can be detected as M-spike and define the stadium of MGUS[59]. Premalignant MGUS cells show a high mutational burden, reminiscent of fully malignant hematologic malignancies like chronic lymphocytic leukemia or acute myeloid leukemia[16,60–62], consisting of a median number of 13 non-synonymous single nucleotide variants (SNVs) per exome[16]. The present clonal cells show slight variations within their V_H loci, indicative of ongoing AID-activity[63,64]. The time window between the first genetic hit and diagnosis (defined as MM or

smoldering myeloma, a high risk MGUS) is between 8 and 66 years[65]. Malignant processes from the initiation of disease to the MGUS stage including translocations affecting MAF transcription factors are referred to as *early* pathogenesis or pre-MGUS[59]. Further genetic events are required for development towards fully malignant MM.

1.2.3 The early pathogenesis of multiple myeloma

In the current model of tumorigenesis, genetic aberrations are distinguished according to their temporal occurrence and their effect on transformation. Classically, primary genetic events are thought to immortalize the COO to give rise to the premalignant clone and MGUS, whereas secondary events are necessary for the transformation into fully malignant MM[66]. Additional groups of mutations have been added to this model, offering a higher resolution of the process. Among them, congenital risk variants and acquired mutations in the time window between classic primary and secondary events[4] belong to the *early* pathogenesis.

1.2.3.1 Risk variants

There are inherited genetic variants associated with the risk of developing PC dyscrasias. Many of the approximately two dozen known SNVs[67] directly increase the risk of developing MGUS, suggesting an effect on the *early* pathogenesis of MM[68]. Proteins affected by such SNVs act in four main molecular biologic fields, including chromatin remodeling, physiological PC differentiation, genome instability and MYC/IRF4 activity[69]. The transcription factor (TF) IRF4 has a central role for MM biology and is indispensable for MM cell survival[70]. It directly regulates transcription of *MYC*[70] and *KLF2*, the candidate gene of risk locus 19p13.11. KLF2 controls homing of MM cells by upregulation of *ITGB7*[38,71].

1.2.3.2 Primary events

Primary genetic aberrations most likely acquired during the GC reaction occur in a large fraction of the tumor, indicating a clonal character and origination from a common progenitor[66,72,73]. There are different primary events, which occur nearly mutually exclusive among patients[74,75]. Therefore, distinct subgroups of MM patients can be genetically distinguished[76,77] that demonstrate different clinical courses including prognosis[78–80].

The largest subgroup, comprising approximately 50 % of patients, is characterized by a variety of trisomies resulting in a hyperdiploid karyotype. Duplication of the chromosomes 9, 15, 18, 19 and 21 show the highest clonality, indicative of *early* events[81] and probably have a dosage effect on gene expression[82]. As recently reported the trisomies occur sequentially[81,83] rather than being the result of a single dysfunctional mitosis as believed initially[4,9].

The genetic architecture of non-hyperploid MM is characterized by recurrent translocations that juxtapose oncogenes to the immunoglobulin locus resulting in overexpression of respective genes by the strong Eμ or 3' enhancer[73,80,84,85]. Sequencing of breakpoints suggested aberrant CSR, SHM or receptor revision as main causes of translocations[55]. Three groups of oncogenes are affected in MM which subdivide the non-hyperdiploid MM into the CCND, t(4;14) and MF subgroup[76]. Cyclin D1 is directly upregulated by the t(11;14) translocation as seen in 15-20 % of patients[86,87]. Also, translocations affecting *CCND2* or *CCND3* are found, albeit less often[4]. The central mechanism of action of the D-type cyclins, whose expression is normally strictly depended on external growth stimuli, is the activation of CDK4/6 that phosphorylates targets like RB1 to promote entry to the synthesis phase of the cell cycle to prepare for mitosis[88]. Overexpression might sensitize cells to growth signals, or even uncouple cell cycle regulation. Further functions of CCND1 in MM concern regulation of adhesion, migration, and redox metabolism[89]. The t(4;14) rearrangement, detectable in 15 % of patients, leads to upregulation of the histone methyltransferase *MMSET* and the tyrosine kinase *FGFR3*[4,86]. Expression of the splice variants *MMSET-II* and *RE-IIBP*[90] is associated with a global increase of the histone-mark H3K36me2, which is likely the predominant mechanism of action, regulating the expression of several genes such as *CCND2*[91–93]. Overexpression of *FGFR3* is lost over time in a quarter of patients, suggesting *MMSET* as the central oncogene of t(4;14)[94,95].

The MF subgroup comprises translocations affecting the large MAF transcriptions factors MAFA, MAFB or MAF[96]. Their similar biochemistry including DNA-binding specificity and protein interaction suggests a common pathogenetic mechanism initiated by regulation of respective target genes. A detailed description of this subgroup will be given further below.

1.2.3.3 MGUS

Mutations detectable in the MGUS clone, but at a lower clonality compared to primary events are potential *early*, but not initiating events. In MGUS patients numerical and structural aberrations can be detected at frequencies of approximately 55 and 45 % respectively[97,98]. Deletions of the short arm as well as of the entire chromosome 13 occur very early[75,97–99], likely resulting in decreased expression of the tumor suppressor *RB1* and deregulation of G1/S transition[4,9,75]. Gain of the long arm of chromosome 1 (+1q) is found in approximately 25 % of MGUS patients[97,98] and can lead to overexpression of *ILF2*, a regulator of splicing and mRNA stability in MM[100]. The deletion of the short arm of chromosome 1 leads to an early loss of several tumor suppressor genes[97,98]. Point mutations detectable at the MGUS state often affect the genes *HIST1H1E* and *EGR1* with especially high clonality[58]. Further mutations can be found in the genes *FAM46C*[58], *DIS3*, *LTB* as well as members of the MAPK/ERK-pathway like *KRAS* and *NRAS*[16,98,101], both within the coding regions and in regulating gene segments[102,103].

Studying the order of occurrence of genetic events is a challenge in MM research. As described above, it is mainly based on clonality of mutations in MGUS and MM probes[16,81,104,105]. Whole genome sequencing (WGS) of MGUS and MM samples and elegant computational approaches have helped to gain a higher resolution of the process[65,106–108]. Comparison of mutational patterns between duplicated chromosomes has shown that abnormally high non-canonical AID-activity is a typical *early* mutational pattern in MM pathogenesis[65]. During the *early* transformation, it is the main driver of kataegis outside of Ig loci whereas in later stages it is mainly induced by APOBEC-activity[65,109] This is consistent with the finding that the MGUS clone is heterogenous regarding V_H mutations. In known target regions of SHM outside of Ig loci, MM cells harbor a 1,000-fold higher mutation frequency than anticipated for post GC B cells[60]. It is unknown, in which setting this high AID-activity, which is normally absent in post GC B cells, takes place. Current explanations include a model of a prolonged GC reaction or multiple rounds of reentry to the GC via the route of a memory B cell state[109]. This could be caused by chronic antigen stimulation[110–114] as antibodies secreted by MM cells are partly specific for chronically presented antigens like epitopes of herpes viruses[110].

1.2.3.4 MGUS to MM progression

The progression of MGUS towards MM is characterized by an increasing tumor mass[115] in addition to branching of subclones by accumulation of heterogenous mutations. The intraclonal heterogeneity regarding the V_H locus gets lost over time[63–65,116–118]. The median number of non-synonymous SNVs increases from 13 to 28, 31 and 59 in the development from MGUS to high risk-SMM, MM and PCL respectively[16], reflecting a high mutation burden with broad heterogeneity[102,104]. Progression-promoting events towards fully malignant MM are hardly found at the MGUS stage and show a subclonal distribution[4]. These include loss of p53, overexpression of *MYC* as well as deregulated NFκB signaling[4,75].

1.3 MAF transcription factors in the pathogenesis of multiple myeloma

1.3.1 Oncogenic function of MAF in MM

Overexpression of MAFA, MAFB and MAF as result of reciprocal translocations constitute initiating events in MM, the most common being t(14;16) deregulating MAF[96,119] in about 5 % of patients[86]. The translocation t(14;16) is associated with a poor prognosis and development of extramedullary disease as well as PCL[9,120–122]. These tumors are only slightly sensitive to proteasome inhibitors such as BTZ[123]. Analogously, melphalan sensitivity is reduced in MAF bearing MM cells[123].

Large MAF transcriptions factors belong to the superfamily of AP1 basic-leucine zippers[124] and form homodimers to bind CRE- (cAMP-responsive element) and TRE- (12-O-tetradecanoyl phorbol 13-acetate-responsive element) consensus sequences, flanked by the palindromic triplet TGC[125]. This MAF recognition element (MARE)[96] shows variations that include degeneration of CRE or TRE sites[126] as well as 5'AT-rich half site MAREs[127]. The aminoterminal regions of large MAF proteins consist of a transactivation domain enabling transcription[96,128]. In contrast, small MAF proteins lacking the transactivation domain act as repressors by competing for DNA-binding sites[125]. MAF transcription factors do not exclusively form homodimers but can also form heterodimers with members of the AP1 superfamily[96] like FOS and JUN *in vitro*[126,129]. Furthermore, MAF interacts with the transcription factors PAX6, HOXD12[130], MYB[131], ETS1[132], NFATC3[133] and SNF2H[134]. MAF

proteins activate transcription via binding to coactivators like P/CAF[135], P300, CBP[136], or TBP[137].

Physiological functions of MAF are represented in both early tissue specification and terminal differentiation, which are best characterized in crystalline gene regulation in the lens[134] and terminal $CD4^+$ T cell differentiation[138], respectively. Interestingly, no physiological function of MAF is known in B cell biology, although MAF is transiently expressed in splenic PBs accompanied by accessibility of MARE sites[139]. In contrast, the small MAF member MAFK is a known critical dimerization partner of BACH2, a suppressor of *BLIMP1*[140,141]. Apart from the original discovery of its homologue v-maf as an oncogene of the transforming avian retrovirus[142,143], little is known about the transforming ability of MAF. However, overexpression in T cells has been found to induce lymphoma in mice[144].

Regarding MM, *MAF* overexpression is expected to constitute a MIE in t(14;16) patients, but is also expressed in other subgroups, especially the MMSET group, as a result of various mechanisms[123]. Such mechanisms include direct upregulation by FOS downstream of MEK1 and ERK1/2[145], XBP1 activity[146] as well as TACI signaling[147]. Furthermore, the long non-coding RNA ANGPTL1-3, upregulated by +1q, competes with miR-30a-3p to increase *MAF* expression[148].

The t(14;16) translocation is mostly a result of erroneous processes during the GC reaction as most breaks at chromosome 14 appear in the switch-regions of *IGHG1* and *IGHG3* and thus can be assigned to aberrant CSR[55]. Furthermore, evidence for homologous recombination that can mediate IGHM to IGHD isotype switching[149] as well as for SHM outside of J_H6 can be found[55,73]. The Ig light-chain translocations t(2;16) and t(16;22) affecting *MAF* exist in patients and human MM cell lines (HMCL) like RPMI-8226 and XG-6[55,73]. The translocation t(14;20) affecting *MAFB* expression may also be a result of errors in DJ recombination in pro-B cells or receptor revision in GC B cells[55]. Nearly all breakpoints on chromosome 16 are localized in the last intron of *WWOX*, centromeric to *MAF*[55]. This region contains the so-termed *fragile site* FRA16D and is prone to DSBs[150,151]. Thus, despite upregulating *MAF*, translocations may also heterozygously disrupt *WWOX*, a known tumor suppressor in MM pathology[152,153]. Of note, the chromosome breakpoint in the HMCL RPMI-8226 lays telomeric to *MAF*[73].

The key mechanism of action of MAF proteins in MM seems to be the deregulation of different target genes. Expression of *CCND2* is directly regulated by MAF[154]. Likewise, the promoters of *ITGB7* and *ARK5* contain MARE sequences that can be bound by MAF[155,156]. Both proteins have a role in tumor-stroma interaction. ITGB7 can form heterodimers to constitute integrin $\alpha_4\beta_7$, which binds MADCAM1 and VCAM1[157] or $\alpha_E\beta_7$ to bind E-cadherin[158]. In that way, upregulation of *ITGB7* by MAF likely enhances adhesion to BM stroma and homing to the BM as well as migration towards SDF1α gradients[159]. In addition, integrin mediated adhesion of MM cells upregulates alternative NFκB and FAC signaling and promotes VEGF, IL6 and CCL4 production[154,159]. ARK5 on the other hand mediates tumor invasion in MM[156]. Further direct targets of MAF and MAFB constitute *SLC25A2*, *NOTCH2* and *ARID2A*[160]. Expression of the chemokine receptors *CCR1* and *CXCR3* as well as the chemokine *CXCL12* is upregulated in the MF subgroup without a proven direct mechanism[76,154]. The same holds true for TLR4, conferring resistance to BTZ[76,161]. DEPTOR, encoded by *DEPDC6*, is overexpressed in the MF subgroup, and inhibits mTORC1 thus activating PI3K/AKT signaling[162]. It furthermore functions as a TF, regulating genes involved in endoplasmic reticulum regulation like *CKAP4*, *ERLIN2* and *KEAP1*[163]. *APOBEC3A* is significantly upregulated among patients of the MF, subgroup which is reflected in an accented APOBEC mutational signature inside and outside of kataegis regions[76,86]. The high number of APOBEC mutations is accompanied by a shift from APOBEC3B to APOBEC3A activity, a mechanism that can also be found in solid cancers[65]. While in the other MM subgroups the ratio of signatures of APOBEC3A to APOBEC3B is about 1, it is raised to 2.5 in the MF subgroup[65]. Importantly, APOBEC is the dominating signature in the MF subgroup from disease initiation onwards[65]. In stark contrast to the other subgroups, no prolonged AID-activity has been found in the MF subgroup suggesting a different *early* pathogenesis[109]. Overall, the MF subgroup shows the highest mutation rate of MM subgroups[86].

In addition to an APOBEC mutational signature, the translocation t(14;16) is generally associated with mutations of the *DIS3* and *TRAF2* genes[153]. Of note, while *BRAF* is altered by a V600 mutation in other subgroups, mutations of D594 predominate the MF subgroup. The t(14;16) is furthermore associated with the structural aberrations +1q and deletion of 13q[98,153].

The transcriptional activity of MAF is tightly regulated by posttranslational modifications in MM. MAFA, MAFB and MAF can be phosphorylated by GSK3B upon phosphorylation of MAFs S65 by a putative initiator kinase, like ERK or MAPK14[135,164–166]. Phosphorylation of MAF proteins in MM increases their transcriptional activity, but also marks them for ubiquitination and degradation[123,165,167]. Increased activity of MAFA is associated with enhanced binding to P/CAF in the model system of COS7 and INS1 cells[135]. Expression of *DEPDC6*, but not *CCND2* and *ITGB7*, is dependent on phosphorylation of MAFB or MAF by GSK3B[165]. Degradation of MAF predominantly occurs via the proteasomal pathway[168]. The ubiquitination of MAF is committed by the activity of HERC4, UBE2O[169,170], TMPAI and NEDD4[171]. In contrast, USP5[172], USP7[173] and OTUB1[174,175] can deubiquitinate and stabilize MAF. Furthermore, MAF proteins underlie a regulation by SUMOylation[176].

1.3.2 Non-GC B cell specific transgenic mouse models to study MAF transcription factors as myeloma-initiating oncogenes

To date, three transgenic approaches were used to study the function of MAF for the development of MM in mice. Morito and colleagues inserted the coding sequence of *Maf* along with the V_H promoter, Eμ enhancer, and 3'Eκ enhancer into the mouse genome and achieved transgene expression in B cells[57]. Based on the analysis of different B cell populations, such as follicular and marginal zone B cells, B cell biology was not restricted, however BMPCs increased in number. After a median age of 80 weeks, about one third of the transgenic mice developed tumors in the spleen in which two cell types were present, showing a $B220^{+}CD138^{+}CD21^{+}CD23^{+}IgM^{+}IgD^{-}$ and a $B220^{low}CD138^{+}$ phenotype, respectively. The tumor cells expressed the MAF target genes *Ccnd2* and *Itgb7*. Concomitantly, serum M-spikes and deposition of Ig in the tubule and mesangium occurred, resembling CAST nephropathy. Thus, these transplantable tumors reflected some features of a plasmacytoma, but failed to induce bone lesions and to resemble the GC origin of MM cells.

The expression of *Mafb* under control of the *Sca1* (*Ly6a*) promoter in hematopoietic stem cells, as performed by Vicente-Duenas and colleagues, resulted in impaired B cell development in the BM from 52 weeks of age onwards, whereas $B220^{low}CD138^{+}FSC^{high}SSC^{high}$ PCs accumulated[56]. These oligoclonal cells infiltrated the lung, liver, kidney and spleens of mice and secreted high amounts of Ig leading to

paraprotein depositions resembling AL-amyloidosis. Transgenic mice showed osteolytic lesions and skeletal destruction. As a downside of the model, the tumor cells did neither express *Mafb* nor known target genes. The authors suggested an epigenetic remodeling of stem cells as a mechanism of the transformation[56].

1.3.3 Previous work from our group: A novel GC B cell specific transgenic mouse model to study MAF as a myeloma-initiating oncogene

Previous work from our group performed by Wiebke Winkler (under the supervision of Martin Janz and Klaus Rajewsky) intended to develop subgroup-specific transgenic mouse models for MM[177]. In this context, a mouse strain was created by Wiebke Winkler (assisted by Hagen Wende and Tomoharu Yasuda) that allowed for the conditional overexpression of *Maf* in mouse GC B cells and their progeny and the characterization of the terminal differentiation of *Maf*-expressing B cells[178].

In general, such cell-specific expression can be achieved by targeting the sequence of the site-specific DNA recombinase Cre to lineage specific genes, like *Mb1*[179] (*Cd79a*), *Cd19*[180] or *Cγ1*[181] (*Ighg1*) in the case of B cells. Cre recombinase can excise or invert DNA fragments depending on the orientation of flanking recombination-sequences termed loxP sites[182,183]. To overexpress genes in a lineage- and stage-specific manner, the gene of interest can be integrated into a ubiquitously transcribed locus (such as the Rosa26 locus in mice) under control of a loxP-flanked STOP cassette. In that way, the STOP cassette gets removed only in cells that express Cre, which in turn results in transgene expression[184,185]. To achieve also temporal control of transgene activation, Cre can be fused to the mutated estrogen receptor ligand-binding domain ERT2, which prevents the recombinase to enter the nucleus. Recombination then only occurs upon application of tamoxifen allowing for nuclear entry[186].

Wiebke Winkler targeted the cDNA of *Maf* linked via an IRES sequence to a BFP reporter under control of a CAG promoter (chicken β-actin promoter with CMV-IE enhancer) as well as a loxP-flanked STOP cassette into the Rosa26 locus, referred to as the R26CAG-Maf-ires-BFPstopF allele, short R26 MafstopF[178]. These mice were crossed to Cγ1-cre mice, in which Cre expression is initiated upon activation of germline transcription from the *Ighg1* locus in activated B cells and early GC B cells[181]. In Cγ1-cre mice, Cre expression reaches

a maximum of 75-85 % BFP reporter-labelled GC B cells 14 days after immunization with NP_{15}-CGG/alum[181].

To compare the biology of oncogene-transgenic cells to a reference and to control cre activity in mouse models generated in our lab, generally, transgenic control mice are used expressing only reporter proteins in a cre/loxP-controlled manner. In the Cγ1-cre; R26 hCD2stopF mouse, a signaling-deficient truncated version of the human T cell surface antigen CD2 is expressed in GC B cells which is assessable by flow cytometry[187]. As shown by previous work, this protein does not interfere with cellular signaling including terminal B cell differentiation and can be used as an appropriate control in transgenic mouse experiments[187,188]. In the Cγ1-cre; R26CAG-BFP-ires-huCD2stopF mouse, BFP and hCD2 are expressed (via linkage of an IRES sequence) which allows for direct assessment of BFP in addition to hCD2 by flow cytometry[189]. In this work, reporter positive cells in the latter mice were detected only via their BFP expression. This allele will hence be referred to as R26 BFPstopF in the following.

Wiebke Winkler first analyzed B cells from the newly created Cγ1-cre; R26 MafstopF mice *in vitro*. When stimulated with αCD40 and IL4 or LPS and IL4, isolated B cells differentiated towards $B220^{int}CD138^{high}$ PCs and switched to IgG1 after 96 h (Fig. 1A). In contrast, *in vivo* experiments showed that numbers of splenic *Maf*-expressing GC B cell were dramatically reduced 14 days after immunization with NP_{15}-CGG/alum (Fig. 1B). The impaired GC reaction was accompanied by reduced numbers of splenic PB/PCs. Splenic antibody-secreting cells (ASC) produced mainly IgM and not IgG on day 14 after immunization. Flow cytometric analysis of BM $CD138^{+}TACI^{+}$ cells found normal numbers of total PCs, whereas *Maf*-expressing PCs were reduced (Fig. 1B). Surprisingly, ELISPOT analysis demonstrated a temporary accumulation of antigen-specific IgM-secreting cells in the BM of Cγ1-cre; R26 MafstopF mice (Fig. 1C) that was already detectable at day 4 after NP_{15}-CGG immunization. Over time, however, *Maf*-expressing GC B and PCs fully disappeared *in vivo,* which could neither be rescued by concomitant *Myc* overexpression nor NFκB activation. Thus, this mouse model stands in contrast to the presumed initial steps of human myelomagenesis. However, the temporary accumulation of antigen-specific IgM-secreting cells in the BM of immunized Cγ1-cre; R26 MafstopF mice is an interesting observation that reflects an important feature of human MM cells. Wiebke Winkler suggested two putative mechanisms for this phenomenon of a reduced GC reaction, but early PC accumulation.

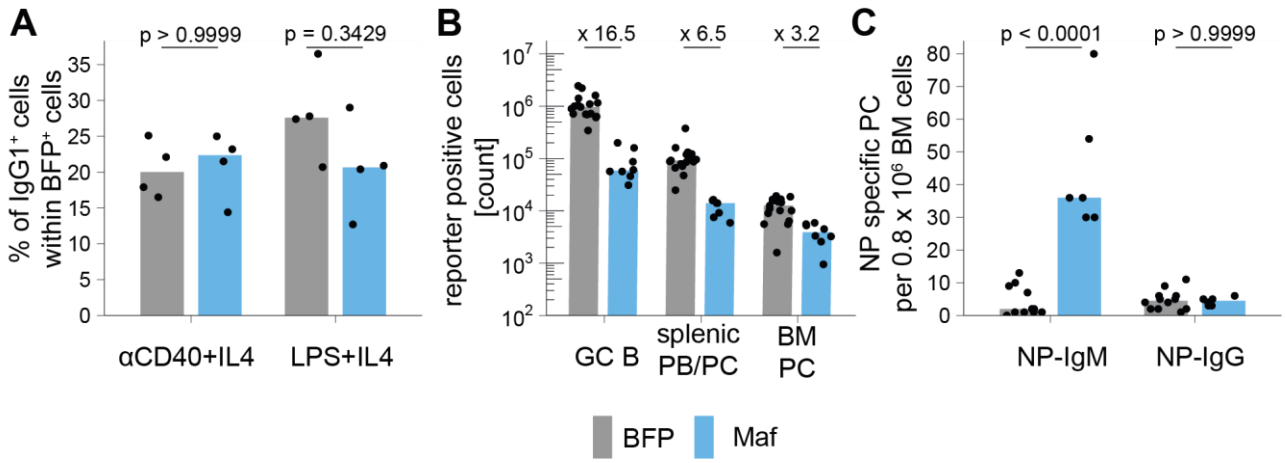

Figure 1: Effect of *Maf* overexpression in activated B cells on the B cell response (modified from [178]). **A)** Naïve B cells were isolated from spleens of Cγ1-cre; R26 MafstopF (Maf) and Cγ1-cre; R26 BFPstopF (BFP) control mice by CD43 depletion. Subsequently, cells were cultured *in vitro* in the presence of either αCD40 (1 µg/ml) + IL4 (25 ng/ml) or LPS (20 µg/ml) + IL4 (25 ng/ml). To assess CSR to IgG1, surface IgG1 expression was measured within transgene-expressing (BFP positive) cells by flow cytometry. **B)** Cγ1-cre; R26 MafstopF (Maf) and BFP control mice were immunized once with NP_{15}-CGG, and the B cell response was analyzed at day 14 after immunization by flow cytometry. Absolute numbers of reporter positive $CD19^+B220^+FAS^{hi}CD38^{lo}$ GC B cells, splenic $CD138^+TACI^+$ PC and $CD138^+TACI^+$ BMPC were back calculated from FACS results. **C)** Maf and control mice were immunized as described before and the NP-specific PC response was analyzed at day 14. Numbers of NP-specific IgM^+ or $IgG1^+$ ASCs per 0.8×10^6 BM cells measured by NP-specific ELISPOT are shown. NP_{28}-BSA served as capturing antigen. Mann-Whitney test. Figure and figure legend are taken and modified with permission of the author from (Winkler, 2018)[178].

First, the specific overexpression of *Maf* in activated B cells could prohibit the GC entry or lead to rapid cell death while (extrafollicular) PBs tolerate *Maf* expression and differentiate into PCs[178]. Alternatively, the observed PCs accumulating in the BM could be the progeny of prematurely differentiated *Maf*-expressing GC B cells[178].

1.4 Aim of this thesis

Overexpression of MAF as a consequence of the translocation t(14;16) is regarded as a primary genetic event[96] in approx. 5 % of multiple myeloma (MM) patients[86]. MAF transcriptional activity is likely to be the initial step in the transformation of GC B cells, the cell of origin of this type of MM[55]. Recent work from our laboratory performed by Wiebke Winkler (under the supervision of Martin Janz and Klaus Rajewsky) aimed to develop genotype-specific MM mouse models by overexpressing translocation-associated initiating oncogenes in germinal center (GC) B cells[177]. Unexpectedly, experiments performed by Wiebke Winkler in Cγ1-cre; R26 MafstopF mice revealed that conditional *Maf*

overexpression in GC B cells and their progeny resulted in a substantial reduction of *Maf*-expressing GC B cells and splenic plasma cells (PC) upon immunization. However, simultaneously, *Maf*-expressing antigen-specific IgM^+ PCs temporary accumulated in the bone marrow (BM)[178].

The goal of this thesis is to further characterize the effect of *Maf* expression on the GC reaction and PC differentiation to better understand the observations made in Cγ1-cre; R26 MafstopF mice. Among others, the restrained GC reaction could be the result of reduced proliferation of GC B cells[178]. Therefore, the proliferative potential of *Maf*-expressing GC B cells in Cγ1-cre; R26 MafstopF mice upon immunization is investigated first by an *in vivo* BrdU incorporation experiment. Of note, in Cγ1-cre; R26 MafstopF mice, *Maf*-expressing IgM^+ PCs emerge early in the bone marrow[178]. To elucidate their origin (prematurely differentiated GC B cells or extrafollicular plasma blasts, PBs), specific overexpression of *Maf* in extrafollicular PBs, GC B cells and differentiating follicular PBs is performed. Therefore, the existing mouse model is modified by using the recently developed Cγ1-creERT2 allele[190]. This cre strain enables the selective activation of a given transgene, here *Maf*, in distinct B cell populations by tamoxifen application during the early, mid, and late GC reaction and the subsequent analysis of their progeny over time. Besides reduced proliferation and effects on differentiation of *Maf*-expressing B cells, expression of a transgene could potentially influence B cell:T cell interactions. Both, T cell support and immune surveillance by T cells are thus assessed in Cγ1-creERT2; R26 MafstopF mice by flow cytometry.

The activity of MAF as a transcription factor requires the interaction with multiple proteins. To gain an unbiased view of such interaction and uncover possible shortcomings of the mouse model, immunoprecipitation of MAF in human MM cell lines is performed and binding proteins analyzed by mass spectrometry. To find the most important interacting candidates and transfer the results to the mouse model, a screening method is developed based on retroviral transduction of candidate interactors into mouse B cells.

2. Materials and methods

2.1 Materials

2.1.1 Bacteria strains

Table 1: Bacteria strains

Name	Genetic background	Supplier
E. coli XL1-blue	*rec*A1 *end*A1 *gyr*A96 *thi*-1 *hsd*R17 *sup*E44 *rel*A1 *lac*	Invitrogen

2.1.2 Cell lines

Table 2: Cell lines

Name	Genetic background / remarks	Reference
ANBL6	$t(14;16)^+$	119
MM1.S	$t(14;16)^+$ IgA lambda MM	119
PlatE	293T cells expressing packaging plasmids pEnv, pGag-pol	191
RPMI8226	$t(16;22)^+$ IgG lambda MM	192

2.1.3 Mouse strains

Table 3: Mouse strains

Name	Full name	Genetic background	Reference
Cγ1-cre		129, backcrossed to C57BL/6	181
Cγ1-creERT2		as above	190
R26 BFPstopF	R26CAG-BFP-ires-huCD2stopF	C57BL/6	189
R26 hCD2stopF		C57BL/6	187
R26 MafstopF	R26CAG-Maf-ires-BFPstopF	C57BL/6	178

2.1.4 Chemicals

Table 4: Chemicals

Name	Supplier, Catalogue Number
Acrylamide 40 %	Roth, #A515.1
Agarose	Biozym, #840004

Alum ($KAl(SO_4)_2$)	Sigma, #31242
Ammonium bicarbonate	Sigma, #09830
Ammonium chloride (NH_4Cl)	Sigma, # 9434
Ammonium persulfate (APS)	Roth, #9592.2
Ammonium sulfate	Sigma, # A4418
Ampicillin	Roth, #K029.2
Bacto Tryptone	BD, #211705
Boric acid	Roth, #5935.2
Bovine Serum Albumin (BSA)	Sigma, #3803
Bromodeoxyuridine (BrdU)	BD; #550891
Bromophenol blue (BPB)	Sigma, #B0126
Calcium chloride ($CaCl_2$)	Fluka, #21079
CHAPS	Roth, #1479.2
Chloroacetamide	Sigma, #22790
Chloroquine	Sigma, #C6628
Cresol Red sodium salt	Sigma, #114480
Deoxycholate	Sigma, #D-6750
Dithiothreitol	Thermo Scientific, # 20290
DTT	Roth, #6908.2
EDTA	Roth, #8040.2
Ethanol	Roth, #9065.1
Glutaraldehyde	Sigma, SLBS4196
Glycerol	PlusOne, #17-1325-01
Glycine	Roth, #3908.3
HCl	Roth, #9277
Isopropanol	Roth, #6752.1
Magnesium chloride ($MgCl_2$)	Sigma, #M-3634
Magnesium sulfate ($MgSO_4$)	Sigma, #M-1880
Methanol	Th. Geyer, #1437.2511
Nonidet P40	Roche, #11754599001
Polybrene	EMD Millipore, #TR-1003
Ponceau S	Roth, #5938.1
Potassium chloride (KCl)	Roth, #6781.1
Potassium dihydrogen phosphate	Roth, #3904.1
Propidium iodide	Sigma, #P-4170
Protein Assay BCA Dye	Thermo Scientific, #23221 #23224
Protein Assay Dye Reagent	Bio-Rad, #500-0006
RetroNectin	Takara, #T100B
SDS	Roth, #CN30.3
Sodium acetate	Sigma, #P-1147
Sodium azide	Roth, #K305.1
Sodium chloride (NaCl)	Roth, #3957.2
Sodium citrate	Roth, #4088.2
Sodium deoxycholate	Sigma, #D6750
Sodium fluoride (NaF)	Roth, #2618
Sodium hydroxide (NaOH)	Roth, #8655
Sodium orthovanadate (Na_3VO_4)	Sigma, #S6508

Sucrose	Roth
Sunflower oil	Sigma, #8001-21-6
Tamoxifen	Sigma, #T5648-5G
TEMED	Roth, #UN-2372
Trifluoroacetic Acid	Sigma, #1.08178
Tris	Roth, #5429.2
TritonX	Roth, #3051
Tween20	Roth, #9127.1
Xylene cyanol blue	Sigma, #X4126
Yeast extract	BD, #288620

2.1.5 Reagents

Table 5: Reagents

Reagent	Supplier, Catalogue number
CD43 MicroBeads	Miltenyi, #130-049-801
Complete, Mini, Protease Inhibitor	Roche, #05 892 791 001
GeneRuler 1 kb DNA ladder	Fermentas, #SM0313
GeneRuler 100 bp Plus DNA ladder	Fermentas, #SM0321
NIP-BSA-APC	in-house preparation
NP_{15}-CGG	Biosearch, #N-5055B-5-BS
PageRuler Plus Prestained Protein Ladder	ThermoFisher Scientific, #26619
Pierce ECL Western Blotting Substrate	Thermo Fisher Scientific, #32106
RNasin Plus	Promega, #N261B
Streptavidin-AP conjugate	Roche; #11-089161-001
TruStain FcX (a-mouse CD16/32) Antibody	BioLegend, #101320
Zombie Aqua	BioLegend, #423102

2.1.6 Oligonucleotides

Oligonucleotides were purchased from Biotez.

Table 6: RT-PCR primer

Name	Sequence	Reference
Hprt-qPCR-F-4	GTTGGGCTTACCTCACTGCT	
Hprt-qPCR-R-4	TCATCGCTAATCACGACGCT	
Itgb7-qPCR-F3	AGTGAGGACTCCAGCAATGTG	
Itgb7-qPCR-R3	TGGGAGTGGAGAGTGCTCAA	
Actb-qPCR-F	CCTTCTTGGGTATGGAATCCTGT	[193]
Actb-qPCR-R	CACTGTGTTGGCATAGAGGTCTTTAC	[193]
Hmbs-qPCR-F	ATGAGGGTGATTCGAGTGGG	[193]
Hmbs-qPCR-R	TTGTCTCCCGTGGTGGACATA	[193]
Tbp-qPCR-F	CCTTGTACCCTTCACCAATGAC	[193]
Tbp-qPCR-R	ACAGCCAAGATTCACGGTAGA	[193]

Maf-qPCR-F	ACTTCGACGACCGCTTCTC	[178]
Maf-qPCR-Rendo2	TCTCCTGCTTGAGGTGGTCT	[178]

Table 7: Genotyping primer

Genotype	Name	Sequence	Ref.	Program
R26 Maf	GT-Maf-for	ACTTCGACGACCGCTTCTC	[178]	GREY
	GT-WW-IRES-rev	CCAAAAGACGGCAATATGGT	[178]	
Cy1-creERT2	Cg1cre IgG1Kpn1	TGTTGGGACAAACGAGCAATC	[190]	ORANGED
	ERT2_fwd	ACTTTGATCCACCTGATGGC	[190]	
	Cg1_3UTR_r	GTCATGACAATGCCAAGGTCGCTAG	[190]	
	Cg1cre IgG1Kpn1	TGTTGGGACAAACGAGCAATC	[190]	ORANGED
Cy1-cre	Cg1cre Cre13	GGTGGCTGGACCAATGTAAATA	[178]	
	Cg1cre IgG1Rev	GTCATGGCAATGCCAAGGTCGCTAG	[178]	
R26 BFP	LC-BFP-for	CACATGAAGCAGCACGACTT	[178]	GREY
	LC-BFP-rev	ACTGGGTGCTCAGGTAGTGG	[178]	
R26 hCD2	HuCD2_F4	GAT GGG AAA CAT CTA AAA CT	[178]	ORANGEH
	HuCD2_REV	GAG GGG TTG AAG CTG GAA TTT GTT G	[178]	
R26 WT	GT-WW-26-3HA-for	TGCTGCATAAAACCCCAGAT	[178]	GREY
	GT-WW-26-5HA-rev	AAGGGAGCTGCAGTGGAGTA	[178]	

2.1.7 Plasmids

Table 8: Plasmids

Name	Source
MSCV-IRES-GFP (MIG)	Achim Leutz laboratory
MSCV-Maf-IRES-GFP	[178]
pEnv	Achim Leutz laboratory
pGagpol	Achim Leutz laboratory

2.1.8 Antibodies

2.1.8.1 Flow Cytometry Antibodies

Table 9: Flow Cytometry Antibodies

Antigen	Fluorescent dye	Supplier, Cat. No.
AA4.1 (CD93)	PE-Cy7	BioLegend, #136506
B220	BV 785	BioLegend, #103245
B220	PE	BioLegend, #103208
BrdU	APC	BD, #51-23619L
CD138	PE	BioLegend, #142504
CD138	Biotin	BD, #553713
CD138	BV 421	BioLegend, #142508
CD19	BV 605	BioLegend, #115540
CD19	BV 650	BioLegend, #115541
CD27	PerCP-Cy5.5	BioLegend, #124214
CD38	Alexa 700	eBioscience, #56-0381-82
CD3e	Biotin	BioLegend, #100303
CD44	BV 785	BioLegend, #103041
CD62L	PE	BioLegend, #161204
FAS (CD95)	PE-Cy7	BD, #557653
GFP	Alexa Fluor 488	ThermoFisher Scientific, #A-21311
hCD2	FITC	BioLegend, #309206
I-A/I-E (mMHC-II)	Biotin	eBioscience, #13-5321-82
I-A/I-E (mMHC-II)	FITC	eBioscience, #11-5321-82
IgD	PerCP-Cy5.5	BioLegend, #405710
IgG1	PE	BD, #550083
IgM	Biotin	SouthernBiotech, #1020-08
IgM	APC	eBioscience, #17-5790-82
IgM	FITC	eBioscience, #11-5790-81
PD1	BV 605	BioLegend, #135219
Streptavidin	BV 605	BioLegend, #405229
Streptavidin	BV 650	BioLegend, #405231
Streptavidin	PE-Cy7	BioLegend, #405206
TACI (CD267)	Alexa Fluor 647	BD, #558453
TCRB	APC	BioLegend, #109211

2.1.8.2 Western blot and Immunoprecipitation Antibodies

Table 10: Western blot and Immunoprecipitation Antibodies

Name	Supplier, Cat. No.
Anti-Guinea pig IgG (H+L), HRP conjugate	ThermoFisher Scientific, #A18769
Anti-Lamin A/C	Cell Signaling, #2032
Anti-MAF	Abcam, BLR045F
Anti-MAF (N-TEAM)	C. Birchmeier-Kohler laboratory
Anti-mouse IgG (H+L), HRP conjugate	Promega, #W402B
Anti-PARP1	Cell Signaling, #9542
Anti-rabbit IgG (H+L), HRP conjugate	Promega, #W401B
Anti-ß-Actin, clone AC-74	Sigma, #A5316
Rabbit IgG Isotype control AB	R&D System AB

2.1.9 Kits

Table 11: Kits

Name	Supplier, Cat. No.
APC BrdU Flow Kit	BD; #552598
NucleoBond Xtra Midi / Maxi	Macherey-Nagel, #740414
Power SYBR Green PCR Master Mix	applied biosystems, #4368708
RNAse-free DNAse Set	Qiagen, #79254
Rneasy Micro Kit	Qiagen, #74004
ZymoClean Gel DNA Recovery Kit	Zymo Research, #D4007

2.1.10 Enzymes and enzyme buffers

Table 12: Enzymes

Name	Supplier, Cat. No.
Benzonase	Merck, #71205-3
DreamTaq DNA Polymerase	ThermoFisher Scientific, #EP0701
EcoRI (FastDigest)	ThermoFisher Scientific, #FD0274
Endopeptidase LysC	Wako, Osaka, Japan
HpaI (FastDigest)	ThermoFisher Scientific, #ER1032
Phusion High-Fidelity DNA Polymerase	ThermoFisher Scientific, #F530L
Proteinase K	Roth, #7528.4
SuperScript II Reverse Transcriptase	Invitrogen, #18064014

Table 13: Enzyme buffers

Name	Supplier, Cat. No.
DreamTaq buffer	ThermoFisher Scientific, #B65
FastDigestion Buffer	ThermoFisher Scientific, #B72
Phusion buffer	ThermoFisher Scientific, #F518L

2.1.11 Cell culture media and supplements

Table 14: Cell culture media and supplements

Name	Supplier, Cat. No.
DMEM, high glucose	Gibco, #11960-085
DMSO	Sigma, #D2438
Fetal calf serum	Biochrom, #S0115, Lot: 1247B
GlutaMAX, 100 x	Gibco, #35050-061
HEPES 100 x	Gibco, #15630-122
LEAF Purified anti-mouse CD40 Antibody	BioLegend, #102908
L-Glutamine, 100 x	Gibco, #25030-081
MEM Non-essential Amino Acids 100 x	Gibco, #11140-035

PBS, pH 7.2	Gibco, #20012-019
Penicillin-Streptomycin 100 x	Gibco, #15140-122
Recombinant human IL6	R&D System, #206-IL-010/CF
Recombinant mouse IL4	R&D Systems, #404-ML-050
RPMI	Gibco, #31870-025
Sodium pyruvate 100 x	Gibco, #11360-039
ß-ME (2-mercaptoethanol)	Sigma, #M6250
Trypsin/EDTA, 10 x	Gibco, #15400-054

2.1.12 Composition of cell culture media

Table 15: Composition of cell culture media

Name	Ingredients
B cell medium (BCM)	DMEM supplemented with 10 % FCS, 1 x NEAA, 1 mM sodium pyruvate, 2 mM L-glutamine, 1 mM HEPES, 1 x Penicillin-Streptomycin, 50 µM ß-Mercaptoethanol
HMCL medium (standard medium)	RPMI-1640 supplemented with 10 % FCS and 1 x Penicillin-Streptomycin
HMCL medium ß-ME (NCI H929)	Standard medium containing 50 µM ß-ME
HMCL medium IL6 (ANBL6 and INA6)	Standard medium containing 20 % FCS and 2 ng/ml human IL6

2.1.13 Buffers

Table 16: Buffers

Name	Ingredients
Tail lysis buffer	0.1 M Tris-HCl pH 8.0, 0.2 M NaCl, 5 mM EDTA, 0.4 % SDS
TBE	0.1 M Tris, 0.1 M boric acid, 2.5 mM EDTA
TBS-T	20 mM Tris (pH 7.5), 0.135 M NaCl, 0.01 % Triton-X
TENS	5 ml 1 M Tris-HCl pH 8.0, 12.5 ml 20 % SDS, 5 ml 10 N NaOH, H_20 to 500 ml

2.1.14 Composition of bacterial media

Table 17: Composition of bacterial media

Name	Ingredients
LB medium	10 g/l Bacto Tryptone, 5 g/l yeast extract, 10 g/l NaCl
SOB medium	20 g/l Bacto Tryptone, 5 g/l yeast extract, 10 mM NaCl, 2.5 mM KCl; pH adjusted to 7.0; then addition of 10 mM $MgCl_2$, 10 mM $MgSO_4$
SOC medium	SOB supplemented with 20 mM glucose

2.1.15 Buffers B cell culture and staining.

Table 18: Buffers B cell culture and staining

Name	Ingredients
2 x HEBS	50 mM HEPES, 280 mM NaCl, 1.5 mM Na_2HPO_4
FACS buffer	PBS (pH 7.2) supplemented with 3 % FCS and 1 mM EDTA
Gey A	35 g/l NH_4Cl, 1.85 g/l KCl, 1.5 g/l Na_2HPO_4 x 12 H_2O, 0.12 g/l KH_2PO_4, 5 g/l glucose, 50 mg/l phenol red
Gey B	4.2 g/l $MgCl_2$ x 6 H_2O, 1.4 g/l $MgSO_4$ x 7 H_2O, 3.4 g/l $CaCl_2$
Gey C	22.5 g/l $NaHCO_3$
Gey Solution mix	3.5 ml ddH_2O, 1 ml Gey A, 0.25 ml Gey B, 0.25 ml Gey C
MACS buffer	PBS (pH 7.2) supplemented with 0.5 % BSA and 2 mM EDTA
PBS, pH 7.2	Gibco, #20012-019

2.1.16 Protein extraction buffers

Table 19: Protein extraction buffers

Name	Ingredients
PBS, pH 7.2	Gibco, #20012-019
PBS, pH 7.4	Gibco, #10010-023
High salt lysis buffer (HSL)	20 mM HEPES (pH 7.4), 350 mM NaCl, 1 mM $MgCl_2$, 0.5 mM EDTA, 0.1 mM EGTA, 0,2 % NP40, 1 mM DTT, supplemented with protease inhibitors (PI): 1x tablet complete Mini EDTA-free Protease Inhibitor Cocktail (PI, #04693159001; Roche) per 10 ml, 1 mM NaF, 1 mM Na_3VO_4
PBS based NP40 buffer (PNP40)	1 mM $MgCl_2$, 1 mM EDTA, 1 % NP40, PI diluted in PBS (137 mM NaCl)
CHAPS buffer	20mM HEPES (pH 7.4), 150mM NaCl, 10% Glycerol, 1mM EDTA, 0,5% CHAPS, PI
Modified RIPA buffer (RIPA)	NaHPO4 (pH 8,0), 150mM NaCl, 0,2% SDS, 1% Deoxycholat, 1% NP40, 1mM DTT, PI,
Cytoskeleton buffer [100 mM NaCl] (CSK100)	10 mM TrisHCl (pH 7.4), 100 mM NaCl, 300 mM Sucrose, 3 mM $MgCl_2$, 1 mM EGTA, PI
Cytoskeleton buffer [50 mM NaCl] (CSK50)	10 mM TrisHCl (pH 7.4), 50 mM NaCl, 300 mM Sucrose, 3 mM MgCl2, 1 mM EGTA, PI
Perinuclear fraction buffer (PNF)	10 mM TrisHCl (pH 7.4), 300 mM Sucrose, 3 mM $MgCl_2$, 1 mM EGTA, 250 mM Ammoniumsulfate
Nuclear fractioning buffer A	10 mM HEPES (pH 8), 1.5 mM $MgCl_2$, 10 mM KCl, PI

Nuclear fractioning buffer B	25 mM HEPES (pH8), 450 mM NaCl, 0.1 mM EDTA, 0.1 mM EGTA, 1.5mM $MgCl_2$, PI

2.1.17 Western blot buffers and gels

Table 20: Western blot buffers and gels

Name	Ingredients
1 x Running buffer	50 mM Tris, 0.5 M glycine, 0.2 % SDS
10 % resolving gel	10 % Rotiphorese Gel 40 (29:1), 0.375 M TRIS (pH 8.8), 0.1 % SDS, 0.1 % APS, 0.05 % TEMED
4 x Laemmli	200 mM TRIS (pH 6.8), 40 % glycerol, 16 % SDS, 20 % ß-ME, 0.02 % BPB
5 % stacking gel	5 % Rotiphorese Gel 40 (29:1), 0.125 M TRIS (pH 6.8), 0.1 % SDS, 0.1 % APS, 0.05 % TEMED
Blot buffer	20 % MetOH, 0.036 % SDS, 48 mM Tris, 39 mM glycine
NuPAGE Antioxidant	ThermoFisher Scientific, #NP0005
NuPAGE 4-12 % Bis-Tris Protein Gels	ThermoFisher Scientific, #NP0322BOX
NuPAGE MOPS SDS Buffer Kit	ThermoFisher Scientific, #NP0050
NuPAGE Sample Reducing Agent	ThermoFisher Scientific, #NP0009
NuPAGE Transfer Buffer (20 x)	ThermoFisher Scientific, #NP00061
Pierce LDS Buffer, Non-Reducing (4 x)	ThermoFisher Scientific, #84788
Ponceau	0.1 % Ponceau in 5 % acetic acid
TBS-T	20 mM Tris (pH 7.5), 0.135 M NaCl, 0.01 % Triton-X

2.1.18 Mass spectrometry buffers

Table 21: Mass spectrometry buffers

Name	Ingredients
Buffer A	3 % acetonitrile and 0.1 % formic acid
Buffer B	80 % acetonitrile and 0.1 % formic acid
Urea buffer	6 M urea, 2M thiourea, 10 mM HEPES, pH 8.0

2.1.19 Laboratory equipment

Table 22: Laboratory equipment

Name	Supplier
Bacterial hood Safe 2020	Thermo Scientific
Bacterial Incubation Shaker Novotron 50	InforsHT
Bacterial Incubator Multitron 2	InforsHT
Bio Doc Analyze System T5	Biometra
Bioruptor	Diagenode
Blue Marine 200 (Agarose gel electrophoresis chamber)	Serva Electrophoresis
Centrifuge Avanti J-26 XP	Beckman
Centrifuge Heraeus Multifuge X3 FR	Thermo Scientific
Centrifuge Heraeus Pico17 Centrifuge	Thermo Scientific
CURIX 60 X-ray film processor	AGFA
DS-11 FX+ spectrophotometer/fluorometer	Biozym (DeNovix)
DU 640 spectrophotometer	Beckman
Duomax 1030 or Unimax 1010	Heidolph Instruments
FACS Aria II	BD
FACS CantoII	BD
FACS LSRFortessa	BD
FiveEasy pH bench meter	Mettler Toledo
Gel Tank and Blot-Modulset	ThermoScientific, #NW2000
High Performance Liquid Chromatography (HPLC) system	ThermoScientific
Horizontal laminar flow hood (eco air)	ENVAIR
Hybridization Incubator Chamber 7601	GFL
Laminary flow hood (cell culture)	BDK
MIC magnetic induction cycler	bms biosystems
Multigel G44 (SDS-PAGE electrophoresis chamber)	Biometra
PCR Cycler C1000 Thermal Cycler	Bio-Rad
Speedvac	Eppendorf
Standard Power Pack 725	Biometra
StepOnePlus	ThermoFisher (applied biosystems)
Thermo Q Exactive Plus instrument	ThermoScientific
Thermomixer compact	eppendorf
Trans-Blot SD Semi-Dry Transfer Cell	Bio-Rad
UV Stratalinker 2400 (UV Crosslinker)	Stratagene
xMark spectrophotometer	Bio-Rad

2.1.20 Miscellaneous

Table 23: Miscellaneous

Name	Supplier
50 mm cell strainer	BD Biosciences; #340632
96 well half-area microplates	greiner bio-one; #675061
Amersham Protran nitrocellulose membrane	Sigma; #GE10600002
CL-Xposure film	Thermo Fisher Scientific; #34089
Disposable cuvettes PMMA	BRAND, #7591-15
Dynal MPC-S magnet	ThermoFisher Scientific, #12321D
Frosted Microscope slides (Menzel glass slides)	ThermoScientific, #AAAA000001##02F
Greiner CELLSTAR 96 well U-bottom plate	Sigma; #M9436
Hybond XL membrane	GE Healthcare, #RPN303S
LS columns	Miltenyi Biotec; #130-042-401
ProbeQuant G-50 Micro Columns	GE Healthcare, #28-9034-08
Reversed-phase column (20 cm fritless silica microcolumns with inner diameter 75 µm, packed with ReproSil-Pur C18-AQ 1.9 µm resin	Dr. Maisch GmbH

2.1.21 Software

Table 24: Applications and packages

Name	Supplier, Reference
Adobe Illustrator	Adobe
Blast	[194]
FlowJo 10	Treestar
ggpubr	Alboukadel Kassambara
ggVenn	[195]
MaxQuant software package (v1.6.3.4)	MaxQuant
Perseus software (v1.6.2.1).	Perseus
reshape2	[196]
RStudio	RStudio Team (2020). RStudio: Integrated Development for R. RStudio, PBC, Boston, MA
SnapGene Viewer	GSL Biotech LLC
STRING	[197]
Tidyverse	[198]
UpsetR	[199]

2.2 Methods

2.2.1 Mouse analysis

Transgenic mice expressing *Maf, hCD2 or BFP* from the Rosa26 locus (R26 MafstopF, R26 hCD2stopF or R26 BFPstopF) were crossed to Cγ1-cre or Cγ1creERT2 mice to overexpress respective transgenes after immunization with NP_{15}-CGG (and tamoxifen application) in B cells. After different time points, described below, mice were sacrificed, and the immune response analyzed by flow cytometry.

2.2.1.1 Genotyping PCR

To verify successful breeding, genotypes of mice were determined by performing PCR of genomic DNA isolated from ear punches. Therefore, biopsies were digested overnight at 56 °C in tail lysis buffer supplemented with 0.16 mg/ml proteinase K. For the PCRs, different programs were used depending on the target sequence.

Table 25: Genotyping PCR mixture

ddH2O	14.5 µl
10 x DreamTaq buffer	2 µl
Cresol red PCR loading dye	2 µl
10 mM dNTPs	0.4 µl
10 µM primer mix	1.5 µl
ear lysate	1.5 µl
DreamTaq DNA Polymerase	0.1 µl

Table 26: Genotyping PCR programs

Program	GREY		Orange H		ORANGE-D	
1	94 °C	5 min	94 °C	5 min	94 °C	3 min
2	94 °C	30 s	94 °C	30 s	94 °C	30 s
3	60 °C	30 s	55 °C	45 s	65 °C	1 min
4	72 °C	30 s	72 °C	1 min	72 °C	1 min
5	back to 2	32 x	back to 2	34 x	back to 2	35 x
6	72 °C	5 min	72 °C	5 min	72 °C	2 min
7	10 °C	keep	10 °C	keep	10 °C	keep

2.2.1.2 NP_{15}-CGG immunization analysis

To induce a valid immune response, Cγ-1cre; MafstopF and Cγ1-creERT2; MafstopF as well as respective control mice were immunized with NP coupled chicken gamma globulin (NP_{15}-CGG) precipitated in alum as adjuvant. Therefore, NP_{15}-CGG was dissolved in a concentration of 1 mg/ml in sterile PBS, filtered (0.45 µm) and stored at -20 °C in aliquots of 500 or 600 µl. Shortly before injection, the same amount of 10 % alum (1 g $KAl(SO_4)_2$ dissolved into 10 ml of PBS) was added to the prepared aliquots and mixed by vortexing. To precipitate the NP_{15}-CGG in alum, pH values were adjusted to 6.5-7.0 by addition of approximately 25 µl NaOH (c=10 mol/l). The precipitates were spinned down at 5'000 x g for 15 s, washed thrice in 1 ml PBS and finally resuspended in PBS at a concentration of 0.5 µg/ml NP_{15}-CGG. Every mouse received 200 µl by intraperitoneal injection using a 1 ml syringe with a 26 G needle.

2.2.1.3 Tamoxifen preparation and injection

At three consecutive days after immunization, mice were treated with tamoxifen. The timepoints were named early (d3-5), mid (d10-12) or late (d31-33), respectively. Technically, 1 g of Tamoxifen was dissolved in 500 µl of 100 % ethanol and 24.5 ml of sunflower oil was added. Tamoxifen was dissolved by four rounds of ultrasound application (Bioruptor Diagenode); each round included: 5 cycles of each 20/50 sec on/off at 21-25 °C. Aliquots of 500 µl were stored at -20 °C. Mice received 100 µl (4 mg) tamoxifen, heated to 37 °C via oral gavage.

2.2.1.4 NP-specific GC and plasma cell analysis by FACS

At distinct timepoints after immunization (specified in the Results part), spleens, femurs, and tibiae were isolated from sacrificed mice. Spleens and bones were smashed using Menzel glasses or a porcelain mortar, respectively, and filtered through a 50 µm filcon cap to receive single cell suspensions. Cells were spinned down at 300 x g and 4 °C for 5 min and resuspended in 5 ml Gey solution to lyse red blood cells. After 3 min on ice, the lysis was stopped by addition of 5 ml BCM. After centrifugation, cells were resuspended in 10 ml BCM, counted, and distributed on 96 well plates for further staining (5 x 10^6 cells/well). The cells were spinned down again and resuspended in 50 µl TruStain fcX (BioLegend, diluted 1:100 in MACS buffer) in the dark at 4 °C. After 10 min, 150 µl MACS buffer was added and cells

were pelleted at 800 x g for 2 min. For staining of surface markers, cells were resuspended in antibody-containing staining cocktail for 20 min in the dark at 4 °C. Staining was stopped by addition of 150 µl MACS buffer and centrifugation. After a washing step in 200 µl MACS buffer, the cells were subjected to the next staining step, respectively. Finally, cells were resuspended in 400 µl FACS buffer supplemented with 1 µg/ml propidium iodide and analyzed by flow cytometry.

Table 27: Staining cocktails for surface markers

cocktail	GC B cell staining	PC staining	T cell staining
1	PE-IgG1	-	
2	Bio-IgM	Bio-MHC-II	
3	FITC-IgM or FITC-hCD2, PECy7-Fas, NIP-BSA-APC, PerCPCy5.5-IgD, AlexaFluor700-CD38, BV605-SA, BV650-CD19, BV785-B220	FITC-sIgk/sIgl or FITC-hCD2 or FITC-MHC-II, PE-CD138, PECy7-CD93, AlexaFluor647-Taci, PerCPCy5.5-CD43 or PerCPCy5.5-CD27, BV605-SA, BV650-CD19, BV785-B220	FITC-hCD2, PE-CD62L, PeCy7-C3e, APC-TCRb, AlexaFlour700-CD19, BV421-BFP, BV605-PD1, BV650-CD8, BV711-CD4, BV785-CD44

2.2.1.5 BrdU injection

To analyze the proliferation of GC B cells, immunized mice were injected with 200 µl of a 10 mg/ml BrdU solution at day 13 after NP_{15}-CGG application.

2.2.1.6 BrdU intracellular staining

Red blood cell-free single cell suspensions of spleens and bones were prepared as described above and plated on 96 well plates (5 x 10^6 cells per well). Cells were washed twice witch 180 µl PBS, then resuspended in 50 µl of Zombie Aqua (diluted 1:400 in PBS) and incubated in the dark at 4 °C for 10 min. After addition of 150 µl MACS buffer and pelleting by centrifugation (800 x g, 2min, 4 °C), surface markers were stained as before. For intracellular staining of incorporated BrdU, the APC BrdU Flow Kit (BD) was used following the manufacturer's instructions. Briefly, after another washing step (MACS buffer), cells were resuspended in 100 µl Cytofix/Cytoperm buffer (BD) for 15 min at 20 °C in the dark. Pelleted cells were then washed in 150 µl Perm/Wash buffer (BD) (diluted 1:10 with H_2O). For the permeabilization, cells were resuspended in 100 µl Cytoperm

Permeabilization buffer Plus (BD) for 10 min at 4 °C in the dark. Following another washing step in 150 µl of diluted Perm/Wash buffer (BD), cells were incubated for 5 min with 100 µl Cytofix/Cytoperm buffer (BD) at 20 °C. After washing, DNA was digested by resuspension of cells in a DNase solution (300 µg/ml) for 1 h at 37 °C. Cells were again washed in 150 µl of diluted Perm/Wash buffer (BD) and finally incubated with the APC conjugated anti-BrdU antibody diluted 1:50 in 1 x BD Cytofix/Cytoperm buffer (BD) for 20 min at 20 °C in the dark. For FACS analysis cells were resuspended in propidium iodide-free FACS buffer.

Table 28: Staining cocktail surface markers before BrdU intracellular staining

cocktail	GC B cell staining before BrdU intracellular staining
1	PE-Fas, PerCPCy5.5-IgD, BV421-hCD2, BV605-CD19, BV785-B220

2.2.2 Work with DNA

To establish an in vitro screen of possible MAF interactors in B cells and overexpress MAF in mouse fibroblasts NIH3T3 as positive controls for Western blotting, the MSCV-Maf-IRES-GFP vector was used[178]. In that vector, based on the murine stem cell virus, Wiebke Winkler previously inserted the cDNA of *Maf* using the HpaI and EcoRI sites[178]. Thus, it is linked to the cDNA of GFP via an IRES site[178]. The empty (Mock) vector only containing GFP is termed MIG. Respective vectors were amplified by cloning and regularly controlled for correctness by restriction enzyme digestion and Sanger sequencing of the insert.

2.2.2.1 Retransformation

50 µL aliquots of chemically competent E. coli XL1-Blue cells were freshly thawed and incubated with 2 µl of the respective vectors on ice, followed by heat shock at 42 °C for 45 s followed incubation. Bacteria were then resuspended in 450 µl SOC medium and rotated for 2 h at 37 °C. A tenth of the bacteria were finally plated on ampicillin-comprising agar plates (100 µg/ml). Plates were incubated overnight at 37 °C.

2.2.2.2 Bacteria cultures

Selected colonies were picked and cultured in 4 ml (small scale), or 200 ml (large scale) LB medium supplemented with ampicillin (100 µg/ml) overnight.

2.2.2.3 Isolation of plasmid DNA

For small scale plasmid DNA isolation (mini prep) an inhouse protocol was applied. Overnight cultures were pelleted in microcentrifuge tubes (3 min, 1’000 x g). Pellets were resuspended in 300 µl of TENS buffer and mixed sharply prior to be chilled on ice for 10 min. After addition of 150 µl of 3.0 M Sodium Acetate (pH 5.2) tubes were mixed again and centrifuged at 17’000 x g for 6 min. Supernatants were transferred to new tubes prefilled with 900 µl EtOH at -20°C. After centrifugation (2 min, 17’000 x g) supernatants were discarded. Pellets were washed in 700 µl ice cold EtOH and finally dried. Dry DNA pellets were resuspended in 99 µl nuclease free water and 1 µl RNase A. Large scale plasmid DNA preparation (maxi prep) was performed using the NucleoBond Xtra Midi / Maxi Kit (Macherey-Nagel) according to the manufacturer’s protocol.

2.2.2.4 Restriction enzyme digestion

To roughly check the integrity of the vector before sequencing, plasmids were incubated by respective enzymes at 37 °C for 1 h according to the manufacturer’s recommendations.

2.2.2.5 Gel electrophoresis

10 x Cresol red was added to restriction enzyme digestion products before separation on 1-2 % agarose gels at 80-120 V for approximately 1 h. TBE was used as running buffer. Determination of fragment sizes was enabled by using 100 bp plus or the 1 kb DNA ladder as a reference scale. Gels initially stained with ethidium bromide (0.5 µg/ml).

2.2.2.6 DNA extraction

Gel slices containing digestion products from ethidium bromide-stained gels were cut with a scalpel under UV light. DNA from gel slices was extracted using ZymoClean Gel DNA Recovery Kit (Zymo Research) following the manufacturer’s protocol.

2.2.2.7 Sequencing of plasmids

Sanger sequencing was applied to sequence plasmid DNA (100-200 ng/ml) and PCR fragments (10-20 ng/m). Sequencing was performed by LGC Genomics company.

2.2.3 Cell culture

Human Multiple Myeloma cell lines were used to study the interactome of MAF *in vitro*. Selected AP1 factors where transduced to *Maf*-transgenic murine B cells in *in vitro* to investigate possible heterodimerization. Single candidate transcription factors were co-expressed together with *Maf* in murine B cells by retroviral transduction to read out expression of known MAF MM target genes.

2.2.3.1 Culture of human MM cell lines

Human Multiple Myeloma cell lines (HMCL) were cultured at 37 °C with 5 % CO_2 in RPMI-1640 medium containing 10 % FCS and antibiotics as described in the Material part. For ANBL6, 2 ng/ml human IL6 and additional 10 % FCS were added to the media.

2.2.3.2 Mouse B cell and fibroblast culture

2.2.3.2.1 Culture of mouse NIH3T3 cells

Mouse embryonic fibroblast NIH3T3 cells were cultured at 37 °C with 5 % CO_2 in DMEM supplemented with 10 % FCS and antibiotics as described in the Material part.

2.2.3.2.2 Isolation and culturing of mouse splenic B cells

To isolate B cells, murine spleens were prepared as before. Following the red blood cell lysis, cells were resuspended in 1920 µl BCM. 80 µl αCD43 loaded magnetic microbeads were added and incubated for 20 min on ice with constant shaking. Incubation was stopped by addition of 5 ml BCM and centrifugation at 300 x g (5 min, 4 °C). LS columns were prepared on a magnetic stand by preloading with 3 ml BCM which was discarded subsequently. The splenocytes resuspended in 2 ml BCM were negative selected for CD43 expression on the columns by collecting the flow through to a new 15 ml tube. After separation, columns were rinsed with 3 ml BCM which was also collected. B cells were spinned down (300 x g, 5 min, 4 °C), resuspended in 10 ml BCM, counted, and distributed in cell culture bottles in a density of 2 x 10^6 cells per ml. αCD40 (1 µg/ml) and IL4 (25 ng/ml) were added to activate B cells and initiate cre-expression.

2.2.3.2.3 Retroviral overexpression

Aiming to co-express different AP1 transcription factors with *Maf*, B cells from Cγ1-cre; R26MafstopF and control mice were retrovirally transduced with MSCV-IRES-GFP (MIG) constructs coding for presumed dimerization partners.

2.2.3.2.4 Production of retroviral supernatants

To produce reproductive viruses, the cDNA encoding MSCV constructs were transfected to PlatE fibroblasts together with packaging plasmids. Therefore, 3.5 x 10^6 PlatE cells were prepared on a 10 cm plate the day before transfection. After night, respective MSCV plasmids and packaging plasmids (10 µg pGagpol, 2 µg pEnv) were mixed with ddH2O to a volume of 450 µl. 50 µl of 2.5 M $CaCl_2$ was added. The solution was vortexed and incubated for 5 min at 20 °C. 15 ml tubes were prefilled with 500 µl 2 x HEBS. The DNA mixture was added dropwise to the buffer while constantly vortexing. After 20 min of incubation at room temperature, the mixture was added slowly to the PlatE cells whose medium was previously changed to 9 ml of PlatE medium supplemented with 25 µM chloroquine. The fibroblasts were kept for 6-8 h with the DNA. Afterwards, the medium was renewed to 10 ml of BCM. After 48 h the supernatant was collected, filtered through a 0.45 µm filter and stored at -80 °C. To verify successful transfection, the PlatE cells were analyzed by flow cytometry for reporter protein expression.

2.2.3.2.5 Transduction

To retrovirally transduce mouse B cells, 6 well plates were coated with RetroNectin (25 µg/ml in PBS) and incubated at 4 °C overnight. After removal of RetroNectin, plates were blocked with 2 % sterile filtered BSA (in PBS) for 1 h and washed once with PBS. Subsequently, 0.6 ml of the supernatant were coated on the wells and incubated for 1 h at 37 °C. 4 x 10^6 cultured murine B cells were added to each well in 1.5 ml new BCM containing 2 x polybrene (8 µg/ml) Additionally 1.5 ml of virus supernatant was added before 6 well plates were centrifuged at 32 °C on 800 x g for 1.5 h. The B cell medium was replaced 24 h later along with restimulation of B cells by αCD40 and IL4. For transduction of mouse NIH3T3 cells, 3 ml of viral supernatants were directly added to the coherent cells seeded in a density of 150’000 cells per well on a 6 well plate the day before. Following an analogous procedure, the median was changed 1 d after transduction and cells were harvested at d 2.

2.2.3.2.6 FACS of cultured murine B cells

At day 3 after transduction, double transgene-expressing B cells were sorted by gating for reporter protein expression BFP, GFP and/or hCD2, respectively. For BFP and GFP sorting, B cells were collected, centrifuged, and resuspended either directly in FACS Buffer to a density of 8 x 10^6 cells per ml. For hCD2 sorting, B cells were resuspended in the same concentration in TruStain fcX solution (BioLegend, diluted 1:100 in PBS) and incubated in the dark at 4 °C for 10 min. After addition of 5 ml MACS buffer, cells were again spinned down and resuspended in anti-hCD2 for 20 min. Cells where washed and resuspended in FACS buffer to be subjected to flow cytometry. Respective cells were directly sorted into 15 ml falcons containing 5 ml BCM, spinned down (300 x g; 4 °C; 5 min), resuspended in 1 ml PBS and transferred to 1.5 ml tubes. Cells were again centrifuged, the PBS removed, and the pellets frozen at -80 °C.

2.2.4 RNA analysis

2.2.4.1 RNA preparation

Total RNA from mouse B cells was isolated applying the RNeasy Micro Kit (Qiagen). The manufacturer's protocol was used. Optional DNAseI digestion was included into the procedure. Finally, RNA was eluted in 12-18 µl RNase-free H_2O.

2.2.4.2 cDNA synthesis

Whole RNA was translated to cDNA before PCR. Therefore, the mixture was prepared and heated for 10 min at 70 °C to enable annealing of the random primers. To gain –RT controls, 5 µL of the mixture were transferred to new 1.5 ml tubes before addition of the SuperScript II Reverse Transcriptase and frozen at -20 °C.

Table 29: Reverse transcription mixture

RNA (1 µg)	ad 13.3 µl
5 x First-strand buffer	5 µl
0.1 M DTT	2.5 µl
50 ng/ml random primers	2.5 µl
10 mM dNTPs	1.2 µl
RNasin Plus	0.5 µl

Table 30: Reverse transcription program

1	70 °C	10 min
2	Ice	10 s
3	room temperature	10 min
4	42 °C	50 min
5	95 °C	5 min

2.2.4.3 Semiquantitative RT-PCR

To test the specificity of used QPCR primers, semiquantitative conventional PCR was performed on gained cDNA. PCR products were separated on an agarose gel and isolated to be sequenced as described before. The Phusion High-Fidelity DNA polymerase was used. Respective primer sequences be found in the Material section.

Table 31: Semiquantitative RT-PCR mixture

5 x Phusion buffer	5 µl
10 mM dNTPs	1 µl
10 µM forward primer	1 µl
10 µM reverse primer	1 µl
25 ng cDNA	1 µl
Phusion High-Fidelity	0.5 µl
DMSO	1 µl
ddH_2O	14.5 µl

Table 32: Semiquantitative RT-PCR program

1	95 °C	3 s
2	95 °C	30 s
3	55-65 °C	30 s
4	72 °C	1 min
5	back to 2	35 cycles
6	72 °C	5 min
7	10 °C	keep

2.2.4.4 Quantitative PCR

For quantitative PCR after Reverse Transcription (RT), the Power SYBR Green PCR Master Mix (applied biosystems) was used. Samples were diluted 1:20 with H_2O. Primer sequences for detection of target genes can be found in the material section.

Table 33: qPCR mixture

Diluted cDNA	4.5 µl
2 x Power SYBR mix	5 µl
10 µM primer mix	0.5 µl

Table 34: qPCR program

1	95 °C	10 min
2	95 °C	15 s
3	60 °C	1 min

The reaction was performed on a magnetic induction cycler MIC (bms biosystems). For baseline estimation and amplification efficiency E calculation the in-built LingRegPCR algorithm was used[200,201]. Amplification cycles until significant signal over baseline are termed Cq. Measurements were performed in triplicates and median values were used for further calculation. Expression levels L of genes of interest x were compared among samples each calculated relative to the geometric mean expression of *Hprt*, *Tbp*, *Hmbs* and as published[202]:

$$L = \frac{{E_x}^{C_q(x,b)-C_q(x,a)}}{geoMEAN_{1-i}({E_{ref,1-i}}^{C_q(ref,1-i,b)-C_q(ref,1-i,1)})} \quad (1)$$

2.2.5 Protein analysis

The interaction of MAF with different transcription factors and nuclear proteins was analyzed by coimmunoprecipitation and subsequent mass spectrometry of MAF binders from HMCL lysates.

2.2.5.1 Cell lysis

Different lysis buffers were used to extract proteins from distinct cellular compartments and conserve protein interactions in specific conditions.

2.2.5.1.1 Whole cell lysis

For whole cell extracts approximately 1 x 10^6 freshly collected or frozen cells were gently resuspended in 40 µl lysis buffer and chilled on ice for 15 min. Compositions of the respective buffers can be found in the Material section. Lysis in modified RIPA buffer required resuspension through a 26 G syringe to completely resolve cells whereas lysis in CHAPS buffer needed shaking for 1 h at 4°C. Lysis was stopped by centrifuging insoluble debris at 4 °C at 17’000 x g for 10 min. Supernatants were transferred to clean tubes.

2.2.5.1.2 Nuclear cytoplasmatic fractioning

The method based on the protocol published by Schreiber and collegues[203]. Lysis of the cells in the hypotonic buffer A leads to disruption of the cytoplasmic membrane. The remaining nuclear parts of cells can then be dissolved in high salt containing buffer B to release chromatin associated proteins. Freshly collected cells were washed once in ice cold PBS, resuspended in 3 volumes of buffer A and vortexed frequently for 10 min while keeping the tubes on ice. Nuclear fractions were subsequently pelleted at 3'500 x g at 4°C. Additional washing steps in buffer A without NP40 increased purity of nuclear fractions. These were resuspended in buffer B and shaken at 4 °C for 30 min. After spinning down, insoluble elements supernatants contained nuclear fractions.

2.2.5.1.3 Dissecting cells to cytoplasm, perinuclear fraction, chromatin fraction and nuclear matrix

To achieve higher purity of chromatin associated proteins, a method was developed to sub dissect the nuclear fractions of HMCL cells based on published protocols[204–207]. Therefore, 1 x 10^6 freshly harvested cells were washed in ice cold PBS and resuspended in 1 ml ice cold CSK100 buffer adding NP40 to a final concentration of 0.2 %. Lysates rotated for 30 min at 4°C and were subsequently spinned at 4 °C, 1'000 x g for 5min. Supernatants were again centrifuged at 3500 x g to retain the cytoplasmatic fraction which was transferred to a new tube. The pellets were washed in CSK100 buffer containing 0.1 % and 0 % NP40 successively. Pellets were then resuspended in two volumes of PNF buffer with 0.5 % NP40 for 5 min at 4 °C. After pelleting at 1'000 x g the supernatants were referred to as perinuclear fraction whereas the core nuclear fraction was subjected to subdissection by resuspending in CSK50 buffer containing benzonase for 20 min on ice, terminated by adding ammonium sulfate to a final concentration of 0.25 M. After centrifuging at 1'000 x g supernatants were stored as chromatin associated protein fraction and pellets resuspended in CSK100 buffer as nuclear matrix fraction.

2.2.5.2 Protein crosslinking

To maintain protein complexes in cell lysis conditions, the crosslinking reagent glutaraldehyde was added to the HSL buffer in different concentrations. More detailed, 1 x 10^6 HMCL cells were freshly collected and washed as above to be lysed in 100 µl of HSL buffer. The expected protein content was used to estimate the required glutaraldehyde

concentration. Glutaraldehyde mainly reacts with lysine residues[208]. Therefore, the expected amount of lysine was calculated assuming lysine to make up 6 % of amino acids of the human proteome[209]. Different molar ratios of glutaraldehyde to lysine residues in the lysis buffer were tested which resulted in concentrations ranging from 0 to 0.4 %. After 5 min, crosslinking was quenched by the addition of Tris-HCl (pH 8) to a final concentration of 100 mM. Then, 0.2 µl Benzonase were added. Samples were chilled on ice for 10 more minutes to then continue the standard cell lysis procedure. The protocol was scaled up to factor 20 to perform IP of crosslinked protein.

2.2.5.3 Protein quantification

After cell lysis protein concentrations were measured using either Bradford assay or BCA dye. In the former case, Protein Assay Dye Reagent Concentrate (Bio-Rad) was diluted 1:5 with water. 2 µl of samples or standard BSA solution was incubated in 1 ml dye for 5 min at room temperature in cuvettes. After creation of a standard curve sample absorbance was determined at 595 nm using DU640 spectrophotometer (Beckman). In the latter case BCA solutions were mixed 1:50. Analogously, samples and standards were incubated at 37 °C for 30 min and measured at 562nm.

2.2.5.4 SDS Page

Proteins were either separated on self-prepared homogenous SDS polyacrylamide gels or on precast gradient gels. If not stated differently, for application of homogenous gels 30 µg of cell lysate were mixed with 4 x Laemmli buffer to a final volume of 20–60 µl and heated to 90 °C for 5 min before separation at 80-120 V for 90-120 min. To separate proteins more precisely NuPAGE 4-12 % Bis-Tris Protein Gels (ThermoFisher Scientific) were used following the manufacturer's protocol. Briefly, 10 µg of protein were incubated with LDS buffer containing reducing agent for 10 min at 70°C and gels were run in respective MOPS buffer containing antioxidant reagent.

2.2.5.5 Western blot

For semidry blotting of proteins from homogenous gels, nitrocellulose membranes and gels were moisturized in blotting buffer and subsequently transfer was performed at 20 V for 30 min. Proteins from gradient gels were transferred to nitrocellulose membranes in a tank

blot system (ThermoFisher Scientific) using the respective transfer buffer containing antioxidant following the manufacturer's protocol. After transfer, membranes were stained in Ponceau red to validate successful blotting and finally blocked in TBS-T containing 10 % milk powder for 1 h at RT or overnight at 4 °C while shaking gently. Primary antibodies were diluted in 1 % TBS-T milk in respective concentrations and incubated the membranes overnight at 4 °C. Afterwards, membranes were washed three times in 1 % TBS-T milk and species-specific secondary antibodies (0.1 µg/ml) were added for 1-2 h at RT. Membranes were again washed three times and incubated with a 1:1 mixture of Pierce ECL Western Blotting Substrate (ThermoFisher Scientific). Exposure to CL-Xposure film for 1-30 min and developing applying the CURIX 60 X-ray film processor (AGFA) followed.

2.2.5.6 Immunoprecipitation

HMCL cells were freshly collected and washed once in ice cold PBS (pH 7.4). 1 x 10^7 cells were lysed in 400 µl of either HSL or modified RIPA buffer, referred to as HSL and RIPA-samples respectively, as described above. Experiments were performed thrice to receive each three biological replicates. After centrifugation, supernatants were diluted to temper concentrations of detergents and salt to retain protein interactions. HSL samples were diluted 3:7 in HSL without NP40 and NaCl to a final concentration of 150 mM NaCl and 0.08 % NP40. RIPA samples were diluted in RIPA buffer without detergents 1:3. Concentrations of protein was measured using Bradford assay for HSL samples and BCA assay for RIPA samples. Protein concentration was set to 1 µg/µl and 450 µl of protein lysate was incubated with αMAF antibody (Abcam, BLR045F) or rabbit isotype control antibody 2 h rotating at 4 °C. Protein A magnetic beads of a storage volume of 45 µl were washed according to the manufacturer's protocol and resuspended in 200 µl PBS containing 0.02 % Tween20. Beads were added to the protein tubes and rotation was continued for 1 h. The bead-antibody-protein complexes were isolated with the help of a Dynal MPC-S magnet and washed twice in diluted lysis buffer and thrice in ice cold PBS (pH 7.4). After resuspension in 300 µl PBS precipitates were transferred to clean tubes. 10 % of the samples were used to ensure successful immunoprecipitation on western blot. Therefore, the beads were resuspended in 15 µl NuPAGE LDS loading buffer (ThermoFisher Scientific) and heated at 70 °C for 10 min to elute proteins from the beads on the magnet. IP input samples were processed analogously. Retained samples were analyzed on a gradient gel western blot. MAF protein was detected using guinea pig αMAF antibody (Carmen Birchmeier lab).

Remaining 90 % of samples were dried on the magnet and frozen at -80 °C to be subjected to mass spectrometry.

2.2.5.7 Mass spectrometry

Analyses of cell line specific MAF interactomes by mass spectrometry and subsequent data analysis was performed by Marieluise Kirchner from the MDC Proteomics Core Facility (Philipp Mertins) applying previously described in-house optimized procedures[210,211].

2.2.5.7.1 Protein digestion

To prepare the bead-antibody-protein complexes from pulldown experiments for mass spectrometry, they were first resuspended in 20 µl urea buffer and subsequently kept at RT for 0.5 h in a 12 mM dithiothreitol solution. The samples were afterwards alkylated with 40 mM chloroacetamide for 20 min at RT. Thereafter, 0.5 µg endopeptidase LysC was used to digest the proteins for 4 h. The following trypsin digestion was performed overnight. Therefore, 80 µl of 50 mM ammonium bicarbonate (pH 8.5) and 1 µg trypsin was added to the samples. The next morning, 10 % trifluoroacetic acid solution was added to adjust the pH below 2.5 to quench the digestion. StageTips were used to extract the peptides following a published protocol[212].

2.2.5.7.2 LC-MS/MS analyses

LC-MS/MS analyses were performed as described before with few modifications[211]. Firstly, digested peptides were eluted from StageTips in 60 µl Buffer B and remaining organic solvent was disposed by high-speed evaporation. Subsequently, dried probes were solved in Buffer A and subjected to reversed-phase column separation. Therefore, 20 cm fritless silica microcolumns with a 75 µm inner diameter were used, packed with “ReproSil-Pur C18-AQ 1.9 µm resin” on a High-Performance Liquid Chromatography system, as previously described[211]. To achieve thorough separation, a 90 min gradient of Buffer B concentration (2 % to 60 %) was applied, and the flow rate was set to 250 nl/min. Afterwards, digested peptides were ionized by electrospray ionization, and the peptides were subsequently analyzed on a “Thermo Q Exactive Plus instrument”. The data dependent mode was chosen on the mass spectrometer with a full scan in the Orbitrap (70 K resolution; 3 x 10^6 ion count target; maximum injection time 50 ms). Eventually, higher-energy collision dissociation (17.5 K resolution, 1 x 10^5 ion count target; 1.6 m/z isolation window; maximum injection

time: 250 ms) was used to perform top 10 MS/MS scans. Therefore, precursors with a charge state of 2–7 were subjected to MS/MS, solely. The dynamic exclusion duration was prescribed to 30 s. A maximum of 10 ppm was tolerated around the selected precursor and its isotopes.

2.2.5.7.3 Data analyses

For mass spectrometry data analysis, established in-house protocols were followed[210]. Raw data were analyzed using the “MaxQuant software package”. Firstly, measured spectra were aligned to a publicly available peptide database. In detail, MS/MS spectra were searched against the forward and reverse sequence-containing decoy UniProt database (HUMAN.2019-07) with the help of the in-built Andromeda search engine. The search conditions were determined as previously well-tried[210]: seven amino acids were chosen as the required minimal peptide length and a maximum of 3 missed cleavages was tolerated. Furthermore, the search conditions comprised deamidation of peptides, different modifications of methionine oxidation and N-terminal acetylation as variable modifications, as well as the fixed modification of carbamidomethyl cysteine. A false discovery rate of 1 % was accepted. Finally, sharp, and unique peptides were included to the quantification. The internal nonlinear time-rescaling algorithm was applied to recalibrate retention times. The option of “Match between runs” was chosen, and the maximal retention time window was determined to 0.7 min. The internal label-free quantification algorithm was used to normalize protein intensities. Possible contaminants, reverse database matches, and proteins only identified by site were excluded prior to statistical data analyses.

2.2.5.7.4 Statistical analysis

The statistical data analysis was done with the “Perseus software” (v1.6.2.1). As the immunoprecipitation experiments were performed in biological triplicates, the three replicates per human MM cell line and lysis condition were grouped. Among the groups intensity values were filtered for “minimum value of 3” in at least one group. If values were missing, they were filled with imputed values in the software based on random noise simulation of the detection limit of the mass spectrometer. In detail, the imputed values for the simulation were chosen from a log normal distribution with 0.3 x the standard deviation of the detected and log2 transformed values, after downshifting by 1.8 standard deviations. Finally, differences in protein abundance between the αMAF antibody and IgG control samples were calculated using Student´s t test, corrected by Benjamini Hochberg (BH)

procedure for multiple testing. Proteins enriched in the αMAF antibody group and passing the significance cut-off (BH 5 %) were considered MAF-associated proteins. Result files were imported to R studio. Plots and diagrams of the data were created using the ggplot2 (Tidyverse) and UpSetR package.

3. Results

3.1 Impact of *Maf* expression on the GC reaction and terminal B cell development *in vivo*

3.1.1 Previous work from our group: Characterization of the B cell response in Cγ1-cre; R26 MafstopF mice

Overexpression of MAF is expected to transform human GC B cells towards MM[96]. Unexpectedly, as shown in recent work from Wiebke Winkler in our laboratory, conditional *Maf* overexpression in activated mouse B cells upon immunization of Cγ1-cre; R26 MafstopF mice led to a massive reduction of *Maf*-expressing GC B cells[178]. Splenic *Maf*-expressing PB/PCs were furthermore reduced in number, whereas antigen-specific IgM-secreting PCs temporary accumulated in the BM[178]. Given these findings, following experiments described here aimed to better characterize the altered terminal differentiation of *Maf*-expressing B cells and to test possible hypotheses to explain the unexpected observations.

3.1.2 Effect of *Maf* expression on the proliferative potential of GC B cells

To investigate if *Maf* overexpression interferes with proliferation of GC B cells in Cγ1-cre; R26 MafstopF mice, the proliferative capacity of *Maf*-transgenic GC B cells was compared to control GC B cells *in vivo*. GC B cells of immunized Cγ1-cre; R26 hCD2stopF mice served as control. These cells express a signaling deficient truncated version of the human CD2 surface maker assessable by flow cytometry which does not interfere with cellular processes, therefore reflecting normal B cell biology[187].

To assess the proliferation of Maf-transgenic GC B cells, Cγ1-cre; R26 MafstopF were immunized by intraperitoneal injection of NP coupled to chicken gamma globulin (NP_{15}-CGG) and subsequently pulse labeled with 5-Bromo-2′-deoxyuridine (BrdU) at day 13 after immunization (post immunization, p.i.). BrdU is a thymidine analogue and is incorporated during DNA replication in dividing cells. Due to its short half-life of 8-11 min[213], only cells that are actively dividing at the time of injection are labeled. Importantly, 65 % of the labeling is lost during the next division and 92 % during the following one[32]. Thus, the analysis at 15 hours after the BrdU application, allowed to measure the proportion of dividing cells at day

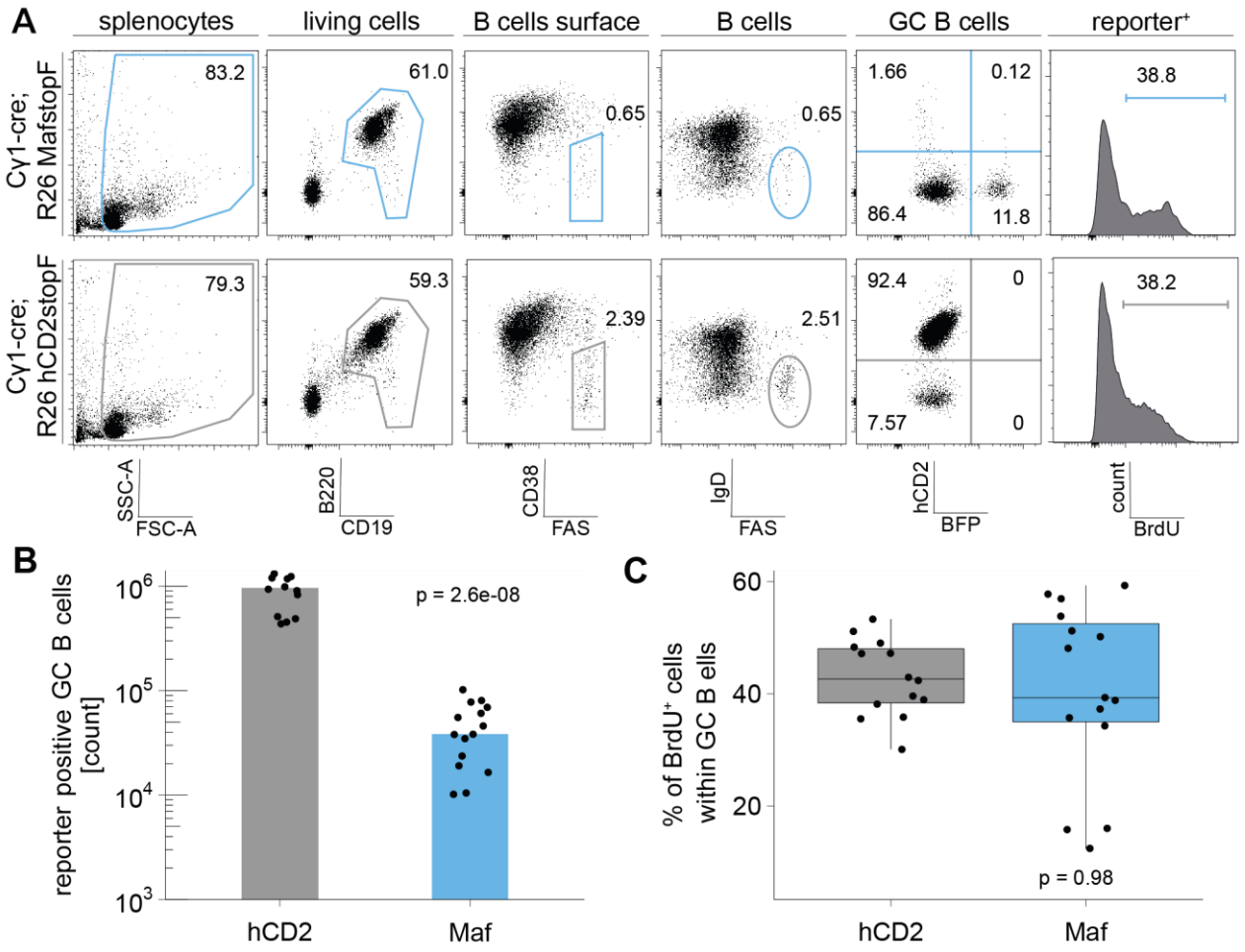

Figure 2: Effect of Maf expression on proliferation of GC B cells in vivo. Cγ1-cre; R26 MafstopF (Maf) and Cγ1-cre; R26 hCD2stopF (hCD2) control mice were immunized once with NP_{15}-CGG (100 µg/200 µl; in alum) and pulse labeled with BrdU (2 mg/200 µl) on day 13 after immunization. GC formation and BrdU incorporation were assessed by staining in two respective antibody-cocktails and subsequent flow cytometry on day 14 p.i. A) Gating strategy illustrated by representative dot plots for a Maf (upper panel) and a hCD2 control mouse (lower panel). Living splenocytes (based on FSC and SSC expression) were further gated for $CD19^+$ B cells, and subsequently for GC B cells, which were distinguished as $FAS^{hi}IgD^-$ or $FAS^{hi}CD38^{lo}$ cells in the two respective staining cocktails. Of these, transgene-expressing cells were identified based on BFP (Maf) or hCD2 (control) expression. Finally, dividing GC B cells were determined by BrdU incorporation. B) Absolute numbers of reporter positive $CD19^+FAS^{hi}CD38^{lo}$ splenic GC B cells, calculated from FACS results. C) Frequency of BrdU positive cells within $CD19^+FAS^{hi}IgD^-$ GC B cells. n=14 for hCD2 mice, n=15 for Maf mice, Wilcoxon test**.**

13 p.i. within BFP reporter expressing cells. Technically, mice were sacrificed, and splenocytes were immunologically stained for either surface markers only or, additionally for intracellular BrdU resulting in two samples per mouse. Finally, splenic B cell populations were analyzed by flow cytometry (Fig. 2A). Among $CD19^+$ B cells, a distinct population of $FAS^{hi}CD38^{lo}$ GC B cells could be found that averaged 2.2 % of control B cells and 0.6 % of *Maf*-expressing B cells (Fig. 2A, column 3). Gating for $FAS^{hi}IgD^-$ can similarly distinguish

GC B cells[214] and was used in the intracellular staining procedure to detect BrdU (Fig. 2A, column 4). As expected, a high proportion, averaging 91.9 % of GC B cells expressed the transgenic reporter protein as judged by hCD2 staining[181,187]. In contrast to this and in agreement with previous work[178], reporter positive *Maf*-expressing GC B cells were diminished to a median proportion of 12.0 % (Fig. 2A, column 5). Calculation of absolute numbers of reporter positive GC B cells provided evidence of a greatly reduced GC reaction in the spleen with approximately 25-fold smaller numbers of *Maf*-expressing GC B cells (Fig. 2B). However, the percentage of BrdU positive cells among $FAS^{hi}IgD^{-}$ GC B cells was not significantly different between *Maf*-expressing and control GC B cells (Fig. 2A, column 6 and Fig. 2C), indicating no restrained proliferation of *Maf*-expressing GC B cells. Of note, the fraction of BrdU-labelled (i.e., dividing) GC B cells showed a wide range between approx. 30-50 %, which is known from *in vivo* BrdU labeling studies[32], but the scattering was particularly pronounced in the Maf group (range between approx. 10-60 %). Taken together, *Maf* overexpression in activated B cells markedly reduced the GC B cell compartment, but this is not caused by an impaired proliferation of the transgenic GC B cells.

3.1.3 Temporally controlled conditional *Maf* expression in B cells

In fact, by using the Cγ1-cre; R26 MafstopF mouse, it was not possible to generate a suitable model for the human $t(14;16)^{+}$ MM. However, the observations made in the same mouse model suggest that different B cell and PB/PC populations react differently to *Maf* overexpression[178]. Therefore, aiming to investigate the effect of *Maf* expression on selected differentiation stages of B cells in more detail and eventually to generate a better MM model, a pilot experiment was set up in the following.

In this experiment, *Maf* was to be expressed at different timepoints after immunization, thereby targeting individual B cell differentiation stages. This was made possible by using a recently developed derivative of the Cγ1-cre allele[190]. In this Cγ1-creERT2 mouse, cre is linked to a mutated version of the estrogen receptor ligand-binding domain that prevents nuclear entry and consequently recombination and transgene expression in the absence of its ligand tamoxifen[190]. Therefore, the timed administration of tamoxifen to the immunized mice allows for external control of transgene expression.

Indeed, previous work has shown that tamoxifen administration on days 4, 5 and 6 p.i. is particularly conducive to express a transgenic eYFP reporter in extrafollicular PBs[190]. Tamoxifen application on day 10 p.i. is furthermore applicable to target somatically hypermutated GC B cells[190]. In contrast, late tamoxifen application on days 29, 30 and 31 achieves expression mainly in B cells of a non-GC phenotype (e.g., memory B cells, among others)[32,190].

Based on these observations, we first aimed to test whether *Maf* can also be specifically overexpressed in these three populations. The second objective was to determine whether a particular population benefits from *Maf* expression, i.e., substantially increases in size over time. Therefore, Cγ1-creERT2; R26 MafstopF mice were immunized with NP_{15}-CGG and given tamoxifen on three consecutive days via oral gavage at an early timepoint (d. 3-5 p.i.), a mid-timepoint (d. 10-12 p.i.) and a late timepoint (d. 30-33 p.i.). Spleens from treated mice were isolated 2 days or 9 days after the last tamoxifen gavage, respectively, and splenic single cell suspensions were stained either for GC B cell markers CD38 and FAS or PC markers CD138, TACI, MHC-II and CD93 and analyzed by flow cytometry (Fig. 3A). Splenic cells where additionally stained for IgG1 surface expression and the NP analogue NIP. To determine the cell populations activating *Maf* expression at the indicated time points, total living single splenocytes were first gated on BFP reporter (i.e., MAF) expression before analyzing the surface expression of B and PC markers (Fig. 3A, column 1).

The experimental design described above, including chosen timepoints of tamoxifen application and the analysis strategy, was based on previously published experiments on Cγ1-creERT2; R26 eYFP mice from our institute[190]. Furthermore, similar antibodies and chemicals as well as the same animal facility was used. We therefore considered it reasonable to compare the data from Cγ1-creERT2; R26 MafstopF mice with the previously published data on Cγ1-creERT2; R26 eYFP mice[190] and to omit new, internal control animals. Besides, we expected to detect a proliferation advantage even with low sample numbers of 2 mice per time point; firstly, based on the internal comparison between the two time points of tamoxifen application and secondly, based on comparison to the published data mentioned above.

Two days after each of the tested time points of tamoxifen administration, approx. 0.1 % of total splenocytes were found to express BFP (i.e., MAF) (shown for the PC staining of one representative mouse each in Fig. 3A, column 1). Of those, $CD19^+B220^+$ B cell populations

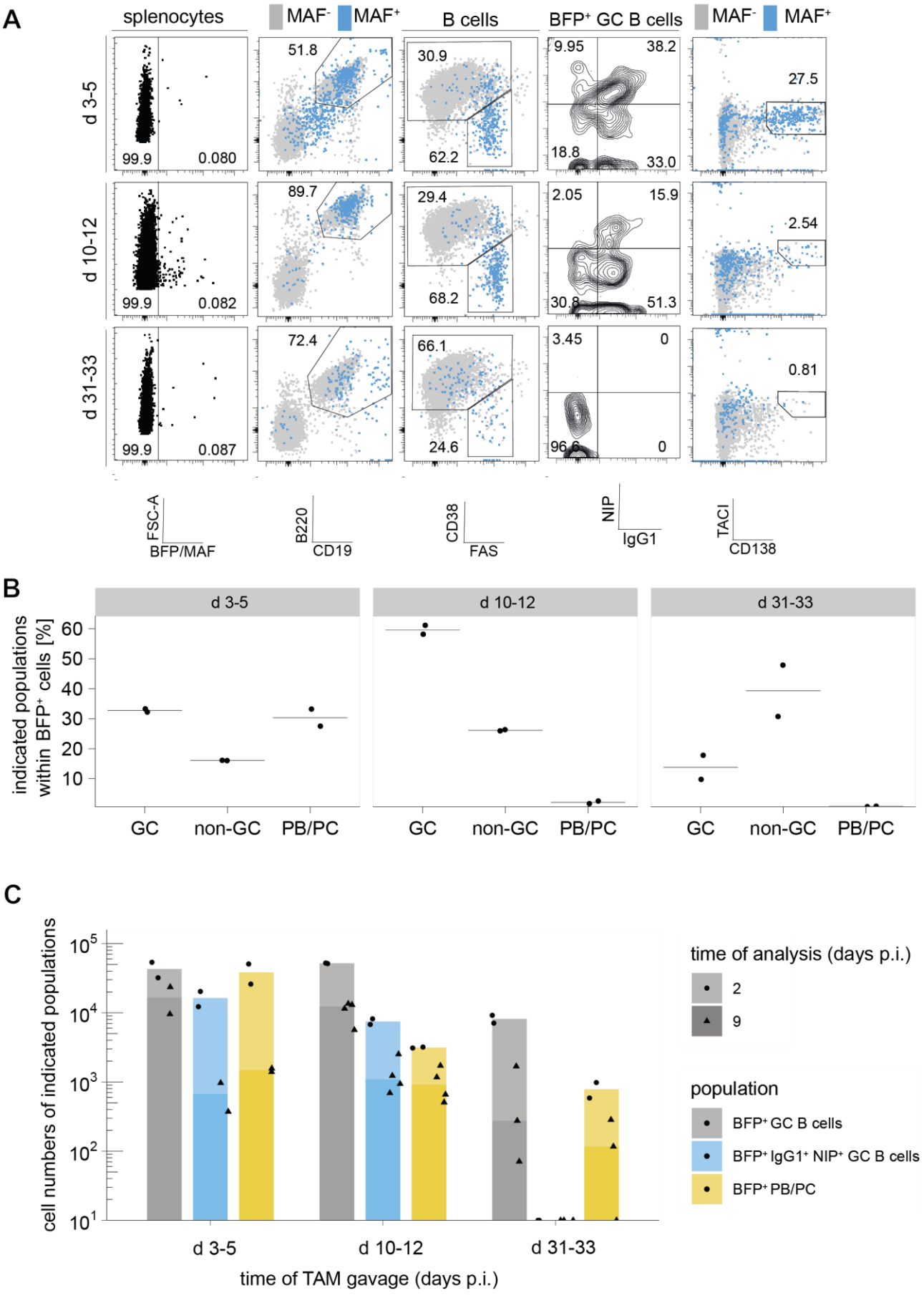
A
splenocytes
MAF- MAF+
B cells
BFP+ GC B cells
MAF- MAF+
d 3-5
d 10-12
d 31-33
99.9
0.080
51.8
30.9
62.2
9.95
38.2
18.8
33.0
27.5
99.9
0.082
89.7
29.4
68.2
2.05
15.9
30.8
51.3
2.54
99.9
0.087
72.4
66.1
24.6
3.45
0
96.6
0
0.81
FSC-A
BFP/MAF
B220
CD19
CD38
FAS
NIP
IgG1
TACI
CD138
B
indicated populations within BFP+ cells [%]
d 3-5
d 10-12
d 31-33
GC
non-GC
PB/PC
C
cell numbers of indicated populations
time of TAM gavage (days p.i.)
time of analysis (days p.i.)
2
9
population
BFP+ GC B cells
BFP+ IgG1+ NIP+ GC B cells
BFP+ PB/PC

Figure 3 (p.59): Targeting specificity of temporally controlled conditional *Maf* expression in B cells. Cγ1-creERT2; R26 MafstopF mice were immunized once with NP_{15}-CGG (100 µg/200 µl; in alum) and treated with tamoxifen (TAM) gavage (4 mg/100 µl) at one of three different time points after immunization (d 3-5, d 10-12, or d 31-33 p.i.) for three consecutive days, respectively. Following, 2 or 9 days after the last gavage, mice were sacrificed, and spleens isolated. Splenocytes were stained using two different antibody cocktails and analyzed by flow cytometry. **A)** Two days after the last tamoxifen gavage, total splenocytes were assessed for BFP reporter expression (i.e., MAF expression) (column 1). Overlay plots illustrate the immunophenotype of MAF^+ versus MAF^- splenocytes. Within BFP^+ cells, splenic B cells ($CD19^+B220^+$), GC ($FAS^{hi}CD38^{lo}$) and non-GC ($CD38^{hi}FAS^{lo}$) B cell as well as PB/PC ($CD138^+TACI^+$) were analyzed. GC B cells were further assessed for class-switching to IgG1 and antigen-specificity (NIP). Dot plots of each one mouse per time point (n = 2 analyzed). **B)** Relative quantification of indicated cell types within BFP^+ cells from mice analyzed at day 2 after TAM gavage respectively. **C)** Absolute quantification of indicated populations each two days after last tamoxifen gavage (light colored, transparent bars and dots) and 9 days after last tamoxifen gavage (dark colored, non-transparent bars and triangles).

could be delineated, which accounted for approx. 52 % at the early timepoint of transgene expression (Fig. 3A, row 1, column 2). The vast majority of these BFP^+ (i.e., MAF-expressing) $CD19^+B220^+$ B cells showed a GC B cell phenotype, defined by high FAS and low CD38 expression, accounting for approx. 33 % of all BFP^+ splenocytes, compared to the reported numbers of ~20 % in similarly treated Cγ1-creERT2; R26 eYFPstopF mice[190] (Fig. 3A, row 1, column 3 and Fig. 3B). Interestingly, approx. 38 % of these were antigen-specific and IgG1-class switched already at that timepoint (Fig. 3, row 1, column 4). Furthermore, a pronounced $CD138^+TACI^+$ PB/PC population could be detected among BFP-expressing splenocytes that making up approx. 30 % (Fig. 3A, row 1, column 5 and Fig. 3B, left panel). These early PB/PCs accounted for the majority of BFP^+ cells at the early time point. Importantly, a gating strategy based on CD138 and TACI expression might underestimate these numbers, as they were reported to account for up to ~80 % of transgene-expressing cells at this early time point when gating for $CD138^+B220^-$ cells[190]. Following tamoxifen administration at days 10-12 p.i., $CD19^+B220^+FAS^{hi}CD38^{lo}$ GC B cells constituted the largest fraction of targeted (i.e., MAF-expressing) cells accounting for approx. 60 % of BFP^+ spleen cells, of which again a substantial fraction was class-switched to IgG1 (Fig. 3A, row 2, Fig. 3B, middle panel). $CD138^+TACI^+$ PB/PC only made up 2 % (Fig. 3A, row 2 and Fig. 3B). Upon late transgene activation (d 31-33 p.i.), the largest population of BFP reporter (i.e., MAF) positive splenocytes showed a non-GC ($FAS^{lo}CD38^{hi}$) B cell phenotype in line with observations from the Cγ1-creERT2; R26 eYFPstopF reporter mouse model[190]. This non-GC B cell population made up approx. 40 % of *Maf*-expressing cells (Fig. 3A, row 3, column 3 and Fig. 3B, right panel), compared to 50 – 85 % observed in Cγ1-

creERT2; R26 eYFPstopF mice. Of note, only approx. 0.8 % of BFP reporter (i.e., MAF) positive splenocytes constituted $CD138^+TACI^+$ PB/PCs at this late time point (d 31-33 p.i.), whereas *Maf*-expressing antigen-specific GC B cells could not be detected (Fig. 3A, row 5 and Fig. 3B).

Thus, time-controlled transgene activation with the Cγ1-creERT2 allele allows for the differential targeting of *Maf* expression to distinct B cell populations. Early transgene activation (d 3-5 p.i.) mostly targets immature (likely extrafollicular) PB/PCs, mid-time activation (d 10-12 p.i.) targets mostly GC B cells and late transgene activation (d 31-33 p.i.) mainly occurs in non-GC B cells (relative to total BFP^+ spleen cells).

To assess whether one of these populations gained a proliferative advantage from *Maf* expression, absolute numbers of BFP^+ (MAF^+) cells were calculated from flow cytometry results 2 and 9 days after the final tamoxifen application, respectively (Fig. 3C). Of note, after a further week of observation, none of the targeted populations markedly increased in number, but rather a reduction of all population sizes was seen. Thus, no apparent growth advantage for selective B cell populations could be found in Cγ1-creERT2; R26 MafstopF mice treated with tamoxifen at different time points.

3.1.4 Developmental fate of *Maf*-expressing GC B cells

Given the finding that the intermediate time point of tamoxifen administration (i.e., day 10-12 p.i.) of Cγ1-creERT2; MafstopF mice resulted in transgene activation predominantly in IgG1 class-switched GC B cells, the believed COO of human MM, further experiments sought to track the fate of differentiating B cells following Maf expression at this timepoint. Therefore, Cγ1-creERT2; R26 MafstopF and Cγ1-cre; R26 hCD2stopF reporter control mice were immunized once with NP_{15}-CGG and treated with tamoxifen at days 10, 11 and 12 p.i., followed by the subsequent analysis at four consecutive time points (d 14, 21, 28 and 35 p.i.). Two mice per genotype and timepoint were analyzed. First, the impact of *Maf* overexpression on the general and antigen-specific GC reaction was evaluated over 5 weeks by flow cytometry (Fig. 4). To do this, splenocytes from Cγ1-creERT2; R26 MafstopF and Cγ1-cre; R26 hCD2stopF control mice were gated for $CD19^+FAS^{hi}CD38^{lo}$ GC B cells and subsequently analyzed for expression of the hCD2 or BFP (i.e., MAF) reporter (shown for a Maf and control mouse at d 14 p.i. in Fig. 4A, left). Based on these, absolute numbers of reporter-expressing GC B cells were calculated. At day 14 after immunization (i.e., d 2

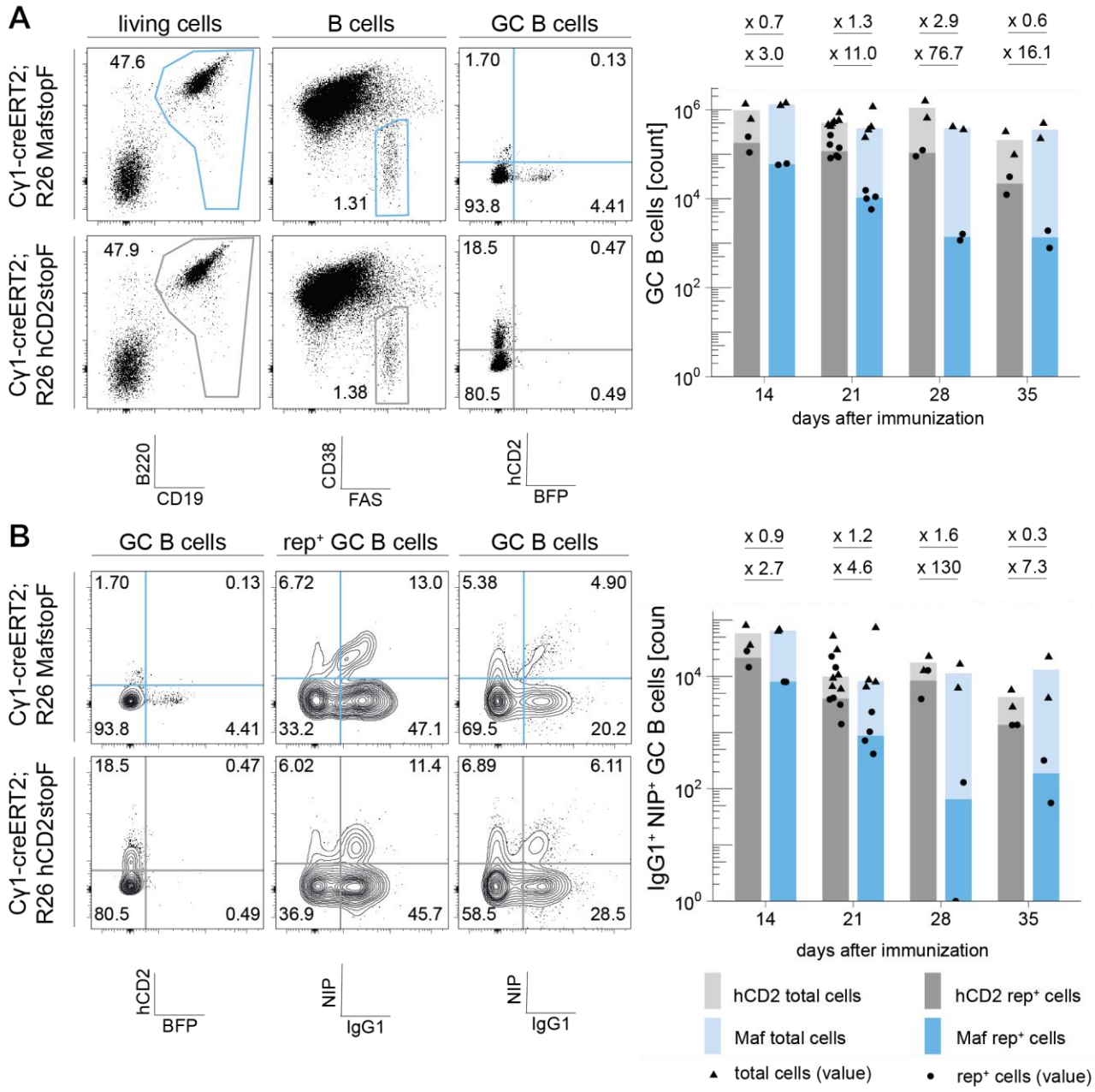

Figure 4: Effect of temporally controlled *Maf* expression in peak GC B cells on total and NP specific GC reaction. Cγ1-creERT2; R26 MafstopF and Cγ1-creERT2; R26 hCD2stopF control mice were immunized and treated with tamoxifen on days 10, 11 and 12 after immunization, followed by analysis at 4 consecutive time points (d 14, 21, 28, 35). The total and antigen specific GC B cell compartment were assessed by flow cytometry based on high FAS and low CD38 surface expression (GC B cells) as well as detection of reporter proteins BFP and hCD2. **A)** Representative dot plots showing splenic CD19⁺ B cells, the GC B cell population and respective reporter expression for a Maf (upper panel) and control mouse (lower panel), each analyzed at d 14 p.i. (left). Absolute numbers of total (light color) and transgene-expressing (dark color) GC B cells were calculated from assessed percentages and are depicted as bar charts (right). **B)** Contour plots showing splenic CD19⁺FAS^{hi}CD38^{lo} GC B cells and the surface expression of IgG1 as well as NIP binding for the same mice as in (A) (left). Absolute numbers of total (light color) and transgene-expressing (dark color) IgG1⁺NIP⁺ GC B cells were calculated from assessed percentages and are depicted as bar charts (right).

after tamoxifen treatment) an approximate number of 1 x 106 total GC B cells was found in the spleens of hCD2 control mice that accounted for 1 % of total $CD19^+$ B cells (Fig. 4A, light grey columns). Of those, approx. 18 % expressed the control reporter gene hCD2 constituting approx. 178'000 cells (Fig. 4B, dark grey columns). The total GC B cell population of Cγ1-creERT2; R26 hCD2stopF mice remained stable at a size of approx. 1 x 10^6 cells until day 28 and then waned to an average number of approx. 0.2 x 10^6 at day 35. The compartment of hCD2 reporter-expressing GC B cells declined more rapidly as its share decreased from the original 18 % (d 14 p.i.) to 11 % (d 35 p.i.) of total GC B cells (Fig. 4A, grey columns). Interestingly, total GC B cells of Cγ1-creERT2; R26 MafstopF mice were similar in number to the hCD2 control CG B cell, although the proportion of $reporter^+$ GC B cells was generally lower. However, at day 14 after immunization, MAF-expressing (BFP^+) cells were reduced by factor 3 in comparison to control mice (whereas it was reduced by factor 25 in Cγ1-cre; R26 MafstopF mice, Fig. 2), indicating that delayed transgene expression with a Cγ1-creERT2 allele can partly rescue the counter-selection of *Maf*-expressing cells. Finally, *Maf*-expressing GC B cells disappeared more rapidly than control cells over time (Fig. 4A, dark blue columns). To gain more insight into the antigen-specific response, GC B cells were further analyzed for NIP binding and IgG1 surface expression (Fig. 4B). Approx. 5 % of the total GC B cells and 13 % of MAF-expressing (BFP^+) GC B cells successfully switched to IgG1 specific for the NP analogue NIP at the first timepoint of assessment (day 14 p.i.) – both fractions being in the range of respective control reporter-expressing cells (6 and 12 %, respectively). However, MAF-expressing $IgG1^+NIP^+$ GC B cells disappeared more rapidly than control cells, suggestive of ongoing counter-selection in Cγ1-creERT2; R26 MafstopF animals.

In summary, the transgenic GC B cell compartment upon delayed *Maf* overexpression in Cγ1-creERT2; R26 MafstopF mice was reduced in size, but less so than in Cγ1-cre; R26 MafstopF mice in which Maf is early activated during the GC response. *Maf*-expressing GC B cells rapidly diminished, but a fraction of the remaining transgene-expressing cells is still antigen-specific and IgG1 class-switched.

3.1.5 Developmental fate of *Maf*-expressing plasma cells

In addition, splenic and BMPC populations were analyzed in the same time course experiment described above, which included NP_{15}-CGG immunization and subsequent

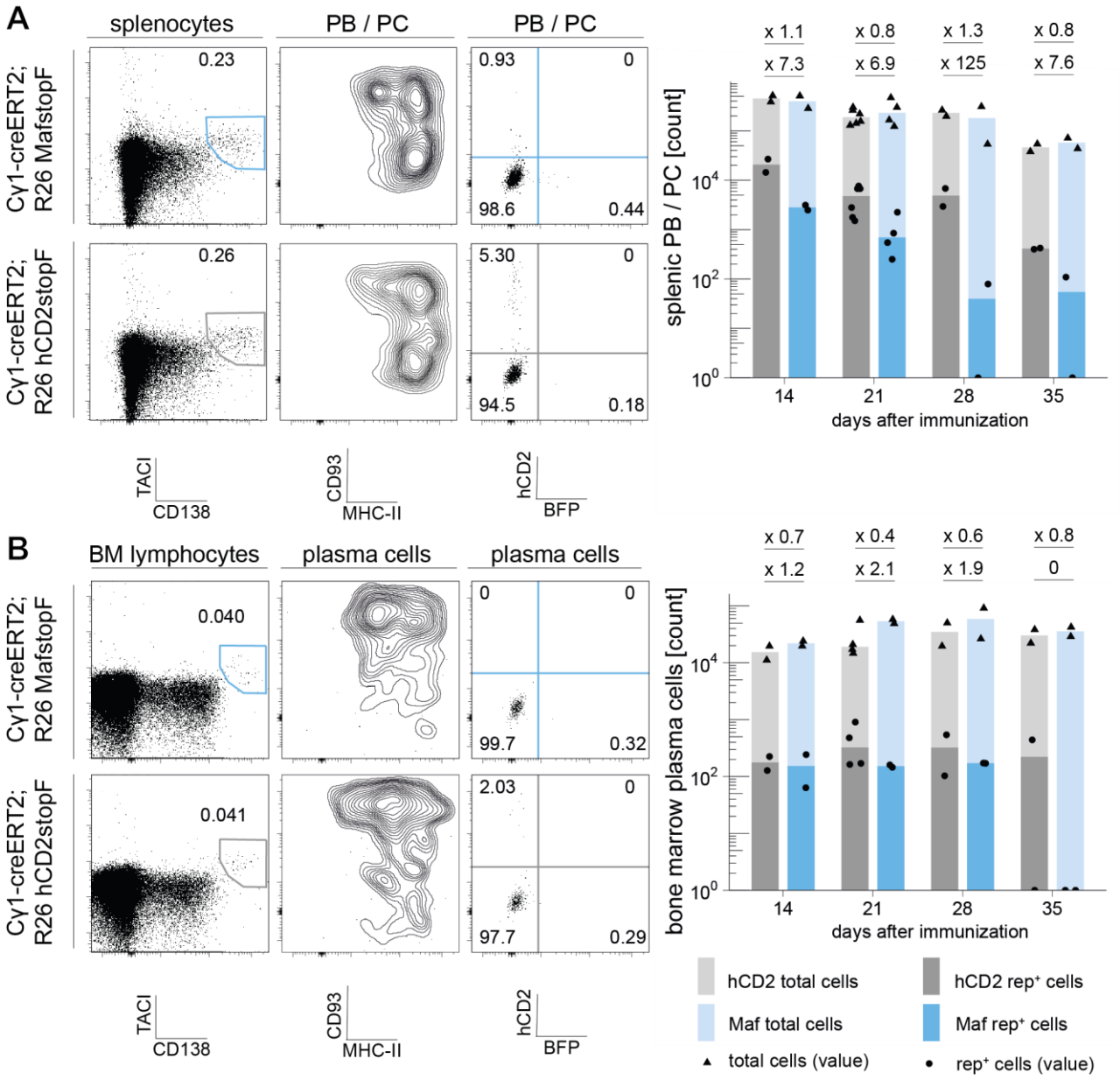

Figure 5: Effect of temporally controlled *Maf* expression in peak GC B cells on the plasma cell response. Cγ1-creERT2; R26 MafstopF mice were immunized, and tamoxifen administered on days 10, 11 and 12 as described before followed by analysis at 4 consecutive time points (d 14, 21, 28, 35). The splenic and bone marrow PC compartment were assessed by flow cytometry based on high CD138 and TACI surface expression as well as detection of reporter proteins BFP and hCD2. **A)** Representative dot plots showing splenic CD138^{+}TACI^{+} PB/PC, expression of MHC-II and CD93 within that population and respective reporter expression for a Maf (upper panel) and control mouse (lower panel), each analyzed at d 14 p.i. (left). Absolute numbers of total (light color) and transgene-expressing (dark color) PB/PC were calculated from assessed percentages and are depicted as bar charts (right). **B)** The same analysis as (A) for bone marrow PC (left). Absolute numbers of total (light color) and transgene-expressing (dark color) bone marrow PCs were calculated from assessed percentages and are depicted as bar charts (right).

administration at the peak of the GC response (i.e., d 10-12 p.i.) of Cγ1-creERT2; R26 MafstopF and R26 hCD2stopF control mice, followed by the analysis at consecutive time points (d 14, 21, 28, 35 p.i.). As before, PCs were identified by CD138 and TACI surface expression using flow cytometry. They accounted for appr. 0.2 % of splenocytes in control and *Maf*-expressing mice until day 28 p.i. (shown for a Maf and control mouse at d 14 p.i. in Fig. 5A, left). Subsequent analysis of maturity markers CD93 and MHC-II showed that both early and more mature PB could be found (Fig. 5A, left). Calculation of absolute cell numbers revealed that the total splenic PB/PC compartment was very similar between Cγ1-creERT2; R26 MafstopF and control mice at all timepoints analyzed (Fig. 5A right, light colored columns). However, the compartment of transgene-expressing (reporter$^+$) splenic PC was substantially smaller in *Maf*-expressing mice and disappeared faster during the experiment than in control animals (Fig. 5A right, dark colored columns). MAF-expressing splenic PCs could only be detected in one out of two mice at day 28 and 35 p.i., respectively, whereas hCD2-expressing PCs could still be found in both control mice at these time points.

Interestingly, a different kinetic was revealed when analyzing BMPCs, which generally exhibit a more mature phenotype as shown by downregulation of MHC-II and upregulation of CD93 (Fig. 5B left). The total BMPC compartment was comparable between *Maf* and hCD2-transgenic mice (Fig. 5B, graph, light-colored columns). Interestingly, the reporter expressing PC population remained comparable in number up to 28 days of observation. While no more BFP$^+$ (i.e., MAF$^+$) BMPCs could be detected at day 35 p.i., the reliability is limited here due to small sample size and no longer allows exact statements regarding this population (Fig. 5B).

3.1.6 T cell support and immunosurveillance upon temporally controlled *Maf* expression

To rule out the possibility that *Maf*-expressing cells rapidly disappear due to lack of T cell support or elimination by cytotoxic T cells[215] in a context of immune surveillance[216], the respective T cell populations in extracted spleens were examined by flow cytometry in the same immunized and tamoxifen treated Cγ1-cre; R26 MafstopF and R26 hCD2 control mice. Technically, T cells were identified by their surface expression of CD3e and TCRb (Fig. 6A). Active T helper cells were assessed by further gating for CD4+CD44+CD62L- cells. Absolute numbers of that population were calculated for all analyzed time points and revealed no apparent difference between Cγ1-cre; R26 MafstopF and R26 hCD2 control mice (Fig. 6B). Among the CD4$^+$ Th cells, PD1$^+$ expression was assessed that allowed for

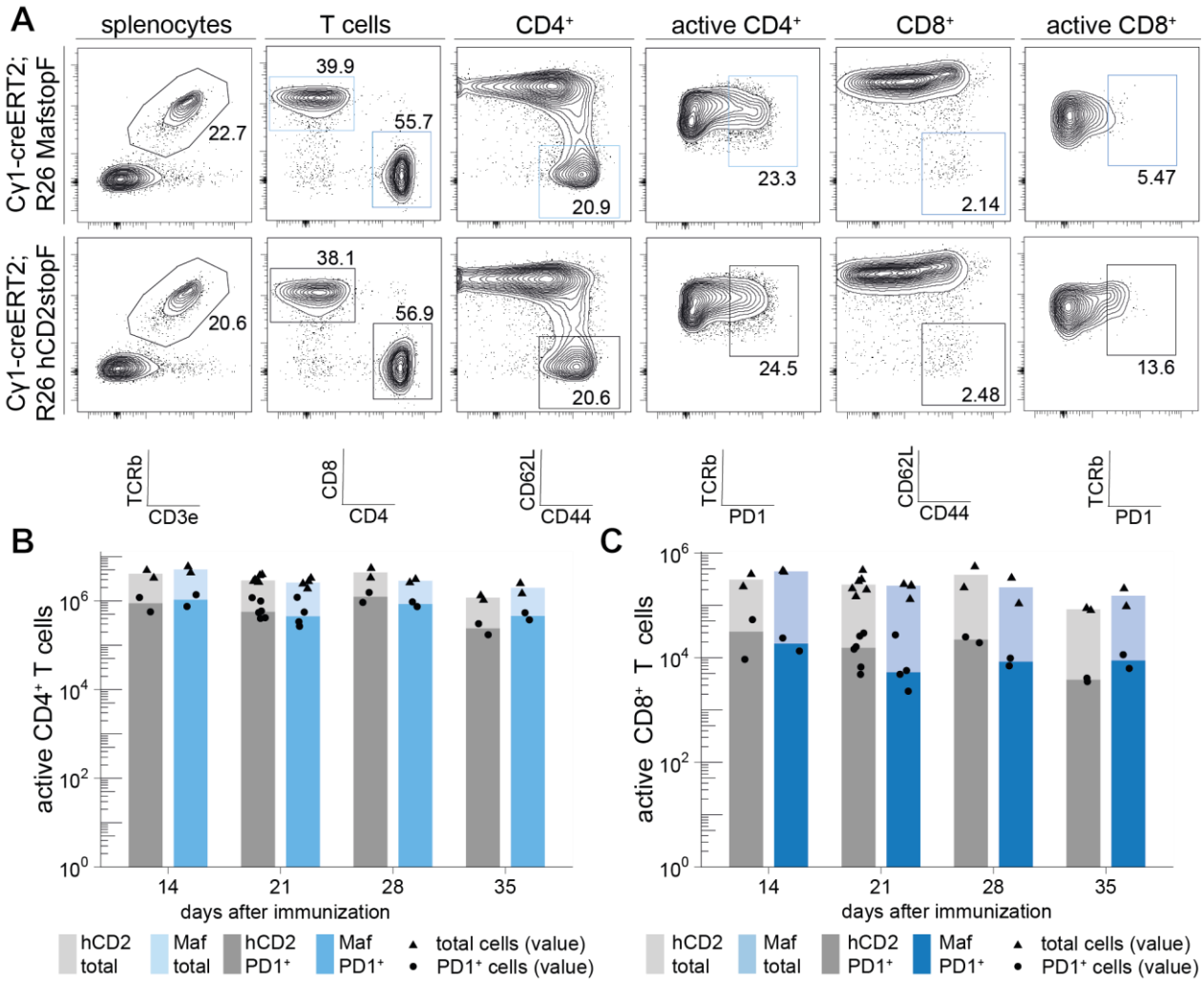

Figure 6: T cell support and immunosurveillance upon conditional *Maf* expression in GC B cells. Cγ1-creERT2; R26 MafstopF (Maf) and Cγ1-creERT2; R26 hCD2 control mice were immunized, and tamoxifen treated at days 10-12 p.i. At 4 consecutive time points (d 14, 21, 28 and 35 p.i.), splenic T cells were assessed by their surface CD3e and TCRb expression. A) Contour plots illustrating the gating strategy for identifying CD4+ and CD8 activated (CD44+CD62L-) T cells in a representative mouse analyzed at day 14 p.i. Both populations were further assessed for PD1 expression marking exhausted T cells and allowing to estimate CD4+ Tfh cells. B) Quantification of the absolute numbers of CD4+ T cell populations in spleens. C) Quantification of the absolute numbers of $CD8^+$ T cell populations in spleens. n = 2.

analysis of exhausted T cells and the estimation of Tfh cells (that are usually defined as $PD1^+CXCR5^{+}$[217]). These populations did not vary concerning absolute numbers between Maf and control mice.

Analogously, $PD1^+$ and $PD1^-$ cytotoxic T effector cells were distinguished as $CD8^+CD44^+CD62L^-$ cells, and absolute numbers for both populations were calculated for all analyzed time points. The numbers revealed no apparent difference between Maf and

control mice (Fig. 6C). Thus, based on an orientating quantitative analysis, no obvious alterations of T cell support or immunosurveillance could be detected.

In summary, delayed transgene expression in Cγ1creERT2; R26 MafstopF mice could attenuate the counter-selection of *Maf*-expressing GC B cells and was compatible with CSR and differentiation into BMPCs. However, a decrease of *Maf*-expressing B cell populations was observed over time that was not caused by reduced proliferation of GC B cells, restrained T cell support or immunosurveillance. Aiming to optimize the transgenic approach, subsequent experiments sought to investigate the molecular biological function of MAF to identify putative shortcomings of the mouse model, such as protein interactions.

3.2 Protein interaction of MAF in MM

The translocation t(14;16) leads to overexpression of the transcription factor MAF in human B cells during the germinal center reaction, a process that is tightly regulated by a network of transcription factors[2,22,26]. To analyze presumable interactions of MAF with other nuclear proteins in MM pathology, an unbiased approach was established based on the immunoprecipitation of MAF followed by mass spectrometric analysis of coprecipitated proteins. Protein-protein interaction studies were carried out in human MAF translocated MM cell lines, which are dependent on MAF expression[154,215] and thus likely conserve the initial MAF mediated oncogenic pathways.

3.2.1 Cellular localization of MAF

To the MAF interactome in its main cellular compartment, first analyses aimed to determine the preferential (nuclear) localization of the target protein. Therefore, a procedure was established that allowed to dissect the cell lysate of human MM cells into a *cytoplasmic*, *perinuclear*, *chromatin* and *nuclear matrix*-fraction. This was achieved by firstly separating the so-termed *perinuclear fraction* from the whole nucleus using a sucrose- and ammonium sulfate- based buffer, before resolving chromatin-bound proteins by benzonase digestion of DNA. All cellular compartments were then analyzed by Western blot (Fig. 7) To control for proper separation, the expression of the cytoplasmic protein ACTB was analyzed and found mainly in its corresponding *cytoplasmic fraction* and to a lesser extend in the *perinuclear matrix* (Fig. 7). Analogously, the nuclear proteins Lamin A/C and PARP1 were analyzed and detected in the *nuclear* subfractions with little to no signal in the *cytoplasmic* fractions. It

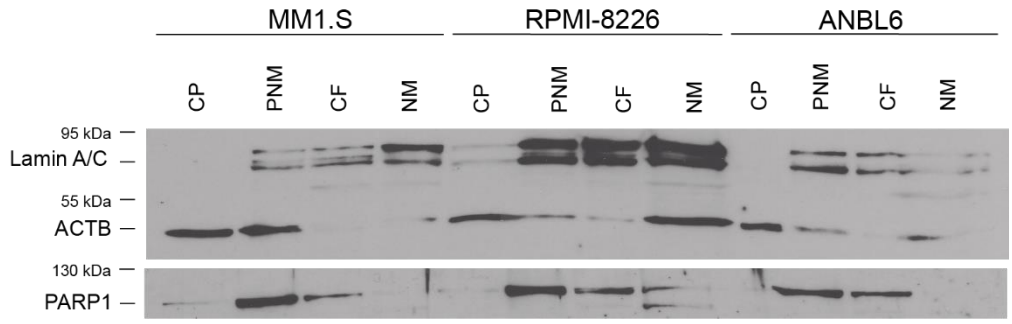

Figure 7: Subdissection of MAF-expressing HMCL cells. Based on published protocols[201–204], a method was established to selectively isolate proteins from the cellular localizations *cytoplasm* (CP), the *perinuclear matrix* (PNM), the *chromatin fraction* (CF) and the *nuclear matrix* (NM) (detailed description in the Methods section). Three MAF translocated MM cells lines were used as model systems (MM1.S, RPMI-8226 and ANBL6). Briefly, approx. 1 x 10^6 HMCL cells were resuspended in CSK100 buffer supplemented with 0.2 % NP40 and centrifuged. Purified supernatants constituted the CP. Nuclear subfractions containing pellets were washed twice before separating the PNM by lysis in PNF buffer with 0.5 % NP40 and centrifugation. The CF was finally isolated by benzonase digestion in CSK50 buffer terminated by adding ammonium sulfate. Remaining pellets after centrifugation constituted the NM. 30 µg of each protein fraction were separated by SDS-Page and analyzed by Western blot for localization of the cytoplasmic protein ACTB (42 kDa) and the nuclear proteins Lamin A/C (74 / 63 kDa) and PARP1 (116 kDa), respectively.

must be noted that dissection into the *nuclear matrix* fraction was challenged by contaminations of cytoplasmic and chromatin-associated proteins. Interestingly, however PARP1 was not detected in the nuclear matrix fraction, unexpectedly from its role as a nuclear enzyme[216]. Nevertheless, the established method allows a reliable statement about the localization of proteins in HMCL cells.

Next, the developed method was used to analyze the cellular localization of MAF and to test the ability of different cell lysis buffers to dissolve MAF from its respective cellular compartment. Therefore, diverse whole cell and nuclear compartment lysis buffers were tested. Technically, the MAF translocated MM1.S cells were harvested and lysed either in a high salt lysis (HSL) buffer, a modified RIPA (mRIPA) buffer, a NP40 buffer or a Chaps based buffer, respectively. In parallel, nuclear extracts from the cells were produced. Protein extracts were analyzed by Western blot and compared to respective extracts from the subdissection method (Fig. 7). As shown in Fig. 8, the MAF translocated human MM cell line MM1.S demonstrated high expression of MAF (48 kDa) controlled by the analysis of retrovirally transduced mouse fibroblast NIH3T3 cells overexpressing mouse MAF (Fig. 8, lanes 12 + 13). Of note, in MM1.S cells, MAF was rarely located in the cytoplasm and predominantly found in the chromatin fraction as expected from its function as a TF. Importantly, protein lysates achieved after HSL also contained high amount of MAF protein.

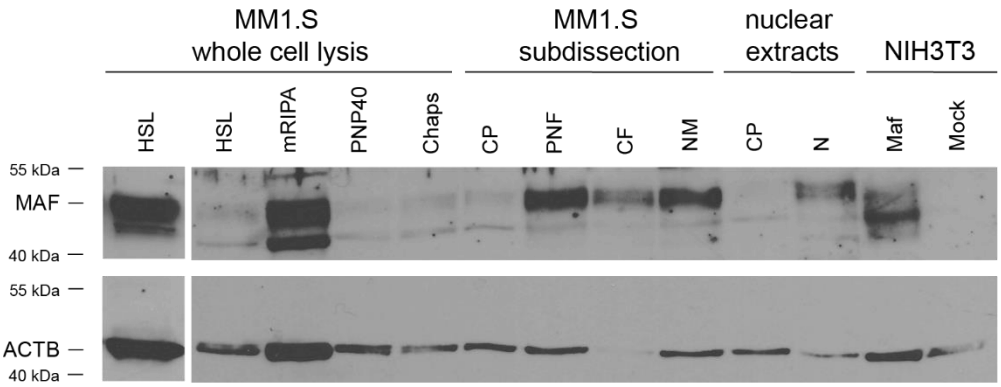

Figure 8: Sufficient isolation of MAF from its nuclear localization. Proteins from MM1.S cells were separated by different lysis conditions to test the ability of different buffers to extract MAF. Briefly, each 1 x 10^6 cells were lysed in the whole cell lysis buffers termed high salt lysis buffer (HSL), a modified RIPA buffer (mRIPA), a PBS-based NP40 containing buffer (PNP40) or a buffer containing the Chaps detergent (Chaps). Analogously, nuclear extracts of MM1.S cells were prepared following a published method[200]. Cells of the mouse fibroblast cell line NIH3T3 were transduced with a murine stem cell virus construct coding for Maf or a GFP reporter protein (Mock) and lysed in HSL buffer as positive control. 30 µg of protein from all procedures were separated by SDS-Page and analyzed for MAF (48 kDa) expression by Western blot together with extracts from the previous subdissection experiment (Fig. 8). An additional blot for the HSL procedure is shown as the MAF band showed an unexpected low signal.

Furthermore, cell lysis in a high detergent containing mRIPA buffer resulted in high MAF concentration even if not classically used for chromatin associated proteins.

Thus, MAF is mainly located in the *chromatin fraction* of the nucleus and can succesfully be dissolved from that localization by a HSL and a mRIPA buffer, both upscalable procedures well suited for mass spectrometry.

3.2.2 MAF interactome in human MM cell lines

To collect MAF immunoprecipitates from HSL and mRIPA lysates of three different MAF-translocated HMCL, samples were incubated with a rabbit αMAF antibody for 2 h before magnetic bead-based pull down assays. As controls, lysates were incubated with a rabbit IgG isotype control antibody. After elution from beads, precipitates were analyzed by Western blot using a guinea pig αMAF antibody. As shown in Fig. 9, MAF protein was successfully immunoprecipitated from both HSL and mRIPA lysates of RPMI-8226, MM1.S and ANBL6 cells.

The procedure was therefore eligible for further analysis of the MAF interactome by mass spectrometry. Thus, samples were prepared and subjected to mass spectrometry

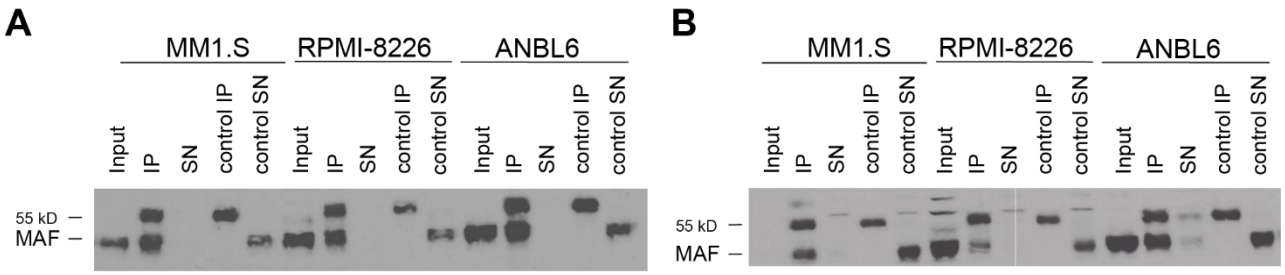

Figure 9: Immunoprecipitation of MAF from lysates of human MM cell lines. 1 x 10^7 freshly collected cells from RPMI-8226, MM1.S and ANBL6 cell lines were lysed in either HSL **(A)** or modified RIPA buffer **(B)** and 450 µg of lysates subjected to magnetic bead-based immunoprecipitation with an αMAF antibody or rabbit IgG isotype control. After elution from magnetic beads, 10 % of resulting proteins (IP) together with 10 µg of protein from input samples and supernatants (SN), respectively, were separated on a gradient SDS-page and subsequently analyzed by Western blot using a guinea pig αMAF antibody.

(performed by Dr. Marieluise Kirchner, Proteomics Core Facility MDC Berlin). The proteomic approach identified a total of 883 protein interactions conserved in HSL lysates (Fig. 10A). The majority of associated proteins (76.3 %) were found in at least two of the three MAF translocated MM cell lines investigated, in agreement with a common mechanism of action of MAF. Interestingly, of the 492 putative MAF interactors shared among all three MM cell lines under HSL conditions, 317 could not be detected in any of the same cell lines under mRIPA conditions (Fig. 10B). Of those, 62 included known DNA binding proteins, suggesting that HSL treatment is more appropriate to elute proteins from the chromatin compartment. Importantly, also 7 TFs (PHF5A, AATF, IFI16, IKZF1, MECP2, REXO4, SPE) could be detected as putative MAF interactors after HSL, but not after mRIPA lysis (Fig. 10B, red triangles). When determining overlapping protein interactors between the two lysis conditions, 62 proteins were associated with MAF in all three human MM cell lines, indicating robust interactors (Fig. 10A and Table 35).

Table 35: Table 36: Common MAF binders in human MM cell lines MM1.S, RPMI8226 and ANBL6 detected after both HSL and mRIPA lysis. Transcription factors are highlighted in blue.

MAF	NFKB1	AQR	NFKB2
BCAS2	NHP2L1	CDC40	PABPC1
CRNKL1	PABPC4	DAP3	PDHA1
DDX21	PDHB	DLAT	PDHX
DLST	PRPF19	EFTUD2	PRPF6
EIF4A3	PRPF8	FASTKD2	PTBP1
HNRNPA1	RALY	HNRNPAB	RBM22
HNRNPC	RBM8A	HNRNPD	RPL10A
HNRNPDL	RPLP2	HNRNPF	RRBP1
HNRNPH1	SEC16A	HNRNPH3	SF3B2
HNRNPK	SNRNP200	HNRNPL	TOP2B
HNRNPM	TRUB2	MRPL17	UPF1
MRPL20	UTP18	MRPL39	WDR36
MRPL41	WDR43	MRPL43	ILF3
MRPL44	ISY1	MRPL51	HIST1H1C
MRPS7	HIST1H1E		

A variety of TF were identified as putative MAF binding proteins (Fig. 11) with a total of 35 binding to MAF in at least one MM cell line in one lysis condition. Interestingly, no AP1 proteins were identified among the interactome, but non-significant enrichment of MAFG peptides was detected. 7 TFs (HNRNPK, NFKB1, NFKB2, MAZ, TARDBP;TDP43, CEBPZ and YBX1) bound to MAF in all three cell lines under HSL conditions plus at least in one more cell line upon mRIPA lysis. Thus, a total of 14 TFs (7 exclusively and 7 in common with mRIPA) were commonly found after HSL extraction. Of those, only NFKB1 and NFKB2 were found under both lysis conditions in all three MM cell lines, indicating a possible cooperation between deregulated MAF expression and the NFκB pathway activity (Table 35). CBFB, a predicted MAF interactor[217] was found solely in the MAF interactome in RPMI-8226 cells after HSL lysis (Fig. 11A)

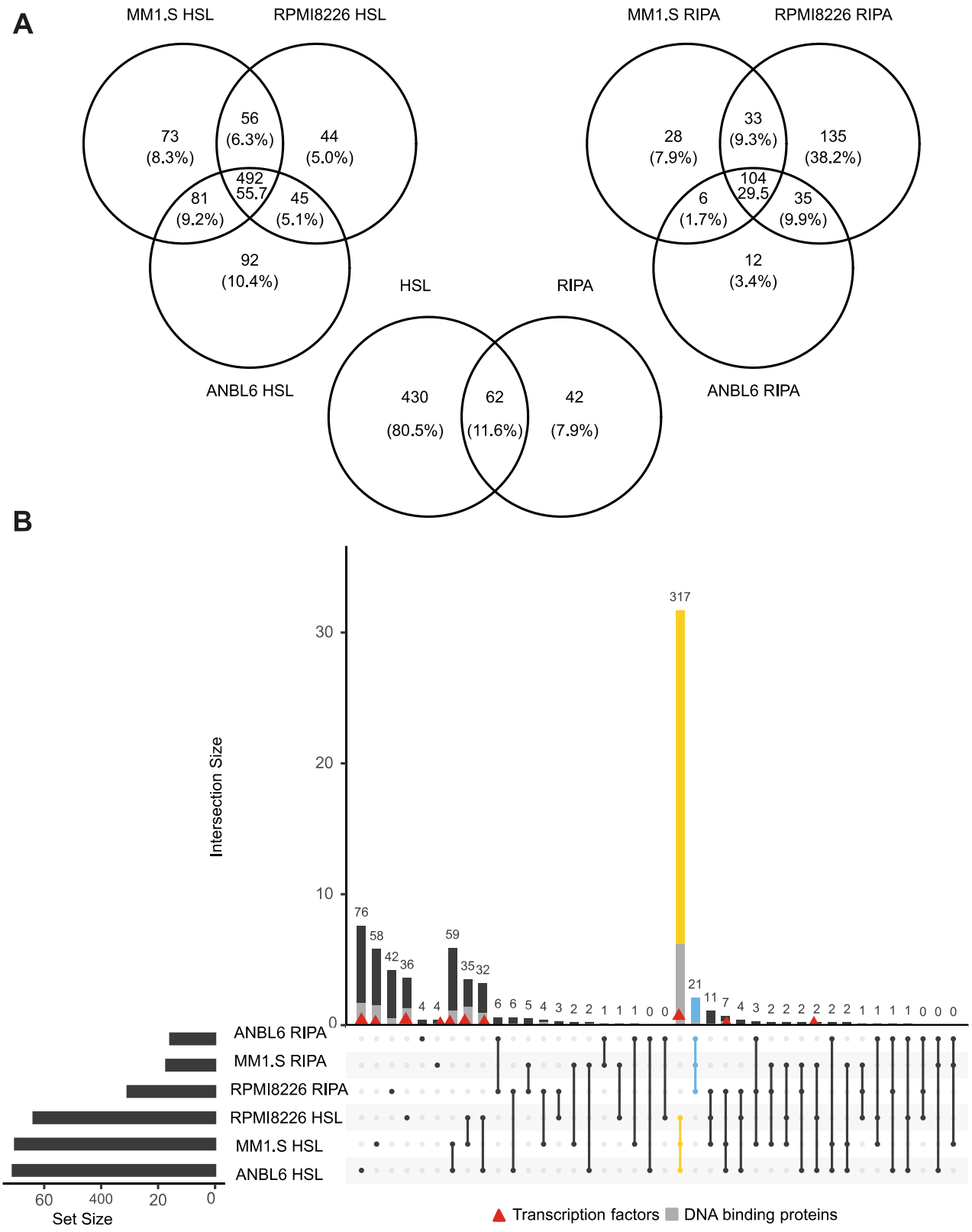
A
MM1.S HSL
RPMI8226 HSL
ANBL6 HSL
73
(8.3%)
56
(6.3%)
44
(5.0%)
492
55.7
81
(9.2%)
45
(5.1%)
92
(10.4%)
MM1.S RIPA
RPMI8226 RIPA
ANBL6 RIPA
28
(7.9%)
33
(9.3%)
135
(38.2%)
104
29.5
6
(1.7%)
35
(9.9%)
12
(3.4%)
HSL
RIPA
430
(80.5%)
62
(11.6%)
42
(7.9%)
B
Intersection Size
30
20
10
0
317
76
58
42
36
59
35
32
21
11
7
ANBL6 RIPA
MM1.S RIPA
RPMI8226 RIPA
RPMI8226 HSL
MM1.S HSL
ANBL6 HSL
60
400
20
0
Set Size
Transcription factors
DNA binding proteins

Figure 10 (page 72): MAF interacting proteins in human MM cell lines. Cells from human *MAF* translocated MM cell lines (RPMI-8226, MM1.S and ANBL6) were lysed in either HSL or modified RIPA buffer and lysates subjected to immunoprecipitation with a rabbit αMAF antibody or rabbit IgG isotype control as described above. Precipitates were analyzed by mass spectrometry. Experiments were performed in technical triplicates; proteins enriched in the MAF antibody group compared to isotype control were considered MAF associated proteins. Two sample student´s t test, corrected by Benjamini Hochberg procedure False discovery rate FDR = 5 % **A)** Venn diagrams depicting MAF associated proteins from HSL lysates (left), and modified RIPA lysates (right) found in the three cell lines analyzed. 62 proteins (including MAF) were found in the interactome in all three cell lines in both conditions (center). **B)** The graphic illustrates proteins that appear in different sets of samples mutually exclusive to one another. Sum of DNA binding proteins as judged by GOMF category analysis is colored in grey. Transcription factors are highlighted by red triangles.

It was previously reported that MAF proteins can interact with the co-activators P/CAF[135], P300, CBP[136], and TBP[137] to initiate transcription. Therefore, the mass spectrometry data were searched for these proteins. Importantly, P/CAF, but none of the other factors robustly bound to MAF in all three MM cell lines following HSL lysis (Fig. 11A). Thus, a diversity of MAF interacting proteins was found showing interesting functions in transcriptional regulation. Further functional analysis are required to determine the importance of putative interactors for the pathogenesis of MM with t(14;16).

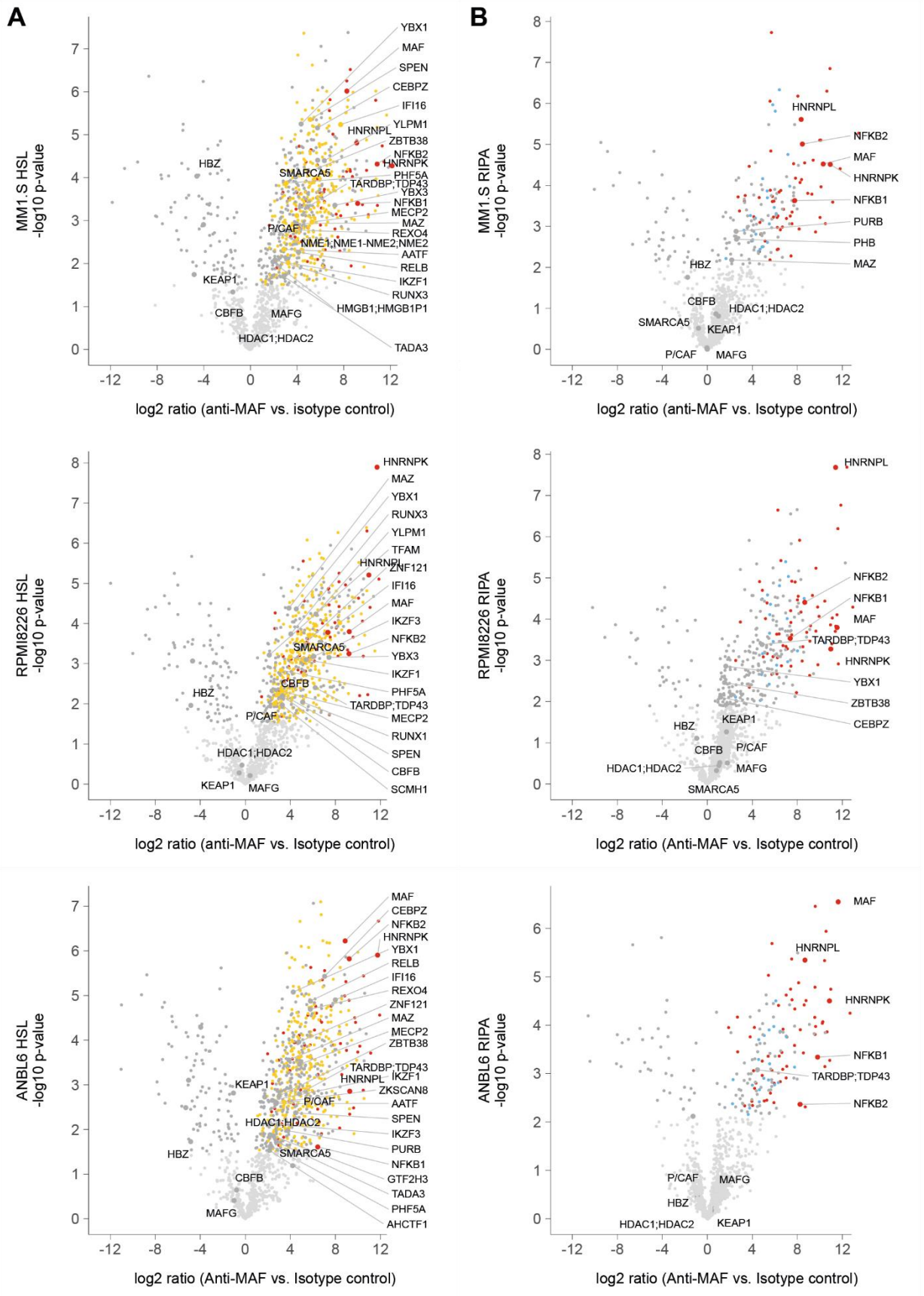
A
B
MM1.S HSL -log10 p-value
MM1.S RIPA -log10 p-value
RPMI8226 HSL -log10 p-value
RPMI8226 RIPA -log10 p-value
ANBL6 HSL -log10 p-value
ANBL6 RIPA -log10 p-value
log2 ratio (anti-MAF vs. isotype control)
log2 ratio (anti-MAF vs. Isotype control)
log2 ratio (Anti-MAF vs. Isotype control)
log2 ratio (Anti-MAF vs. Isotype control)
YBX1
MAF
SPEN
CEBPZ
IFI16
YLPM1
HNRNPL
ZBTB38
NFKB2
HNRNPK
PHF5A
TARDBP;TDP43
YBX3
NFKB1
MECP2
MAZ
REXO4
NME1;NME1-NME2;NME2
AATF
RELB
IKZF1
RUNX3
HMGB1;HMGB1P1
TADA3
HBZ
SMARCA5
P/CAF
KEAP1
CBFB
MAFG
HDAC1;HDAC2
PURB
PHB
ZNF121
TFAM
RUNX1
SCMH1
ZKSCAN8
GTF2H3
AHCTF1

Figure 11 (page 74): MAF binding transcription factors in MM. Volcano plots presenting MAF associated proteins detected by mass spectrometry of MAF pull downs from lysates of the cell lines MM1.S, RPMI8226 and ANBL6 respectively, as described before. **A)** MAF interactome as detected after HSL lysis. Substantial binders after Benjamini Hochberg correction are colored dark grey. Proteins that were found to bind MAF in all three cell lines, but mutually exclusive in one buffer condition are colored yellow (HSL) or blue (RIPA), as encoded in Figure 11B, respectively. Transcription factors substantially binding MAF are labeled at the edge. Known or predicted MAF binders are labeled in the center of the diagrams and corresponding data points colored dark grey. **B)** Same analysis as A, but cells were lysed in a modified RIPA buffer.

3.2.3 MAF protein interaction in a mouse model and screening for candidates

Proteomic analysis of MAF immunoprecipitates from human MM cell lines found a variety of TFs and chromatin associated proteins in the interactome of MAF suggesting that the oncogenic activity of MAF in MM requires its cooperation with other (e.g., DNA-binding) cofactors. This is also implied by the observation that the overexpression of Maf on its own in mouse GC B cells does not induce myelomagenesis. One possible explanation for this observation could be that essential oncogenic protein-protein interactions cannot form in the mouse model either due to a wrong timing of MAF overexpression or because of complete absence in the murine situation. Therefore, further experiments aimed to establish an in vitro screening platform to assess the interaction of MAF and possible interactors in mouse B cells to eventually enable future research on the MAF interactome.

To gain a first insight into the protein interactions of MAF in the Cγ1cre; R26 MafstopF mouse model, a glutaraldehyde crosslinking approach was established. To test for the minimal amount of glutaraldehyde required to crosslink MAF protein, increasing amounts of glutaraldehyde were added to the HSL buffer during the lysis of MAF expessing human MM cell lines. The respective lysates were then analyzed by Western blot to observe the formation of bands of higher molecular weight. Interestingly, upon addition of 0.004 % glutaraldehyde a new band at approx. 100 kDa appeared, interacting with a MAF specific antibody, indicating the presence of a MAF containing protein complex (Fig. 12A). Of note, upon addition of 0.04 % of glutaraldehyde, the monomeric band of MAF disappeared, suggesting complete crosslinking. Interestingly, the 100 kDa protein complex could also be immunoprecipitated with an αMAF antibody from HSL lysates, rendering the method suitable for analysis of protein interactions in human MM cell lines and probably conserving also unstable or transient protein interactions (Fig. 12B).

To compare the protein interactions of MAF in HMCL with those found in *in vitro* activated splenic B cells from the Cγ1cre; R26 MafstopF mouse, *Maf*-expressing B cells were also lysed in glutaraldehyde containing HSL buffer, analogously to MM1.S and RPMI-8226 human MM cells. Importantly, in the presence of glutaraldehyde, the same 100 kDa band originally identified in HMCL samples also appeared in *Maf*-expressing mouse B cell lysates, indicating the occurrence of a similar MAF containing protein complex in the mouse and suggesting that the method could potentially be used in the future to analyse mouse protein interactions (Fig. 12C).

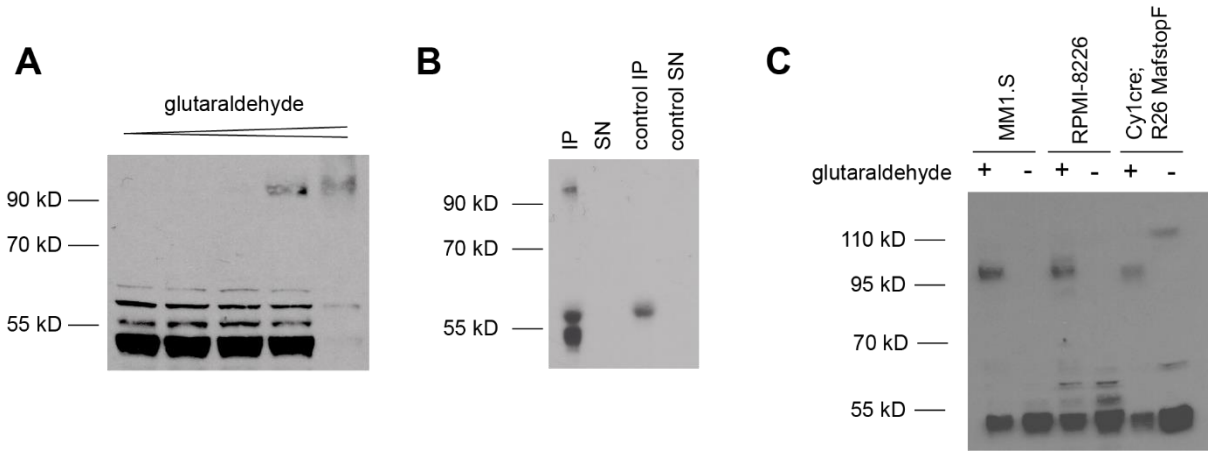

Figure 12: Oligomerization of MAF in human MM cells and mouse B cells. A) Crosslinking approach to analyze protein interaction of MAF. 1 x 10^6 freshly collected MM1.S cells were lysed in HSL buffer containing increasing amounts of the crosslinker glutaraldehyde (0 %, 0.0004 %, 0.001 %, 0.004 % and 0.04 %, indicated by the crescendo). Crosslinking was quenched by addition of Tris-HCl (pH 8). Lysates were subjected to Western blotting with the rabbit αMAF antibody (MAF, 48 kDa). **B)** Lysates from (A) with 0.004 % GA were subjected to IP as described before. Eluted immunoprecipitates, 10 µg supernatant protein and respective controls (rabbit IgG isotype) were analyzed by Western blot using a guinea pig αMAF antibody. **C)** Splenic B cells from Cγ1-cre; R26 MafstopF mice were isolated by CD43 depletion and cultured in the presence of αCD40 (1 µg/ml) and IL4 (25 ng/ml) overnight to activate *Maf* transcription. Subsequently, mouse B cells and human MM cells from the HMCL MM1.S cells and RPMI8226 were lysed in HSL buffer with or without glutaraldehyde crosslinking (0.004 % GA). Lysates were separated by SDS page and analyzed by Western blot using a rabbit αMAF antibody.

Next, an approach was developed to investigate the possible functional interactions of transgenic mouse MAF with proteins identified in the mass spectrometric analysis of MAF immunoprecipitates in HMCL. The concept is based on the hypothesis that enforced coexpression of possible interactors together with transgenic *Maf* in mouse B cells might enhance its transcriptional activity and upregulate known MAF-regulated genes. Thus, the expression of such target genes can be measured as read-out. To allow for the overexpression of selected interaction candidates, splenic B cells isolated either from Cγ1-cre; R26 MafstopF or reporter control mice can be transduced with MSCV-based retroviruses encoding respective interactors and GFP or only GFP. Double reporter positive B cells can be FACS sorted for coexpression of MAF (BFP) and the interactor (GFP) or respective single transgenes and reporter controls. Finally, the transcriptional activity of MAF can be delineated based on the mRNA expression levels of selected MM target genes. To simplify the concept during establishment, only MAF itself was initially transduced as a possible interaction partner, and only the expression of *Itgb7* was used as read-out. Importantly, *ITGB7* is considered one of the most important target genes of MAF in MM pathology and is expressed upon direct binding of MAF to its promoter[57,154,155,159].

Stimulation of isolated splenic B cells with IL4 and αCD40 resulted in an expected[181] transgene activation in >90 % of B cells both in *Maf*-transgenic and control cells as judged by the respective reporter protein expression (Fig. 13A). Retroviral transduction with a MSCV-based retrovirus, empty or encoding for *Maf*, was highly efficient allowing for a decent amount of double reporter positive cells to be FACS sorted (Fig. 13A). Upon stimulation, B cells from Cγ1-cre; R26 MafstopF mice showed a 5-fold higher relative expression of *Maf* mRNA compared to control B cells (Fig. 13B, light blue). Transduction of the *Maf*-encoding retrovirus increased *Maf* expression within normal B cells approx. 35-fold (Fig. 13B, green), which was further elevated in the additional presence of the *Maf* transgene (Fig. 13B, dark blue). Interestingly, the increasing expression level of *Maf* had a direct effect on the expression of its target gene *Itgb7* whose expression was upregulated approx. 3.5-fold by the *Maf* transgene (Fig. 13C, light blue) or 4.5-fold by the *Maf* retrovirus (Fig. 13C, green) alone, but was enhanced up to 8-fold in double *Maf*-expressing B cells (Fig. 13C, dark blue).

Thus, stimulated B cells from Cγ1-cre; R26 MafstopF mice can be transduced with MSCV constructs encoding for putative interaction partners and the MAF MM target gene *Itgb7* can be used as a read-out for MAF transcriptional activity. Therefore, the established protocol is suitable to screen proteins identified in the mass spectrometric approach from HMCL as oncogenic partners of MAF in the Cγ1cre; R26 MafstopF mouse model in future work. Promising candidates might finally be coexpressed with *Maf in vivo* to develop a convenient mouse model for the pathology of t(14;16) translocated MM cases.

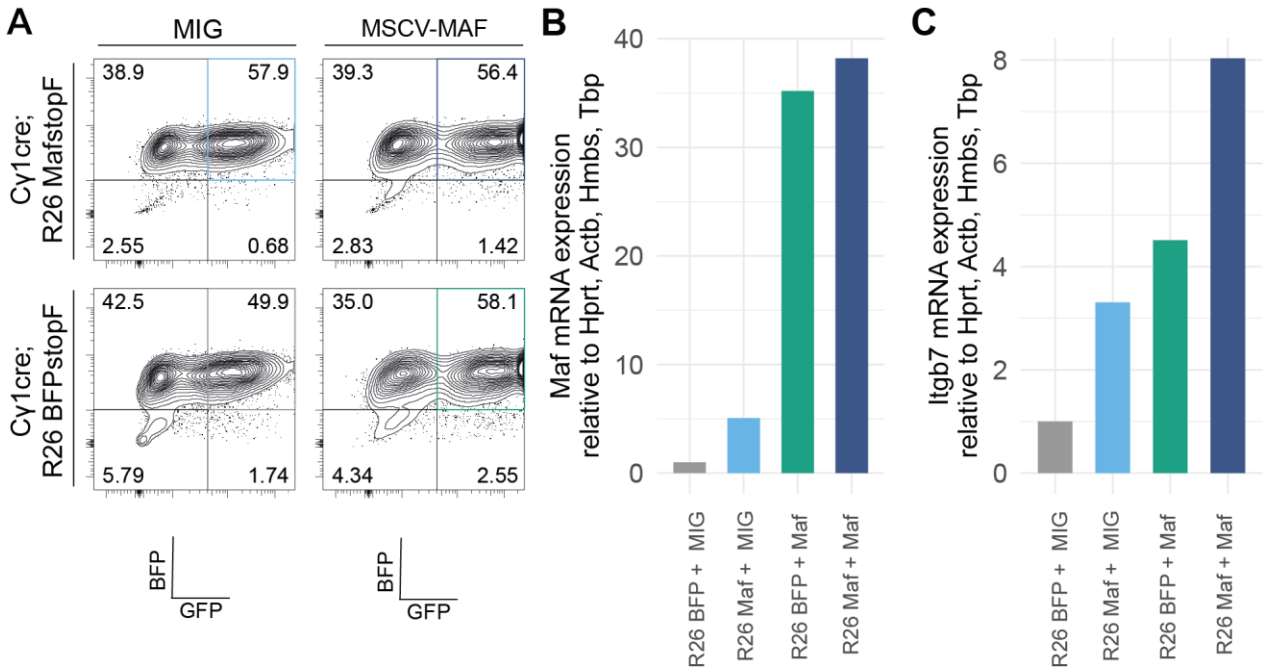

Figure 13: Establishment of an *in vitro* screen of candidate MAF interactors in mouse B cells. Splenic B cells from Cγ1-cre; R26 MafstopF and Cγ1-cre; R26 BFPstopF control mice were isolated by CD43 depletion, cultured in the presence of αCD40 (1 µg/ml) and IL4 (25 ng/ml) overnight and transduced with MSCV-based retroviral supernatants encoding for GFP only (=MIG) or *Maf* and GFP. **A)** Double reporter positive B cells were FACS sorted after 72 h based on BFP and GFP protein expression. Four samples were generated per experiment; (1) BFP control B cells transduced with an empty MIG virus (grey), (2) *Maf* transgenic B cells transduced with an empty MIG virus (light blue), (3) BFP control B cells transduced with a *Maf*-encoding virus (green) and (4) *Maf* transgenic B cells transduced with a *Maf*-encoding virus (dark blue). Contour plots illustrate the sorting strategy after transduction. **B-C)** Quantitative RT-PCR to detect *Maf* (B) and *Itgb7* (C) mRNA expression in the sorted samples. Of note, the expression values are plotted as normalized values in comparison to the respective reporter control sample (control B cells and control virus, grey-colored). *Actb*, *Hmbs*, *Tbp* and *Hprt* were used as reference genes. The RT-PCR was performed in technical triplicates. MIG: MSCV-IRES-GFP vector.

4. Discussion

4.1 Impact of *Maf* expression on terminal B cell differentiation in a novel mouse model

MM is a tumor of terminally differentiated B cells, namely PCs, and is characterized by a stepwise acquisition of genetic aberrations that lead to malignant transformation[4]. The beginning of this process likely happens during the GC reaction of B cells and is defined by the emergence of classical primary genetic events, referred to as myeloma-initiating events (MIE)[9,83]. In approximately 50 % of MM cases, these MIEs include the overexpression of single oncogenes because of translocations which place these genes under control of the strong Ig enhancer region[4]. Next to cyclin D members and MMSET, overexpression of three MAF transcription factors constitute MIEs, with c-MAF being the most frequently found TF as a consequence of the translocation t(14;16) in 5 % of MM cases[96].

Surprisingly, as previously shown in our laboratory by Wiebke Winkler, the conditional overexpression of *Maf* in early mouse GC B cells of the Cγ1-cre; R26 MafstopF strain led to a massive reduction of *Maf*-expressing GC B cells, the believed COO of this type of MM[178]. At the same time, *Maf*-expressing antigen-specific IgM-secreting PCs temporarily accumulated in the BM. It is not known whether these cells are derived from the early GC or extrafollicular immune response. Thus, the reduced GC reaction can be explained by transgenic *Maf* expression either impairing entry into the GC, inducing apoptosis, and/or reducing proliferation of GC B cells. The early accumulation of BMPCs from day 4 onwards could be caused by a better toleration of *Maf* overexpression in PBs[178]. On the other hand, *Maf* expression in GC B cells could enforce terminal differentiation towards PCs[178]. Additionally, containment of transgenic GC B cells by T cell dominated immunosurveillance must be regarded.

This thesis aimed to characterize the altered terminal B cell differentiation upon *Maf* overexpression in the Cγ1-cre; R26 MafstopF mouse model in more detail, mainly focusing on the unexpected observations of the strongly reduced mature B cell populations[178]. Therefore, BrdU incorporation studies as well as fate tracking experiments to target *Maf* expression more precisely to specific B cell differentiation stages were conducted to assess

the proliferative capacity, differentiation choice and further development of *Maf*-transgenic B cells *in vivo*.

4.1.1 Impact of *Maf* expression on early GC B cells

Impaired cell division of GC B cells upon *Maf* overexpression constitutes a possible reason for the reduced GC reaction in Cγ1-cre; R26 MafstopF mice. To analyze the effect of *Maf* expression on the proliferation of GC B cells, BrdU incorporation experiments were performed. The absolute amount of *Maf*-expressing GC B cells on day 14 post immunization was approx. 25-fold lower in Cγ1-cre; R26 MafstopF mice compared to control mice (Fig. 2B), in line with the previously described 16.5-fold reduction[178]. However, BrdU incorporation within *Maf*-expressing GC B cells did not differ from control animals (Fig. 2C), indicating that *Maf* overexpression *per se* does not impair the ability of B cells to proliferate. Cell division is a central mechanism in the terminal differentiation of B cells[218]. Upon challenge with a type-I TI antigen, a division-specific regulation of gene expression can be found in B cells differentiating towards PCs[219]. This regulation is strongly dependent on division-specific changes in the DNA methylome and overall DNA accessibility[219–221]. Unfortunately, such analyses have not yet been conducted for TD antigens, such as NP_{15}-CGG. However, if one assumes an analogy, the precondition to differentiate terminal would be fulfilled in *Maf*-expressing GC B cells. Of note, the fraction of $BrdU^+$ cells within the GC B cell compartment was rather heterogenous among the Cγ1-cre; R26 MafstopF mice analyzed and especially low in 3 of them. Importantly, the experiment was performed in four runs (i.e., four separate days) with a minimum of 3 mice per group being analyzed in parallel. The three mentioned dropouts were analyzed in different runs of the experiment each together with respective control mice, minimizing errors in the process. Large variances of $BrdU^+$ fractions within whole cell compartments are commonly observed[32]. However, it can also reflect a limitation of the experimental setup, which depicts only a snap-shot-like view of the proliferation status. Due to the short half-life of BrdU[213], it is incorporated in cells that enter the S-phase shortly after intraperitoneal injection. GC B cells divide every 7-12 h[222,223] and BrdU labeling is reduced to 8 % within 2 divisions[32]. Thus, 15 h after injection, cells are detected which have actively divided at day 13. However, it cannot be determined how many divisions a GC B cell performed upon activation, and how many may follow. Upon immunization with TI antigen, a minimum of eight divisions is needed for the differentiation into ASCs[224]. Such

dependency has not been investigated for TD antigens. Of note, PBs and PCs can be found in *Maf*-transgenic mice, implying no differentiation block *per se*. Nevertheless, the application of cell division tracking dyes like carboxyfluorescein succinimidyl ester or CellTrace Violet (available from Molecular Probes, Invitrogen) could enable a more long-term analysis of cell division to explicitly analyze GC B cells and their progeny[225]. These substances accumulate in the cytoplasm of cells and are distributed equally to the daughter cells upon cell division, resulting in distinct fluorescence intensities that allow tracking up to 11 divisions[225]. Hence, proliferation could be tracked over a longer period and compared to reporter control-expressing cells to more profoundly rule out reduced cell division of *Maf*-expressing GC B cells as the reason for the reduced GC B cell compartment in Cγ1-cre(ERT2); R26 MafstopF mice. As a downside, these dyes can only be subjected to cells *ex vivo* and require transplantation for *in vivo* analysis[218], a challenge in GC B cell studies. The addition of CXCR4 and CXCR5 staining could furthermore improve the analysis of proliferation within the GC compartment by allowing to specifically analyze LZ and DZ cells that show different cycling behaviors[222].

Apart from restricted proliferation, activation of apoptosis should be considered as a potential reason for the reduced GC reaction in Cγ1-cre; R26 MafstopF mice. In addition to its role in terminal $CD4^+$ T cell differentiation[138], MAF was reported to contribute to apoptosis induction by BCL2 depletion in $CD4^+$ T cells[226] and by caspase 6 upregulation in $CD8^+$ T cells[227]. *Ex vivo* intracellular staining for active caspase 3 or incubation with fluorophore coupled pan-caspase inhibitors like FITC-VAD-FMK and subsequent flow cytometric analysis of transgene-expressing GC B cells would allow to measure the fraction of apoptotic cells within that compartment. It must be noted that incubation of unstimulated transgenic B cells *ex vivo* carries the risk of premature cell death and must be kept as short as possible, as preliminary work has shown. A further possibility to gain a broader insight into the effect of *Maf* overexpression including apoptosis is RNA-seq of sorted *Maf*-expressing cell populations, an ongoing work in our laboratory. Furthermore, to assess possible apoptosis induction by *Maf in vivo*, the Cγ1-cre; R26 MafstopF mouse could be crossed to a conditional *Bcl2* allele[228]. Of note, *Bcl2* overexpression in Eμ-Bcl2 mice enforces an initial ASC accumulation[228] and can also lead to plasmacytoma like diseases[229] which must be controlled properly.

4.1.2 Impact of *Maf* expression on peak GC B cells

Aiming to assess the impact of *Maf* overexpression on different developmental stages in terminal B cell differentiation, the Cγ1-creERT2[190] allele was used. Technically, the exact timing of *Maf* expression could be externally determined by tamoxifen application at different time points after immunization of Cγ1-creERT2; R26 MafstopF mice (Fig. 3). As expected from published work on eYFP-transgenic mice[190], tamoxifen application at days 10, 11 and 12 after immunization enabled to target *Maf* expression predominantly to peak GC B cells (approx. 60 % of BFP^+ cells, Fig. 3) so that the effect of a delayed transgene activation could be studied in comparison to the Cγ1-cre; R26 MafstopF allele that leads to early transgene induction in the GC reaction.

In general, cre recombination in GC B cells can be expected in only up to 10 % of GC B cells when using the Cγ1-creERT2 allele[190] compared to 85 % in Cγ1-cre mice[181]. Similarly, the absolute numbers of reporter-expressing GC B cells in control mice at day 14 were approx. 5-fold lower when activated by the Cγ1-creERT2 allele than by the in Cγ1-cre allele. The same held true for antigen-specific, IgG1 class-switched GC B cells. In stark contrast, the *Maf*-expressing GC B cell population was of the same size on day 14 after immunization, regardless of activation by the Cγ1-cre or Cγ1-creERT2 allele (tam d 10-12) and only reduced 3-fold in comparison to control GC B cells in the latter case. Interestingly, numbers of antigen-specific, IgG1 class-switched B cells were approx. 4-times larger upon delayed transgene activation in a smaller initial fraction of cells in Cγ1-creERT2; R26 MafstopF mice. This suggests that the counter-selection of *Maf*-expressing GC B cells could happen very early in the GC (i.e., before CSR) and can partly be overcome by delayed transgene activation. However, this initial rescue did not change the long-term fate of *Maf*-expressing GC B cells, as both total and antigen-specific ones were lost during the experiment (Fig. 4).

Nevertheless, the observation suggests that the development of a mouse model for the translocation t(14;16) in human myelomagenesis requires an exact timing of transgene activation. In contrast, in a previously developed mouse model, expression of *Maf* in naïve B cells under the control of the V_H promoter, Eμ enhancer, and 3'Eκ enhancer led to accumulation of $CD138^{hi}B220^-$ PCs with age, resembling a plasmacytoma-like phenotype[57]. This model implies that an exact timing is not needed, even though the PCs did not exhibit a post-GC phenotype[57]. Astonishingly, in another model, even the overexpression of *Mafb*

in hematopoietic stem cells led to the accumulation of pathogenic PCs even though these cells expressed neither *Mafb* nor known target genes[56]. A mechanism of epigenetic remodeling was suggested by the authors[56]. Indeed, the exact time point of acquisition of the translocation t(14;16) in human myelomagenesis in not known, but examples like follicular lymphoma and mantle cell lymphoma show that the initial acquisition of the genetic aberrations can take place well before a malignant phenotype of a given differentiation stage is formed[18].

Nevertheless, to further validate the R26 MafstopF allele, it could be crossed to other cre alleles that target the expression to naïve B cells with the Cd19-cre allele[180] (close to the Eμ-*Maf* mouse model[57]) or to hematopoietic stem cells using Vav-cre[230] (close to the Sca1-*Mafb* mouse model[56]). The first method has the additional advantage of minimizing counter-selection mechanisms, as *Maf* would be expressed in 90–95 % of naïve B cells[180].

Somatic cells underlie a constant surveillance by the immune system controlling possible malignant transformation and infection, to a great extend based on the presentation of self-antigen by MHC-I[231]. To rule out the possibility that transgenic overexpression of *Maf* activates a cytotoxic immune response against *Maf*-transgenic B cells in Cγ1-creERT2; R26 MafstopF mice, T cell populations were assessed by flow cytometry. Splenic active $CD8^+$ T cells in *Maf*-transgenic mice did not differ in the number compared to control mice, implying no ongoing cytotoxic T cell attack against *Maf*-expressing B cells. This was expected, since the transgenic *Maf* is of murine origin and should be tolerated. As the generation of a fully functional GC is highly dependent on Tfh cells[2], respective populations were furthermore assessed. The numbers of Tfh cells in the spleen of Cγ1-creERT2; R26 MafstopF mice were equal to control animals, estimated by assessment of $CD4^+CD44^+CD62L^-PD1^+$ cells (Fig. 7B) implying normal Tfh support. Of note, this population also includes exhausted $CD4^+$ T helper cells.

4.1.3 Impact of *Maf* expression on plasma cell populations

In Cγ1-cre; R26 MafstopF mice, *Maf*-expressing cells of more mature stages of terminal B cell differentiation were less reduced than GC B cells, and the early generation of antigen-specific IgM^+ ASC in the BM significantly exceeded (albeit only transiently) the response in hCD2-expressing control animals[178]. To gain a more detailed insight into the impact of *Maf* overexpression on PC differentiation, splenic PB and PC populations were assessed in Cγ1-creERT2; R26 MafstopF mice following early, mid, and late tamoxifen application as well as BMPCs upon mid-term activation.

Immunization of Cγ1-creERT2; R26 MafstopF mice and subsequent early *Maf* activation offered a suitable method to investigate the effect of *Maf* overexpression on splenic differentiating PBs (Fig. 3B). This was expected based on previous studies that targeted eYFP to those cells[190]. Such *Maf*-expressing PBs are most likely of extrafollicular origin and should show only limited SHM which can be confirmed by sorting of the respective cells followed by isolation of genomic DNA and sequencing of the VDJ rearrangements as well as the J_H4 intron. The number of these cells decreased within one week of observation, explainable by induced cell death and/or terminal differentiation or homing to the BM. However, it must be noted that *Maf* overexpression in B cells does not drive PC differentiation *in vitro*, neither upon stimulation with LPS (mimicking a type-I TI response)[178] nor upon stimulation with IL4 and αCD40 (a TD model, unpublished work) or in culture with 40LB feeder cells[232] (TD model with continuous CD40L and BAFF and subsequent IL4 or IL21 provision)[233].

The targeting of *Maf* expression to mainly peak GC B cells (mid tamoxifen application) did not lead to an accumulation of splenic or BMPCs (Fig. 5). However, *Maf*-expressing BMPCs were the most stable population and only 1-2-fold lower in numbers than their respective control cells. Upon mid time point *Maf* activation, transgene-expressing BMPCs only disappeared after 35 days (Fig. 5B). It can be speculated, whether this population derives from a steady influx, or whether it is rather a remnant of early, perhaps even extrafollicular PBs whose disappearance must be regarded as physiological.

Late tamoxifen application (d 31-33 p.i.) to Cγ1-creERT2; R26 MafstopF mice targeted *Maf* expression mainly to non-GC B cells (Fig. 3). This is consistent with similarly conducted

previous work with the same mouse strain that showed eYFP reporter expression mainly in $CD19^{+}B220^{+}FAS^{lo}CD38^{hi}$ B cells in the spleen, which partly had switched to IgG1 indicative of memory B cells[190]. In contrast to this finding, BrdU pulse chase experiments suggest that the late GC reaction is rather the main source of post-mitotic long-lived PCs whereas memory B cells appear to emerge earlier[32]. Unfortunately, late-stage GC B cells are not sufficiently targeted by the tamoxifen application at days 31-33 p.i. Therefore, this injection protocol is not useful to investigate the effect of transgene expression on the fate of PC differentiation.

It has been described that especially the upregulation of ITGB7 by MAF enhances the homing of PCs to the BM[159], a feature that is tremendously important for the survival of long-lived PCs[234]. Binding to ITGB7 upregulates survival signals such as the alternative NFκB pathway and enhances VEGF, IL6 and CCL4 production[154,159]. The promoter of ITGB7 contains MARE sites that are bound by MAF in human macrophages[155]. *Ex vivo* stimulated B cells from Cγ1cre; R26 MafstopF mice expressed *Itgb7* mRNA in a *Maf* dosage dependent manner (Fig. 13). Thus, the observations made *in vivo* might be explained in part by upregulated ITGB7 expression. Once again, the application of cell division dyes would allow for determination of division dependent upregulation of maturity markers like previously used to study TI responses[218], thus making it possible to compare such dynamics to reporter control-expressing cells. Finally, also the previously mentioned RNA-seq experiments of respective cell populations will help to unravel the effect that *Maf* expression exerts on mature mouse B cells.

In non-hyperdiploid MM subgroups other than the MAF group, pronounced AID activity and respective mutational signatures can be found during *early* pathogenesis[65]. This has been explained with a prolonged GC reaction[109] and chronic antigen stimulation[110–114]. This is in line with slightly enlarged GC B cell populations upon overexpression of MMSET or CCND1 in activated mouse B cells[177,178], the oncogenes of the t(4,14) or t(11,14), respectively. Further genetic events arise before silencing of AID activity in these subgroups[65]. However, a contrastive profile was found in MM cells carrying the t(14;16) translocation, which do not exhibit evidence of prolonged AID activity, but show an early APOBEC signature instead[65]. This is accompanied by overexpression of APOBEC3A[76] in the MF subgroup and a shift from APOBEC3B to APOBEC3A activity[65]. The reduced GC reaction and early rise of PC populations upon *Maf* overexpression in B cells may therefore reflect fundamental

differences in the *early* pathogenesis of t(14;16)$^{+}$ MM compared to the other MM subgroups. RNA-seq and/or WGS to detect mutational signatures will help to confirm this hypothesis.

4.1.4 Limitations of the transgenic approach

It must be noted that the performed *in vivo* studies were challenged by the presence of small cell populations and presumably rapid cell death of fragile PB/PCs *ex vivo*. Furthermore, the relatively small number of mice analyzed impedes the interpretation of data. To overcome this obstacle and further focus the analysis on the possibly enforced differentiation of *Maf*-expressing cells, low-input methods are needed, such as RNA-seq studies[177]. Another possibility to circumvent the handling of cells *ex vivo* is e.g., bioluminescence based *in vivo* cell tracing, which allows to analyze the migration of cells including B cells[235]. Conditional alleles harboring cre activatable luciferase genes are available, which could be combined with conditional *Maf* overexpression to track the migration of terminally differentiated B cells to the BM. In addition to SHM analyses such studies would be helpful to prove the GC origin of Maf expression BMPCs, an important prerequisite for the development of a COO specific mouse model.

The expression level of transgenic *Maf* in R26 MafstopF which is approx. 3-times higher than in HMCL[178]. In that allele the CAG promoter was used to achieve high transgene expression. Indeed, studies on chicken embryo fibroblasts[126,128,236] and mouse T cells[144] suggest that a certain threshold level of *Maf* expression is needed to induce transformation[96]. In line with that, both the expression of CCND2[77], a central initiator of the enhanced proliferation, and the expression of *Itgb7* in *Maf*-transgenic mouse B cells, is MAF dosage dependent[77]. For CCND2, this can be explained by enhanced chromatin accessibility and binding of the TF to the respective promoter[77,237]. Nevertheless, it might be possible that excessively high expression levels can inhibit cell growth or lead to apoptosis. Thus, other promoters inserted into the R26 locus may have to be tested to adapt the expression level of the *Maf* transgene.

4.2 The function of MAF in the malignant transformation of B cells

To gain more detailed information about the molecular function of MAF in MM pathology, the protein interactome of the TF was investigated *in vitro*. To this end, immunoprecipitation of endogenously overexpressed MAF in t(14;16)$^{+}$ human MM cell lines was carried out and coimmunoprecipitated proteins analyzed by mass spectrometry.

Lysis of human MM cells in a high salt containing buffer was especially successful to elute MAF from its main localization in the chromatin fraction of cells (Fig. 9) and preserved more interactions with other TFs than lysis in a modified RIPA buffer (Fig. 12). This is expected, since NaCl can disrupt charge-based protein-DNA bindings, and chromatin associated proteins are better eluted upon increasing concentration of NaCl[238].

Until today, only MAFA was found to bind P/CAF in animal model cell lines[135]. Strikingly, this work shows the first indication of also a putative MAF-P/CAF interaction in human MM cells (Fig. 11). Of note, previously reported interactions of MAF with the coactivators P300, CBP[136], and TBP[137] could not be detected. Interestingly, P/CAF is a co-activator with intrinsic histone acetylase activity[239,240] that can bind the preinitiation complex[241]. Indeed, increased chromatin accessibility in comparison to normal PCs is linked to MM pathology[242,243] and different accessibility has been found among the different MM subgroups[215]. Binding of MAF to chromatin modifiers like P/CAF could in part explain such different DNA accessibility in line with previously suggested pioneer activity of MAF[77]. Pioneer TFs can bind their target DNA motifs in heterochromatin and mediate stable chromatin remodeling[244].

Interestingly, many TFs previously reported to interact with MAF do not bind MAF in MM, including PAX6, HOXD12[130], MYB[131], ETS1[132] and NFATC3[133]. Surprisingly, no large MAF proteins or other AP1 factors were found in the interactome of MAF in HMCLs, since it was recently suggested that the malignant function of MAF in MM pathology requires its heterodimerization with other AP1 factors[96]. However, experiments with heterodimerization deficient mutants have shown that binding to FOS or JUN is not necessary for MAF induced transformation of chicken embryo fibroblasts[128]. In contrast, weak binding to MAFG peptides was detected by mass spectrometry under some conditions which were not significant, requiring further validation and analysis of their biological relevance. Of note, MAF and

MAFG share a 112 amino acids long sequence of 59 % homology and antibody cross reactivity must be considered.

Many of the TFs binding MAF have known functions in MM pathology, including NFKB1, NFKB2 and RELB. Elevated NFκB pathway activity is important in the (later) pathogenesis of MM. This is illustrated by from a wide range of mutations in genes of the canonical and alternative NFκB pathways leading to the inactivation of negative regulators (e.g. TRAF2, TRAF3, CYLD) or constitutive activation positive regulators such as NFKB1, NFKB2, CD40, LTBR, TACI, and NIK[245,246]. With regard to MAF, TRAF2 mutations frequently arise among the t(14;16) sugroup of patients[153], however a mechanistic cooperation with MAF is unknown. Furthermore, RUNX proteins are involved in MM pathology via their interaction with IKZF1 and IKZF3 in a complex with CBFB, inhibiting their CRBN-mediated degradation[247]. Strikingly, all proteins from that complex were found to interact with MAF. ILF2 and ILF3 bind to MAF, stabilize RNA, and facilitate splicing of DNA damaging control genes in MM[100]. Interestingly, ILF2 is overexpressed by +1q, an early genomic aberration highly associated with t(14;16)[153].

Applying a glutaraldehyde based crosslinking approach to the lysis of MM cell lines widens the possibilities to perform protein interaction analysis of MAF (Fig. 13). Crosslinking of MAF resulted in the appearance of an approximately 100 kDa band in the Western blot, which presumably contains MAF homodimers or other MAF complexes, the exact composition of which will be exciting to investigate. The crosslinking approach is furthermore applicable to mouse B cells and can be combined with immunoprecipitation. As a major advantage, crosslinking prior to immunoprecipitation will allow to study also weak or transient protein interactions, including enzymes conferring posttranslational modifications like phosphorylation, SUMOylation and ubiquitination, known to interfere with MAF activity[123,135,164–175].

To further investigate the biological relevance of candidate MAF interactors, different strategies can be followed. To find common mechanism between different MAF TFs in MM pathology, the conducted coimmunoprecipitation experiments could be repeated precipitating MAFB and MAFA in respective t(14;20)$^{+}$ and t(8;14)$^{+}$ cell lines. Further functional validation can be achieved by using CRISPR/Cas9 or shRNA knockout screens to investigate oncogene dependencies. Such methods have previously underlined the role of IRF4 in MM[70]. Motif analysis of both MAF CHIP-seq and ATAC-seq results from human

MM cell lines with t(14;16) will provide further information on relevant TFs possibly interacting with MAF in MM pathogenesis. Of note, both analyses have recently been published[77]. A multiomics approach, meaning the overlay of these four high-throughput analyses, i.e., CHIP-seq, ATAC-seq, CRIPSR-screen and proteomics would help to find the most important interacting TFs of MAF in human MM biology. Knockout screens could for example confirm dependency on CBFB, RELB, NFKB1, NFKB2, RUNX3 and MAFG in MM1.S and RPMI-8226 cell lines as well as on RUNX1 in the RPMI-8226 cell line, all candidates that showed binding to MAF in the coimmunoprecipitation approach (Fig. 11). Interestingly, footprint analysis of MAF CHIP-seq data found significant enrichment of RUNX motifs[77], indicating functional MAF-RUNX cooperation in MM pathology. CBFB and MAZ, bound by MAF, belong to a gene regulatory network of six TFs (CXXC1, BPTF, MAZ, KLF13, CBFB and RFX5) found in all MM subgroups[77].

Of note, all these experiments rely on the model system of established human MM cell lines or primary patient cells. It must be noted that the biology of HMCLs, often originating from PC leukemia rather than from MM, can be significantly different to the molecular and biological environment of the COO in which MAF transcriptional activity initially arises. Therefore, as a final part of this work, a screening approach was developed that uses a model system much closer to the putative COO, namely activated mouse B cells. First, proof was established that putative MAF interactors can be sufficiently coexpressed in *Maf*-expressing B cells from Cγ1-cre; R26 MafstopF mice following retroviral transduction (Fig. 13). The subsequent measurement of MAF specific MM target genes, like *Itgb7* allows to evaluate the transcriptional activity of formed MAF-protein complexes. Besides *Itgb7*, *Ccnd2* can also be used as an additional readout gene since it is an important gene in MM pathology and directly regulated by MAF[154,215]. However, its high baseline expression in activated B cells must considered[2]. An even closer model of the GC reaction can be achieved *ex vivo*, by the coculture of B cells with so-termed LB40 feeder cells enabling continuous provision of CD40L and BAFF in combination with IL4 or IL21[233]. This approach has been followed in our laboratory as a continuation of my work by Angelos Rigopoulos. Based on the findings from the proteomic approach and the in vitro co-transfection protocol presented here, he investigated the effect of coexpressing *Maf* and different molecules of the NFκB pathway[232]. However, no survival advantage was found for mouse B cells coexpressing *Maf* with *Rel*, *Rela*, *Relb*, *p52* or *Nfkb2* (*p100*)[232]. To study protein interactions *in vivo*, putative interactors could be coexpressed with *Maf* in Cγ1-cre(ERT2); R26 MafstopF

mice – preferentially upon tamoxifen application at days 10-12 p.i. to target transgene activation to class-switched GC B cells. Along that line, in our laboratory, Wiebke Winkler tried to rescue the counter-selection of *Maf*-expressing GC B cells by coexpressing *Maf* together with a constitutive active mutant of *Ikk2* in mouse GC B cells as such introducing a classical secondary genetic event[178]. Of note, canonical NFκB pathway activation could partly rescue the reduction of splenic and BMPC in these mice, however GC B cells were still dramatically reduced in number[178]. Since Ikk2ca specifically activates the canonical pathway[248], the role of alternative NFκB signaling in *Maf*-expressing B cell should be additionally analyzed *in vivo* e.g., by use of the R26 NIKstopF strain[249].

4.3 Concluding remarks, summary and outlook

In conclusion, the use of a temporarily controlled conditional gene targeting approach (based on the Cγ1-creERT2 strain) allowed to specifically overexpress *Maf* in extrafollicular PBs, peak GC B cells and differentiating PCs. As a major advancement to the previous Cγ1-cre model, tamoxifen application at days 10-12 p.i. indeed induced *Maf* activation in class-switched GC B cells, the presumed COO of t(14;16)$^{+}$ MM. However, as before, activation of the *Maf* transgene resulted in a reduction of absolute numbers of splenic GC B cells, splenic PB/PCs, and BMPCs whereby delayed transgene expression attenuated the counter-selection of *Maf*-expressing GC B cells. The counter-selection decreased towards later differentiation stages. The reasons for this are not fully understood and it is not clear to the last whether overexpression of *Maf* drives terminal B cell differentiation *per se*, or if its expression is simply better tolerated in terminally differentiated PCs. Some evidence argues for the latter, including the upregulation of *Itgb7* in *Maf*-expressing B cells and the independency of the BMPC population from the size of its precursor populations. However, final proof of a GC origin of *Maf*-expressing BMPCs is lacking. Based on additional data obtained in this thesis, reduced proliferation of GC B cells and immunosurveillance mechanisms by T cells could largely be excluded as reasons for the apparent counter-selection.

It must be noted that the investigation of the impact of *Maf* on B cell differentiation was mainly based on immunophenotypic characterization of B cell populations in *Maf*-transgenic mice. As knowledge of the precise function of MAF in MM continues to increase, future work on *Maf*-based mouse model should also use molecular biology approaches as a read-out of

MAF activity. This should include the ongoing work of RNA-seq of *Maf*-expressing B cell and PC populations and the investigation of MAF-mediated changes in chromatin accessibility by ATAC-seq, CHIP-seq and/or newly arising low input techniques such as CUT&Tag[250]. Furthermore, protein-protein interactions of MAF in mouse B and PCs can be assessed by immunoprecipitation and mass spectrometry with the aim of comparing the functional interactome of MAF in the mouse model with that derived from human MM cells.

The present work and the remaining open questions underscored the difficulties and challenges that arise during the establishment of appropriate models for human cancer development[251]. Such models are necessary to test or screen for new therapeutic options and drugs and to answer molecular questions related to the pathogenesis of human malignancies. At the same time, however, the development of the model itself generates an immense amount of knowledge.

It should be noted that the overexpression of a single oncogene in mice offers the unique possibility to change a single variable and subsequently analyze the consequences on the transformation of B cells, as successfully done for MMSET and CCND1 in our laboratories (by Wiebke Winkler, Research groups Martin Janz and Klaus Rajewsky)[177]. On the other hand, there are limitations of this simplified gene targeting approach. For example, the transgenic mice show an isogenic background with no consideration of risk variants that can influence tumor development. Furthermore, they live under almost sterile conditions, a fact that can constitute a major limiting factor given the importance of the immune response and the strong interaction of myeloma cells with the BM microenvironment[5]. In addition, the impact of heterozygotic WWOX deletion that accompany the t(14;16)[152,153] translocation is not considered in the current approach that is solely based on the overexpression of *Maf*[178]. Moreover, not all human genes have murine analogues, for example the mouse genome contains only one APOBEC3-encoding gene whereas the human genome contains several APOBEC3 variants. To overcame certain limitations, the use of selected additional models will be helpful for future work. Thus, in addition to mouse models and cell lines with known (mono) genetic background, primary patient cells, patient-derived induced pluripotent stem cells and organoid like models can be used too[251]. This has been done to study the complete reciprocal t(11;14) in normal B cell derived induced pluripotent stem cells[252].

In conclusion, transgenic *Maf* expression was successfully targeted to class-switched GC B cells, the presumed COO of t(14;16)$^{+}$ MM. However, *Maf*-expressing mouse GC B cells were

still counter-selected which was most likely not due to impairment of proliferation or enhanced T cell surveillance. Future work should focus on the molecular biologic impact of *Maf* expression in mouse B cells and investigate its transforming mode of function. Regarding the latter, an unbiased coimmunoprecipitation coupled to mass spectrometry approach identified NFKB and RUNX proteins as putative MAF partners in t(14;16) HMCLs. Such results should be verified in appropriate COO-close models like in the retrovirus-based screen presented here, eventually helping to improve current *Maf*-based mouse models of MM.

5. References

1. Rajewsky, K. The advent and rise of monoclonal antibodies. *Nature* **575,** 47–49 (2019).

2. Silva, N. S. & Klein, U. Dynamics of B cells in germinal centres. *Nature Reviews Immunology* **15,** 137–148 (2015).

3. Nutt, S. L., Hodgkin, P. D., Tarlinton, D. M. & Corcoran, L. M. The generation of antibody-secreting plasma cells. *Nature Reviews Immunology* **15,** 160–171 (2015).

4. Manier, S., Salem, K. Z., Park, J., Landau, D. A., Getz, G. & Ghobrial, I. M. Genomic complexity of multiple myeloma and its clinical implications. *Nature Reviews Clinical Oncology* **14,** 100–113 (2017).

5. Hideshima, T., Mitsiades, C., Tonon, G., Richardson, P. G. & Anderson, K. C. Understanding multiple myeloma pathogenesis in the bone marrow to identify new therapeutic targets. *Nature Reviews Cancer* **7,** nrc2189 (2007).

6. Jones, H. B. On a new substance occurring in the urine of a patient with mollities ossium. *Abstr Pap Commun Royal Soc Lond* **5,** 673–673 (1851).

7. Korngold, L. & Lipari, R. Multiple-myeloma proteins. III. The antigenic relationship of Bence Jones proteins to normal gamma-globulin and multiple-myeloma serum proteins. *Cancer* **9,** 262–272 (1956).

8. Barwick, B. G., Gupta, V. A., Vertino, P. M. & Boise, L. H. Cell of Origin and Genetic Alterations in the Pathogenesis of Multiple Myeloma. *Front Immunol* **10,** 1121 (2019).

9. Morgan, G. J., Walker, B. A. & Davies, F. E. The genetic architecture of multiple myeloma. *Nat Rev Cancer* **12,** 335–348 (2012).

10. Becker, N. Multiple Myeloma. *Recent Results Canc* **183,** 25–35 (2011).

11. Du, Z., Weinhold, N., Song, G. C., Rand, K. A., Berg, D. J. V. D., Hwang, A. E., Sheng, X., Hom, V., Ailawadhi, S., Nooka, A. K., Singhal, S., Pawlish, K., Peters, E. S., Bock, C., Mohrbacher, A., Stram, A., Berndt, S. I., Blot, W. J., Casey, G., Stevens, V. L., Kittles, R., Goodman, P. J., Diver, W. R., Hennis, A., Nemesure, B., Klein, E. A., Rybicki, B. A., Stanford, J. L., Witte, J. S., Signorello, L., John, E. M., Bernstein, L., Stroup, A. M., Stephens, O. W., Zangari, M., Rhee, F. V., Olshan, A., Zheng, W., Hu, J. J., Ziegler, R., Nyante, S. J., Ingles, S. A., Press, M. F., Carpten, J. D., Chanock, S. J., Mehta, J., Colditz, G. A., Wolf, J., Martin, T. G., Tomasson, M., Fiala, M. A., Terebelo, H., Janakiraman, N., Kolonel, L., Anderson, K. C., Marchand, L. L., Auclair, D., Chiu, B. C.-H., Ziv, E., Stram, D., Vij, R., Bernal-Mizrachi, L., Morgan, G. J., Zonder, J. A., Huff, C. A., Lonial, S., Orlowski, R. Z., Conti, D. V., Haiman, C. A. & Cozen, W. A meta-analysis of genome-wide association studies of multiple myeloma among men and women of African ancestry. *Blood Adv* **4,** 181–190 (2020).

12. Kristinsson, S. Y., Björkholm, M., Goldin, L. R., Blimark, C., Mellqvist, U., Wahlin, A., Turesson, I. & Landgren, O. Patterns of hematologic malignancies and solid tumors among 37,838 first-degree relatives of 13,896 patients with multiple myeloma in Sweden. *Int J Cancer* **125,** 2147–2150 (2009).

13. Röllig, C., Knop, S. & Bornhäuser, M. Multiple myeloma. *Lancet* **385,** 2197–2208 (2015).

14. Kyle, R. A. & Rajkumar, S. V. Monoclonal gammopathy of undetermined significance and smouldering multiple myeloma: emphasis on risk factors for progression. *Brit J Haematol* **139,** 730–743 (2007).

15. Rajkumar, S. V., Dimopoulos, M. A., Palumbo, A., Blade, J., Merlini, G., Mateos, M.-V., Kumar, S., Hillengass, J., Kastritis, E., Richardson, P., Landgren, O., Paiva, B., Dispenzieri, A., Weiss, B., LeLeu, X., Zweegman, S., Lonial, S., Rosinol, L., Zamagni, E., Jagannath, S., Sezer, O., Kristinsson, S. Y., Caers, J., Usmani, S. Z., Lahuerta, J. J., Johnsen, H. E., Beksac, M., Cavo, M., Goldschmidt, H., Terpos, E., Kyle, R. A., Anderson, K. C., Durie, B. G. M. & Miguel, J. F. S. International Myeloma Working Group updated criteria for the diagnosis of multiple myeloma. *Lancet Oncol* **15,** e538–e548 (2014).

16. Walker, Wardell, C., Melchor, L., Brioli, A., Johnson, D., Kaiser, M., Mirabella, F., Lopez-Corral, L., Humphray, S., Murray, L., Ross, M., Bentley, D., Gutiérrez, N., Garcia-Sanz, R., Miguel, S. J., Davies, F., Gonzalez, D. & Morgan, G. Intraclonal heterogeneity is a critical early event in the development of myeloma and precedes the development of clinical symptoms. *Leukemia* **28,** 384–390 (2014).

17. Terpos, E., Berenson, J., Raje, N. & Roodman, G. D. Management of bone disease in multiple myeloma. *Expert Rev Hematol* **7,** 113–125 (2014).

18. Lieber, M. R. Mechanisms of human lymphoid chromosomal translocations. *Nature Reviews Cancer* **16,** 387–398 (2016).

19. Jankovic, M., Casellas, R., Yannoutsos, N., Wardemann, H. & Nussenzweig, M. C. RAGs and Regulation of Autoantibodies. *Immunology* **22,** 485–501 (2004).

20. Jourdan, M., Caraux, A., Caron, G., Robert, N., Fiol, G., Rème, T., Bolloré, K., Vendrell, J.-P., Gallou, S., Mourcin, F., Vos, J., Kassambara, A., Duperray, C., Hose, D., Fest, T., Tarte, K. & Klein, B. Characterization of a Transitional Preplasmablast Population in the Process of Human B Cell to Plasma Cell Differentiation. *The Journal of Immunology* **187,** 3931–3941 (2011).

21. Srinivasan, L., Sasaki, Y., Calado, D. P., Zhang, B., Paik, J. H., DePinho, R. A., Kutok, J. L., Kearney, J. F., Otipoby, K. L. & Rajewsky, K. PI3 Kinase Signals BCR-Dependent Mature B Cell Survival. *Cell* **139,** 573–586 (2009).

22. Zhang, Y., Garcia-Ibanez, L. & Toellner, K. Regulation of germinal center B-cell differentiation. *Immunological Reviews* **270,** 8–19 (2016).

23. Kouzine, F., Wojtowicz, D., Yamane, A., Resch, W., Kieffer-Kwon, K.-R., Bandle, R., Nelson, S., Nakahashi, H., Awasthi, P., Feigenbaum, L., Menoni, H., Hoeijmakers, J., Vermeulen, W., Ge, H., Przytycka, T. M., Levens, D. & Casellas, R. Global Regulation of Promoter Melting in Naive Lymphocytes. *Cell* **153,** 988–999 (2013).

24. Nie, Z., Hu, G., Wei, G., Cui, K., Yamane, A., Resch, W., Wang, R., Green, D. R., Tessarollo, L., Casellas, R., Zhao, K. & Levens, D. c-Myc Is a Universal Amplifier of Expressed Genes in Lymphocytes and Embryonic Stem Cells. *Cell* **151,** 68–79 (2012).

25. Kieffer-Kwon, K.-R., Nimura, K., Rao, S. S. P., Xu, J., Jung, S., Pekowska, A., Dose, M., Stevens, E., Mathe, E., Dong, P., Huang, S.-C., Ricci, M. A., Baranello, L., Zheng, Y., Ardori, F. T., Resch, W., Stavreva, D., Nelson, S., McAndrew, M., Casellas, A., Finn, E., Gregory, C., Hilaire, B. G. St., Johnson, S. M., Dubois, W., Cosma, M. P., Batchelor, E., Levens, D., Phair, R. D., Misteli, T., Tessarollo, L., Hager, G., Lakadamyali, M., Liu, Z., Floer, M., Shroff, H., Aiden, E. L. & Casellas, R. Myc Regulates Chromatin Decompaction and Nuclear Architecture during B Cell Activation. *Mol Cell* **67,** 566-578.e10 (2017).

26. Basso, K. & Dalla-Favera, R. Germinal centres and B cell lymphomagenesis. *Nature Reviews Immunology* **15,** 172–184 (2015).

27. Holmes, A. B., Corinaldesi, C., Shen, Q., Kumar, R., Compagno, N., Wang, Z., Nitzan, M., Grunstein, E., Pasqualucci, L., Dalla-Favera, R. & Basso, K. Single-cell analysis of germinal-center B cells informs on lymphoma cell of origin and outcome. *J Exp Med* **217,** (2020).

28. Roco, J. A., Mesin, L., Binder, S. C., Nefzger, C., Gonzalez-Figueroa, P., Canete, P. F., Ellyard, J., Shen, Q., Robert, P. A., Cappello, J., Vohra, H., Zhang, Y., Nowosad, C. R., Schiepers, A., Corcoran, L. M., Toellner, K.-M., Polo, J. M., Meyer-Hermann, M., Victora, G. & Vinuesa, C. G. Class-Switch Recombination Occurs Infrequently in Germinal Centers. *Immunity* (2019). doi:10.1016/j.immuni.2019.07.001

29. Paus, D., Phan, T. G., Chan, T. D., Gardam, S., Basten, A. & Brink, R. Antigen recognition strength regulates the choice between extrafollicular plasma cell and germinal center B cell differentiation. *J Exp Medicine* **203,** 1081–1091 (2006).

30. O'Connor, B. P., Vogel, L. A., Zhang, W., Loo, W., Shnider, D., Lind, E. F., Ratliff, M., Noelle, R. J. & Erickson, L. D. Imprinting the Fate of Antigen-Reactive B Cells through the Affinity of the B Cell Receptor. *J Immunol* **177,** 7723–7732 (2006).

31. Kitano, M., Moriyama, S., Ando, Y., Hikida, M., Mori, Y., Kurosaki, T. & Okada, T. Bcl6 Protein Expression Shapes Pre-Germinal Center B Cell Dynamics and Follicular Helper T Cell Heterogeneity. *Immunity* **34,** 961–972 (2011).

32. Weisel, F. J., Zuccarino-Catania, G. V., Chikina, M. & Shlomchik, M. J. A Temporal Switch in the Germinal Center Determines Differential Output of Memory B and Plasma Cells. *Immunity* **44,** 116–130 (2016).

33. Kallies, A., Hasbold, J., Fairfax, K., Pridans, C., Emslie, D., McKenzie, B. S., Lew, A. M., Corcoran, L. M., Hodgkin, P. D., Tarlinton, D. M. & Nutt, S. L. Initiation of Plasma-Cell Differentiation Is Independent of the Transcription Factor Blimp-1. *Immunity* **26,** 555–566 (2007).

34. Sabbattini, P., Canzonetta, C., Sjoberg, M., Nikic, S., Georgiou, A., Kemball-Cook, G., Auner, H. W. & Dillon, N. A novel role for the Aurora B kinase in epigenetic marking of silent chromatin in differentiated postmitotic cells. *Embo J* **26,** 4657–4669 (2007).

35. Herviou, L., Jourdan, M., Martinez, A.-M., Cavalli, G. & Moreaux, J. EZH2 is overexpressed in transitional preplasmablasts and is involved in human plasma cell differentiation. *Leukemia* **33,** 2047–2060 (2019).

36. Mohr, E., Serre, K., Manz, R. A., Cunningham, A. F., Khan, M., Hardie, D. L., Bird, R. & MacLennan, I. C. M. Dendritic Cells and Monocyte/Macrophages That Create the IL-6/APRIL-Rich Lymph Node Microenvironments Where Plasmablasts Mature. *J Immunol* **182,** 2113–2123 (2009).

37. Kabashima, K., Haynes, N. M., Xu, Y., Nutt, S. L., Allende, M. L., Proia, R. L. & Cyster, J. G. Plasma cell S1P1 expression determines secondary lymphoid organ retention versus bone marrow tropism. *J Exp Medicine* **203,** 2683–2690 (2006).

38. Winkelmann, R., Sandrock, L., Porstner, M., Roth, E., Mathews, M., Hobeika, E., Reth, M., Kahn, M. L., Schuh, W. & Jäck, H.-M. B cell homeostasis and plasma cell homing controlled by Krüppel-like factor 2. *Proc National Acad Sci* **108,** 710–715 (2011).

39. Chevrier, S., Emslie, D., Shi, W., Kratina, T., Wellard, C., Karnowski, A., Erikci, E., Smyth, G. K., Chowdhury, K., Tarlinton, D. & Corcoran, L. M. The BTB-ZF transcription factor Zbtb20 is driven by Irf4 to promote plasma cell differentiation and longevityZbtb20 regulates late B cell differentiation. *J Exp Medicine* **211,** 827–840 (2014).

40. Ochiai, K., Kondo, H., Okamura, Y., Shima, H., Kurokochi, Y., Kimura, K., Funayama, R., Nagashima, T., Nakayama, K., Yui, K., Kinoshita, K. & Igarashi, K. Zinc finger–IRF composite elements bound by Ikaros/IRF4 complexes function as gene repression in plasma cell. *Blood Adv* **2,** 883–894 (2018).

41. Cortés, M. & Georgopoulos, K. Aiolos Is Required for the Generation of High Affinity Bone Marrow Plasma Cells Responsible for Long-Term Immunity. *J Exp Medicine* **199,** 209–219 (2004).

42. Rozanski, C. H., Arens, R., Carlson, L. M., Nair, J., Boise, L. H., Chanan-Khan, A. A., Schoenberger, S. P. & Lee, K. P. Sustained antibody responses depend on CD28 function in bone marrow–resident plasma cells. *J Exp Medicine* **208,** 1435–1446 (2011).

43. Wols, H. A. M., Underhill, G. H., Kansas, G. S. & Witte, P. L. The Role of Bone Marrow-Derived Stromal Cells in the Maintenance of Plasma Cell Longevity. *J Immunol* **169,** 4213–4221 (2002).

44. Chevrier, S., Genton, C., Kallies, A., Karnowski, A., Otten, L. A., Malissen, B., Malissen, M., Botto, M., Corcoran, L. M., Nutt, S. L. & Acha-Orbea, H. CD93 is required for maintenance of antibody secretion and persistence of plasma cells in the bone marrow niche. *Proc National Acad Sci* **106,** 3895–3900 (2009).

45. Tokoyoda, K., Egawa, T., Sugiyama, T., Choi, B.-I. & Nagasawa, T. Cellular Niches Controlling B Lymphocyte Behavior within Bone Marrow during Development. *Immunity* **20,** 707–718 (2004).

46. Chu, V. T. & Berek, C. Immunization induces activation of bone marrow eosinophils required for plasma cell survival. *European Journal of Immunology* **42,** 130–137 (2012).

47. Carrington, E. M., Vikstrom, I. B., Light, A., Sutherland, R. M., Londrigan, S. L., Mason, K. D., Huang, D. C. S., Lew, A. M. & Tarlinton, D. M. BH3 mimetics antagonizing restricted prosurvival Bcl-2 proteins represent another class of selective immune modulatory drugs. *Proc National Acad Sci* **107,** 10967–10971 (2010).

48. Tangye, S. G. Staying alive: regulation of plasma cell survival. *Trends in Immunology* **32,** 595–602 (2011).

49. Peperzak, V., Vikström, I., Walker, J., Glaser, S. P., LePage, M., Coquery, C. M., Erickson, L. D., Fairfax, K., Mackay, F., Strasser, A., Nutt, S. L. & Tarlinton, D. M. Mcl-1 is essential for the survival of plasma cells. *Nat Immunol* **14,** 290–297 (2013).

50. Nussenzweig, A. & Nussenzweig, M. C. Origin of Chromosomal Translocations in Lymphoid Cancer. *Cell* **141,** 27–38 (2010).

51. Và, M. C. D., Ziccheddu, B., Maeda, A., Bagnoli, F., Perrone, G. & Bolli, N. A Journey Through Myeloma Evolution: From the Normal Plasma Cell to Disease Complexity. *Hemasphere* **4,** e502-1–13 (2020).

52. Bakkus, M., Heirman, C., Riet, I. V., Camp, B. V. & Thielemans, K. Evidence that multiple myeloma Ig heavy chain VDJ genes contain somatic mutations but show no intraclonal variation. *Blood* **80,** 2326–2335 (1992).

53. Cowan, G., Weston-Bell, N. J., Bryant, D., Seckinger, A., Hose, D., Zojer, N. & Sahota, S. S. Massive parallel IGHV gene sequencing reveals a germinal center pathway in origins of human multiple myeloma. *Oncotarget* **6,** 13229–13240 (2015).

54. Rettig, M., Vescio, R., Cao, J., Wu, C., Lee, J., Han, E., DerDanielian, M., Newman, R., Hong, C., Lichtenstein, A. & Berenson, J. VH gene usage is multiple myeloma: complete absence of the VH4.21 (VH4- 34) gene. *Blood* **87,** 2846–2852 (1996).

55. Walker, B. A., Wardell, C. P., Johnson, D. C., Kaiser, M. F., Begum, D. B., Dahir, N. B., Ross, F. M., Davies, F. E., Gonzalez, D. & Morgan, G. J. Characterization of IGH locus breakpoints in multiple myeloma indicates a subset of translocations appear to occur in pregerminal center B cells. *Blood* **121,** 3413–3419 (2013).

56. Vicente-Dueñas, C., Romero-Camarero, I., González-Herrero, I., Alonso-Escudero, E., Abollo-Jiménez, F., Jiang, X., Gutierrez, N. C., Orfao, A., Marín, N., Villar, L. M., Criado, M. C. F., Pintado, B., Flores, T., Alonso-López, D., Rivas, J. D. L., Jiménez, R., Criado, F. J. G., Cenador, M. B. G., Lossos, I. S., Cobaleda, C. & Sánchez-García, I. A novel molecular mechanism involved in multiple myeloma development revealed by targeting MafB to haematopoietic progenitors. *Embo J* **31,** 3704–3717 (2012).

57. Morito, N., Yoh, K., Maeda, A., Nakano, T., Fujita, A., Kusakabe, M., Hamada, M., Kudo, T., Yamagata, K. & Takahashi, S. A Novel Transgenic Mouse Model of the Human Multiple Myeloma Chromosomal Translocation t(14;16)(q32;q23). *Cancer Research* **71,** 339–348 (2011).

58. Maura, F., Rustad, E. H., Yellapantula, V., Łuksza, M., Hoyos, D., Maclachlan, K. H., Diamond, B. T., Greenbaum, B. D., Morgan, G., Lesokhin, A., Papaemmanuil, E. & Landgren, O. Role of AID in the temporal pattern of acquisition of driver mutations in multiple myeloma. *Leukemia* **34,** 1476–1480 (2020).

59. Dhodapkar, M. V. MGUS to myeloma: a mysterious gammopathy of underexplored significance. *Blood* **128,** 2599–2606 (2016).

60. Chapman, M. A., Lawrence, M. S., Keats, J. J., Cibulskis, K., Sougnez, C., Schinzel, A. C., Harview, C. L., Brunet, J.-P., Ahmann, G. J., Adli, M., Anderson, K. C., Ardlie, K. G., Auclair, D., Baker, A., Bergsagel, P. L., Bernstein, B. E., Drier, Y., Fonseca, R., Gabriel, S. B., Hofmeister, C. C., Jagannath, S., Jakubowiak, A. J., Krishnan, A., Levy, J.,

Liefeld, T., Lonial, S., Mahan, S., Mfuko, B., Monti, S., Perkins, L. M., Onofrio, R., Pugh, T. J., Rajkumar, S. V., Ramos, A. H., Siegel, D. S., Sivachenko, A., Stewart, A. K., Trudel, S., Vij, R., Voet, D., Winckler, W., Zimmerman, T., Carpten, J., Trent, J., Hahn, W. C., Garraway, L. A., Meyerson, M., Lander, E. S., Getz, G. & Golub, T. R. Initial genome sequencing and analysis of multiple myeloma. *Nature* **471,** 467–472 (2011).

61. Vogelstein, B., Papadopoulos, N., Velculescu, V. E., Zhou, S., Diaz, L. A. & Kinzler, K. W. Cancer Genome Landscapes. *Science* **339,** 1546–1558 (2013).

62. Ley, T. J., Mardis, E. R., Ding, L., Fulton, B., McLellan, M. D., Chen, K., Dooling, D., Dunford-Shore, B. H., McGrath, S., Hickenbotham, M., Cook, L., Abbott, R., Larson, D. E., Koboldt, D. C., Pohl, C., Smith, S., Hawkins, A., Abbott, S., Locke, D., Hillier, L. W., Miner, T., Fulton, L., Magrini, V., Wylie, T., Glasscock, J., Conyers, J., Sander, N., Shi, X., Osborne, J. R., Minx, P., Gordon, D., Chinwalla, A., Zhao, Y., Ries, R. E., Payton, J. E., Westervelt, P., Tomasson, M. H., Watson, M., Baty, J., Ivanovich, J., Heath, S., Shannon, W. D., Nagarajan, R., Walter, M. J., Link, D. C., Graubert, T. A., DiPersio, J. F. & Wilson, R. K. DNA sequencing of a cytogenetically normal acute myeloid leukaemia genome. *Nature* **456,** 66–72 (2008).

63. Sahota, S., Leo, R., Hamblin, T. & Stevenson, F. Ig VH gene mutational patterns indicate different tumor cell status in human myeloma and monoclonal gammopathy of undetermined significance. *Blood* **87,** 746–755 (1996).

64. Zojer, N., Ludwig, H., Fiegl, M., Stevenson, F. K. & Sahota, S. S. Patterns of somatic mutations in VH genes reveal pathways of clonal transformation from MGUS to multiple myeloma. *Blood* **101,** 4137–4139 (2003).

65. Rustad, E. H., Yellapantula, V., Leongamornlert, D., Bolli, N., Ledergor, G., Nadeu, F., Angelopoulos, N., Dawson, K. J., Mitchell, T. J., Osborne, R. J., Zicchedda, B., Carniti, C., Montefusco, V., Corradini, P., Anderson, K. C., Moreau, P., Papaemmanuil, E., Alexandrov, L. B., Puente, X. S., Campo, E., Siebert, R., Avet-Loiseau, H., Landgren, O., Munshi, N., Campbell, P. J. & Maura, F. Timing the initiation of multiple myeloma. *Nat Commun* **11,** 1917 (2020).

66. Kuehl, M. W. & Bergsagel, L. P. Multiple myeloma: evolving genetic events and host interactions. *Nat Rev Cancer* **2,** 175–187 (2002).

67. Janz, S., Zhan, F., Sun, F., Cheng, Y., Pisano, M., Yang, Y., Goldschmidt, H. & Hari, P. Germline Risk Contribution to Genomic Instability in Multiple Myeloma. *Frontiers Genetics* **10,** 424 (2019).

68. Weinhold, N., Johnson, D. C., Rawstron, A. C., Försti, A., Doughty, C., Vijayakrishnan, J., Broderick, P., Dahir, N. B., Begum, D. B., Hosking, F. J., Yong, K., Walker, B. A., Hoffmann, P., Mühleisen, T. W., Langer, C., Dörner, E., Jöckel, K.-H., Eisele, L., Nöthen, M. M., Hose, D., Davies, F. E., Goldschmidt, H., Morgan, G. J., Hemminki, K. & Houlston, R. S. Inherited genetic susceptibility to monoclonal gammopathy of unknown significance. *Blood* **123,** 2513–2517 (2014).

69. Went, M., consortium, T. P., Sud, A., Försti, A., Halvarsson, B.-M., Weinhold, N., Kimber, S., Duin, M. van, Thorleifsson, G., Holroyd, A., Johnson, D. C., Li, N., Orlando, G., Law, P. J., Ali, M., Chen, B., Mitchell, J. S., Gudbjartsson, D. F., Kuiper, R., Stephens, O. W., Bertsch, U., Broderick, P., Campo, C., Bandapalli, O. R., Einsele, H., Gregory, W. A., Gullberg, U., Hillengass, J., Hoffmann, P., Jackson, G. H., Jöckel, K.-H., Johnsson, E., Kristinsson, S. Y., Mellqvist, U.-H., Nahi, H., Easton, D., Pharoah, P., Dunning, A., Peto, J., Canzian, F., Swerdlow, A., Eeles, R. A., Kote-Jarai, Zs., Muir, K., Pashayan, N., Nickel, J., Nöthen, M. M., Rafnar, T., Ross, F. M., Filho, M. I. da S., Thomsen, H., Turesson, I., Vangsted, A., Andersen, N. F., Waage, A., Walker, B. A., Wihlborg, A.-K., Broyl, A., Davies, F. E., Thorsteinsdottir, U., Langer, C., Hansson, M., Goldschmidt, H., Kaiser, M., Sonneveld, P., Stefansson, K., Morgan, G. J., Hemminki, K., Nilsson, B. & Houlston, R. S. Identification of multiple risk loci and regulatory mechanisms influencing susceptibility to multiple myeloma. *Nat Commun* **9,** 3707 (2018).

70. Shaffer, A. L., Emre, T. N., Lamy, L., Ngo, V. N., Wright, G., Xiao, W., Powell, J., Dave, S., Yu, X., Zhao, H., Zeng, Y., Chen, B., Epstein, J. & Staudt, L. M. IRF4 addiction in multiple myeloma. *Nature* **454,** 226 (2008).

71. Ohguchi, H., Hideshima, T., Bhasin, M. K., Gorgun, G. T., Santo, L., Cea, M., Samur, M. K., Mimura, N., Suzuki, R., Tai, Y.-T., Carrasco, R. D., Raje, N., Richardson, P. G., Munshi, N. C., Harigae, H., Sanda, T., Sakai, J. & Anderson, K. C. The KDM3A–KLF2–IRF4 axis maintains myeloma cell survival. *Nature Communications* **7,** 10258 (2016).

72. Fonseca, R., Barlogie, B., Bataille, R., Bastard, C., Bergsagel, L. P., Chesi, M., Davies, F. E., Drach, J., Greipp, P. R., Kirsch, I. R., Kuehl, M. W., Hernandez, J. M., Minvielle, S., Pilarski, L. M., Shaughnessy, J. D., Stewart, K. A. & Avet-Loiseau, H. Genetics and Cytogenetics of Multiple Myeloma A Workshop Report. *Cancer Res* **64,** 1546–1558 (2004).

73. Bergsagel, P. & Kuehl, W. Chromosome translocations in multiple myeloma. *Oncogene* **20,** 5611–22 (2001).

74. Weston-Bell, N., Gibson, J., John, M., Ennis, S., Pfeifer, S., Cezard, T., Ludwig, H., Collins, A., Zojer, N. & Sahota, S. S. Exome sequencing in tracking clonal evolution in multiple myeloma following therapy. *Leukemia* **27,** 1188–1191 (2013).

75. Kuehl, M. W. & Bergsagel, L. P. Molecular pathogenesis of multiple myeloma and its premalignant precursor. *Journal of Clinical Investigation* **122,** 3456–3463 (2012).

76. Zhan, F., Huang, Y., Colla, S., Stewart, J. P., Hanamura, I., Gupta, S., Epstein, J., Yaccoby, S., Sawyer, J., Burington, B., Anaissie, E., Hollmig, K., Pineda-Roman, M., Tricot, G., Rhee, F. van, Walker, R., Zangari, M., Crowley, J., Barlogie, B. & Shaughnessy, J. D. The molecular classification of multiple myeloma. *Blood* **108,** 2020–2028 (2006).

77. Alvarez-Benayas, J., Katsarou, A., Trasanidis, N., Chaidos, A., May, P. C., Ponnusamy, K., Xiao, X., Bua, M., Atta, M., Roberts, I. A., Auner, H. W., Hatjiharissi, E., Maria, P. M., Caputo, V. S., Ian, S. M. & Karadimitris, A. Over-accessible chromatin links myeloma initiating genetic events to oncogenic transcriptomes and aberrant transcription factor regulatory networks. *Biorxiv* 2020.06.11.140855 (2020). doi:10.1101/2020.06.11.140855

78. Avet-Loiseau, H., Facon, T., Grosbois, B., Magrangeas, F., Rapp, M.-J., Harousseau, J.-L., Minvielle, S. & Bataille, R. Oncogenesis of multiple myeloma: 14q32 and 13q chromosomal abnormalities are not randomly distributed, but correlate with natural history, immunological features, and clinical presentation. *Blood* **99,** 2185–2191 (2002).

79. Fonseca, R., Blood, E., Rue, M., Harrington, D., Oken, M. M., Kyle, R. A., Dewald, G. W., Ness, B. V., Wier, S. A. V., Henderson, K. J., Bailey, R. J. & Greipp, P. R. Clinical and biologic implications of recurrent genomic aberrations in myeloma. *Blood* **101,** 4569–4575 (2003).

80. Kuehl, W. M. & Bergsagel, P. L. Early Genetic Events Provide the Basis for a Clinical Classification of Multiple Myeloma. *ASH Education Program Book* **2005,** 346–352 (2005).

81. Samur, A. A., Minvielle, S., Shammas, M., Fulciniti, M., Magrangeas, F., Richardson, P. G., Moreau, P., Attal, M., Anderson, K. C., Parmigiani, G., Avet-Loiseau, H., Munshi, N. C. & Samur, M. K. Deciphering the chronology of copy number alterations in Multiple Myeloma. *Blood Cancer J* **9,** 39 (2019).

82. Chng, W. J., Santana-Dávila, R., Wier, S. A. V., Ahmann, G. J., Jalal, S. M., Bergsagel, P. L., Chesi, M., Trendle, M. C., Jacobus, S., Blood, E., Oken, M. M., Henderson, K., Kyle, R. A., Gertz, M. A., Lacy, M. Q., Dispenzieri, A., Greipp, P. R. & Fonseca, R. Prognostic factors for hyperdiploid-myeloma: effects of chromosome 13 deletions and IgH translocations. *Leukemia* **20,** 807–813 (2006).

83. Maura, F., Bolli, N., Angelopoulos, N., Dawson, K. J., Leongamornlert, D., Martincorena, I., Mitchell, T. J., Fullam, A., Gonzalez, S., Szalat, R., Abascal, F., Rodriguez-Martin, B., Samur, M. K., Glodzik, D., Roncador, M., Fulciniti, M., Tai, Y. T., Minvielle, S., Magrangeas, F., Moreau, P., Corradini, P., Anderson, K. C., Tubio, J. M. C., Wedge, D. C., Gerstung, M., Avet-Loiseau, H., Munshi, N. & Campbell, P. J. Genomic landscape and chronological reconstruction of driver events in multiple myeloma. *Nat Commun* **10,** 3835 (2019).

84. Küppers, R. & Dalla-Favera, R. Mechanisms of chromosomal translocations in B cell lymphomas. *Oncogene* **20,** 5580–5594 (2001).

85. González, D., Burg, M. van der, García-Sanz, R., Fenton, J. A., Langerak, A. W., González, M., Dongen, J. J. M. van, Miguel, J. F. S. & Morgan, G. J. Immunoglobulin gene rearrangements and the pathogenesis of multiple myeloma. *Blood* **110,** 3112–3121 (2007).

86. Walker, B. A., Wardell, C. P., Murison, A., Boyle, E. M., Begum, D. B., Dahir, N. M., Proszek, P. Z., Melchor, L., Pawlyn, C., Kaiser, M. F., Johnson, D. C., Qiang, Y.-W., Jones, J. R., Cairns, D. A., Gregory, W. M., Owen, R. G., Cook, G., Drayson, M. T., Jackson, G. H., Davies, F. E. & Morgan, G. J. APOBEC family mutational signatures are associated with poor prognosis translocations in multiple myeloma. *Nat Commun* **6,** 6997 (2015).

87. Chesi, M., Bergsagel, P., Brents, L., Smith, C., Gerhard, D. & Kuehl, W. Dysregulation of cyclin D1 by translocation into an IgH gamma switch region in two multiple myeloma cell lines [see comments]. *Blood* **88,** 674–681 (1996).

88. Poon, R. Y. C. Cell Cycle Oscillators, Methods and Protocols. *Methods Mol Biology* **1342,** 3–19 (2016).

89. Bustany, S., Bourgeais, J., Tchakarska, G., Body, S., Hérault, O., Gouilleux, F. & Sola, B. Cyclin D1 unbalances the redox status controlling cell adhesion, migration, and drug resistance in myeloma cells. *Oncotarget* **7,** 45214–45224 (2016).

90. Garlisi, C. G., Uss, A. S., Xiao, H., Tian, F., Sheridan, K. E., Wang, L., Billah, M. M., Egan, R. W., Stranick, K. S. & Umland, S. P. A Unique mRNA Initiated within a Middle Intron of WHSC1/MMSET Encodes a DNA Binding Protein That Suppresses HumanIL-5 Transcription. *Am J Resp Cell Mol* **24,** 90–98 (2001).

91. Kuo, A. J., Cheung, P., Chen, K., Zee, B. M., Kioi, M., Lauring, J., Xi, Y., Park, B. H., Shi, X., Garcia, B. A., Li, W. & Gozani, O. NSD2 Links Dimethylation of Histone H3 at Lysine 36 to Oncogenic Programming. *Mol Cell* **44,** 609–620 (2011).

92. Martinez-Garcia, E., Popovic, R., Min, D.-J., Sweet, S. M. M., Thomas, P. M., Zamdborg, L., Heffner, A., Will, C., Lamy, L., Staudt, L. M., Levens, D. L., Kelleher, N. L. & Licht, J. D. The MMSET histone methyl transferase switches global histone methylation and alters gene expression in t(4;14) multiple myeloma cells. *Blood* **117,** 211–220 (2011).

93. Bergsagel, P. L., Kuehl, W. M., Zhan, F., Sawyer, J., Barlogie, B. & Shaughnessy, J. Cyclin D dysregulation: an early and unifying pathogenic event in multiple myeloma. *Blood* **106,** 296–303 (2005).

94. Keats, J. J., Reiman, T., Maxwell, C. A., Taylor, B. J., Larratt, L. M., Mant, M. J., Belch, A. R. & Pilarski, L. M. In multiple myeloma, t(4;14)(p16;q32) is an adverse prognostic factor irrespective of FGFR3 expression. *Blood* **101,** 1520–1529 (2003).

95. Santra, M., Zhan, F., Tian, E., Barlogie, B. & Shaughnessy, J. A subset of multiple myeloma harboring the t(4;14)(p16;q32) translocation lacks FGFR3 expression but maintains anIGH/MMSET fusion transcript. *Blood* **101,** 2374–2376 (2003).

96. Eychène, A., Rocques, N. & Pouponnot, C. A new MAFia in cancer. *Nature Reviews Cancer* **8,** 683–693 (2008).

97. Mikulasova, A., Smetana, J., Wayhelova, M., Janyskova, H., Sandecka, V., Kufova, Z., Almasi, M., Jarkovsky, J., Gregora, E., Kessler, P., Wrobel, M., Walker, B. A., Wardell, C. P., Morgan, G. J., Hajek, R. & Kuglik, P. Genomewide profiling of copy-number alteration in monoclonal gammopathy of undetermined significance. *Eur J Haematol* **97,** 568–575 (2016).

98. Mikulasova, A., Wardell, C. P., Murison, A., Boyle, E. M., Jackson, G. H., Smetana, J., Kufova, Z., Pour, L., Sandecka, V., Almasi, M., Vsianska, P., Gregora, E., Kuglik, P., Hajek, R., Davies, F. E., Morgan, G. J. & Walker, B. A. The spectrum of somatic mutations in monoclonal gammopathy of undetermined significance indicates a less complex genomic landscape than that in multiple myeloma. *Haematologica* **102,** 1617–1625 (2017).

99. Kaufmann, H., Ackermann, J., Baldia, C., Nösslinger, T., Wieser, R., Seidl, S., Sagaster, V., Gisslinger, H., Jäger, U., Pfeilstöcker, M., Zielinski, C. & Drach, J. Both IGH translocations and chromosome 13q deletions are early events in monoclonal gammopathy of undetermined significance and do not evolve during transition to multiple myeloma. *Leukemia* **18,** 1879–82 (2004).

100. Marchesini, M., Ogoti, Y., Fiorini, E., Samur, A. A., Nezi, L., D'Anca, M., Storti, P., Samur, M. K., Ganan-Gomez, I., Fulciniti, M. T., Mistry, N., Jiang, S., Bao, N., Marchica, V., Neri, A., Bueso-Ramos, C., Wu, C.-J., Zhang,

L., Liang, H., Peng, X., Giuliani, N., Draetta, G., Clise-Dwyer, K., Kantarjian, H., Munshi, N., Orlowski, R., Garcia-Manero, G., DePinho, R. A. & Colla, S. ILF2 Is a Regulator of RNA Splicing and DNA Damage Response in 1q21-Amplified Multiple Myeloma. *Cancer Cell* **32,** 88-100.e6 (2017).

101. Rossi, A., Voigtlaender, M., Janjetovic, S., Thiele, B., Alawi, M., März, M., Brandt, A., Hansen, T., Radloff, J., Schön, G., Hegenbart, U., Schönland, S., Langer, C., Bokemeyer, C. & Binder, M. Mutational landscape reflects the biological continuum of plasma cell dyscrasias. *Blood Cancer J* **7,** e537–e537 (2017).

102. Lohr, J. G., Stojanov, P., Carter, S. L., Cruz-Gordillo, P., Lawrence, M. S., Auclair, D., Sougnez, C., Knoechel, B., Gould, J., Saksena, G., Cibulskis, K., McKenna, A., Chapman, M. A., Straussman, R., Levy, J., Perkins, L. M., Keats, J. J., Schumacher, S. E., Rosenberg, M., Consortium, T. M. M. R., Anderson, K. C., Richardson, P., Krishnan, A., Lonial, S., Kaufman, J., Siegel, D. S., Vesole, D. H., Roy, V., Rivera, C. E., Rajkumar, S. V., Kumar, S., Fonseca, R., Ahmann, G. J., Bergsagel, P. L., Stewart, A. K., Hofmeister, C. C., Efebera, Y. A., Jagannath, S., Chari, A., Trudel, S., Reece, D., Wolf, J., Martin, T., Zimmerman, T., Rosenbaum, C., Jakubowiak, A. J., Lebovic, D., Vij, R., Stockerl-Goldstein, K., Getz, G. & Golub, T. R. Widespread Genetic Heterogeneity in Multiple Myeloma: Implications for Targeted Therapy. *Cancer Cell* **25,** 91–101 (2014).

103. Hoang, P. H., Dobbins, S. E., Cornish, A. J., Chubb, D., Law, P. J., Kaiser, M. & Houlston, R. S. Whole-genome sequencing of multiple myeloma reveals oncogenic pathways are targeted somatically through multiple mechanisms. *Leukemia* **32,** 2459–2470 (2018).

104. Bolli, N., Avet-Loiseau, H., Wedge, D. C., Loo, P. V., Alexandrov, L. B., Martincorena, I., Dawson, K. J., Iorio, F., Nik-Zainal, S., Bignell, G. R., Hinton, J. W., Li, Y., Tubio, J. M. C., McLaren, S., Meara, S. O., Butler, A. P., Teague, J. W., Mudie, L., Anderson, E., Rashid, N., Tai, Y.-T., Shammas, M. A., Sperling, A. S., Fulciniti, M., Richardson, P. G., Parmigiani, G., Magrangeas, F., Minvielle, S., Moreau, P., Attal, M., Facon, T., Futreal, P. A., Anderson, K. C., Campbell, P. J. & Munshi, N. C. Heterogeneity of genomic evolution and mutational profiles in multiple myeloma. *Nat Commun* **5,** 2997 (2014).

105. Keats, J. J., Chesi, M., Egan, J. B., Garbitt, V. M., Palmer, S. E., Braggio, E., Wier, S. V., Blackburn, P. R., Baker, A. S., Dispenzieri, A., Kumar, S., Rajkumar, S. V., Carpten, J. D., Barrett, M., Fonseca, R., Stewart, A. K. & Bergsagel, P. L. Clonal competition with alternating dominance in multiple myeloma. *Blood* **120,** 1067–1076 (2012).

106. Alexandrov, L. B., Kim, J., Haradhvala, N. J., Huang, M. N., Ng, A. W. T., Wu, Y., Boot, A., Covington, K. R., Gordenin, D. A., Bergstrom, E. N., Islam, S. M. A., Lopez-Bigas, N., Klimczak, L. J., McPherson, J. R., Morganella, S., Sabarinathan, R., Wheeler, D. A., Mustonen, V., Alexandrov, L. B., Bergstrom, E. N., Boot, A., Boutros, P., Chan, K., Covington, K. R., Fujimoto, A., Getz, G., Gordenin, D. A., Haradhvala, N. J., Huang, M. N., Islam, S. M. A., Kazanov, M., Kim, J., Klimczak, L. J., Lopez-Bigas, N., Lawrence, M., Martincorena, I., McPherson, J. R., Morganella, S., Mustonen, V., Nakagawa, H., Ng, A. W. T., Polak, P., Prokopec, S., Roberts, S. A., Rozen, S. G., Sabarinathan, R., Saini, N., Shibata, T., Shiraishi, Y., Stratton, M. R., Teh, B. T., Vázquez-García, I., Wheeler, D. A., Wu, Y., Yousif, F., Yu, W., Getz, G., Rozen, S. G. & Stratton, M. R. The repertoire of mutational signatures in human cancer. *Nature* **578,** 94–101 (2020).

107. Alexandrov, L. B., Jones, P. H., Wedge, D. C., Sale, J. E., Campbell, P. J., Nik-Zainal, S. & Stratton, M. R. Clock-like mutational processes in human somatic cells. *Nat Genet* **47,** 1402–1407 (2015).

108. Lee, J. J.-K., Park, S., Park, H., Kim, S., Lee, J., Lee, J., Youk, J., Yi, K., An, Y., Park, I. K., Kang, C. H., Chung, D. H., Kim, T. M., Jeon, Y. K., Hong, D., Park, P. J., Ju, Y. S. & Kim, Y. T. Tracing Oncogene Rearrangements in the Mutational History of Lung Adenocarcinoma. *Cell* **177,** 1842-1857.e21 (2019).

109. Maura, F., Rustad, E. H., Boyle, E. M. & Morgan, G. J. Reconstructing the evolutionary history of multiple myeloma. *Best Pract Res Cl Ha* **33,** 101145 (2020).

110. Bosseboeuf, A., Feron, D., Tallet, A., Rossi, C., Charlier, C., Garderet, L., Caillot, D., Moreau, P., Cardó-Vila, M., Pasqualini, R., Arap, W., Nelson, A. D., Wilson, B. S., Perreault, H., Piver, E., Weigel, P., Girodon, F., Harb, J., Bigot-Corbel, E. & Hermouet, S. Monoclonal IgG in MGUS and multiple myeloma targets infectious pathogens. *Jci Insight* **2,** e95367 (2017).

111. Nair, S., Branagan, A. R., Liu, J., Boddupalli, C. S., Mistry, P. K. & Dhodapkar, M. V. Clonal Immunoglobulin against Lysolipids in the Origin of Myeloma. *New Engl J Medicine* **374,** 555–561 (2016).

112. Babel, N., Schwarzmann, F., Pruss, A., Volk, H.-D. & Reinke, P. Monoclonal gammopathy of undetermined significance (MGUS) is associated with an increased frequency of Epstein-Barr Virus (EBV) latently infected B lymphocytes in long-term renal transplant patients. *Transplant P* **36,** 2679–2682 (2004).

113. Bigot-Corbel, E., Gassin, M., Corre, I., Carrer, D. L., Delaroche, O. & Hermouet, S. Hepatitis C virus (HCV) infection, monoclonal immunoglobulin specific for HCV core protein, and plasma-cell malignancy. *Blood* **112,** 4357–4358 (2008).

114. Hermouet, S., Corre, I., Gassin, M., Bigot-Corbel, E., Sutton, C. A. & Casey, J. W. Hepatitis C Virus, Human Herpesvirus 8, and the Development of Plasma-Cell Leukemia. *New Engl J Medicine* **348,** 178–179 (2003).

115. López-Corral, L., Gutiérrez, N. C., Vidriales, M., Mateos, M., Rasillo, A., García-Sanz, R., Paiva, B. & Miguel, J. F. The Progression from MGUS to Smoldering Myeloma and Eventually to Multiple Myeloma Involves a Clonal Expansion of Genetically Abnormal Plasma Cells. *Clin Cancer Res* **17,** 1692–1700 (2011).

116. Ledergor, G., Weiner, A., Zada, M., Wang, S.-Y., Cohen, Y. C., Gatt, M. E., Snir, N., Magen, H., Koren-Michowitz, M., Herzog-Tzarfati, K., Keren-Shaul, H., Bornstein, C., Rotkopf, R., Yofe, I., David, E., Yellapantula, V., Kay, S., Salai, M., Yehuda, D., Nagler, A., Shvidel, L., Orr-Urtreger, A., Halpern, K., Itzkovitz, S., Landgren, O., San-Miguel, J., Paiva, B., Keats, J. J., Papaemmanuil, E., Avivi, I., Barbash, G. I., Tanay, A. & Amit, I. Single cell dissection of plasma cell heterogeneity in symptomatic and asymptomatic myeloma. *Nat Med* **24,** 1867–1876 (2018).

117. Rustad, E. H., Misund, K., Bernard, E., Coward, E., Yellapantula, V. D., Hultcrantz, M., Ho, C., Kazandjian, D., Korde, N., Mailankody, S., Keats, J. J., Akhlaghi, T., Viny, A. D., Mayman, D. J., Carroll, K., Patel, M., Famulare, C. A., Bruinink, D. H., Hutt, K., Jacobsen, A., Huang, Y., Miller, J. E., Maura, F., Papaemmanuil, E., Waage, A., Arcila, M. E. & Landgren, O. Stability and uniqueness of clonal immunoglobulin CDR3 sequences for MRD tracking in multiple myeloma. *Am J Hematol* **94,** 1364–1373 (2019).

118. Puig, N., Conde, I., Jiménez, C., Sarasquete, M. E., Balanzategui, A., Alcoceba, M., Quintero, J., Chillón, M. C., Sebastián, E., Corral, R., Marín, L., Gutiérrez, N. C., Mateos, M.-V., González-Díaz, M., San-Miguel, J. F. & García-Sanz, R. The predominant myeloma clone at diagnosis, CDR3 defined, is constantly detectable across all stages of disease evolution. *Leukemia* **29,** 1435–1437 (2015).

119. Chesi, M., Bergsagel, L. P., Shonukan, O. O., Martelli, M., Brents, L. A., Chen, T., Schröck, E., Ried, T. & Kuehl, M. W. Frequent Dysregulation of the c-maf Proto-Oncogene at 16q23 by Translocation to an Ig Locus in Multiple Myeloma. *Blood* **91,** 4457–4463 (1998).

120. Abdallah, N., Rajkumar, S. V., Greipp, P., Kapoor, P., Gertz, M. A., Dispenzieri, A., Baughn, L. B., Lacy, M. Q., Hayman, S. R., Buadi, F. K., Dingli, D., Go, R. S., Hwa, Y. L., Fonder, A., Hobbs, M., Lin, Y., Leung, N., Kourelis, T., Warsame, R., Siddiqui, M., Lust, J., Kyle, R. A., Bergsagel, L., Ketterling, R. & Kumar, S. K. Cytogenetic abnormalities in multiple myeloma: association with disease characteristics and treatment response. *Blood Cancer J* **10,** 82 (2020).

121. Usmani, S. Z., Heuck, C., Mitchell, A., Szymonifka, J., Nair, B., Hoering, A., Alsayed, Y., Waheed, S., Haider, S., Restrepo, A., Rhee, F. V., Crowley, J. & Barlogie, B. Extramedullary disease portends poor prognosis in multiple myeloma and is over-represented in high-risk disease even in the era of novel agents. *Haematologica* **97,** 1761–1767 (2012).

122. Boyd, K. D., Ross, F. M., Chiecchio, L., Dagrada, G. P., Konn, Z. J., Tapper, W. J., Walker, B. A., Wardell, C. P., Gregory, W. M., Szubert, A. J., Bell, S. E., Child, J. A., Jackson, G. H., Davies, F. E., Morgan, G. J. & Group, N. H. O. S. A novel prognostic model in myeloma based on co-segregating adverse FISH lesions and the ISS: analysis of patients treated in the MRC Myeloma IX trial. *Leukemia* **26,** 349–355 (2012).

123. Qiang, Y.-W., Ye, S., Chen, Y., Buros, A. F., Edmonson, R., Rhee, F. van, Barlogie, B., Epstein, J., Morgan, G. J. & Davies, F. E. MAF protein mediates innate resistance to proteasome inhibition therapy in multiple myeloma. *Blood* **128,** 2919–2930 (2016).

124. Vinson, C., Acharya, A. & Taparowsky, E. J. Deciphering B-ZIP transcription factor interactions in vitro and in vivo. *Biochimica Et Biophysica Acta Bba - Gene Struct Expr* **1759,** 4–12 (2006).

125. Kataoka, K., Noda, M. & Nishizawa, M. Transactivation activity of Maf nuclear oncoprotein is modulated by Jun, Fos and small Maf proteins. *Oncogene* **12,** 53–62 (1996).

126. Kataoka, K., Noda, M. & Nishizawa, M. Maf Nuclear Oncoprotein Recognizes Sequences Related to an AP-1 Site and Forms Heterodimers with both Fos and Jun. *Molecular and Cellular Biology* **14,** 700–712 (1994).

127. Yoshida, T., Ohkumo, T., Ishibashi, S. & Yasuda, K. The 5′-AT-rich half-site of Maf recognition element: a functional target for bZIP transcription factor Maf. *Nucleic Acids Research* **33,** 3465–3478 (2005).

128. Kataoka, K., Shioda, S., Yoshitomo-Nakagawa, K., Handa, H. & Nishizawa, M. Maf and Jun nuclear oncoproteins share downstream target genes for inducing cell transformation. *The Journal of biological chemistry* **276,** 36849–56 (2001).

129. Kerppola, T. & Curran, T. Maf and Nrl can bind to AP-1 sites and form heterodimers with Fos and Jun. *Oncogene* **9,** 675–84 (1994).

130. Kataoka, K., Yoshitomo-Nakagawa, K., Shioda, S. & Nishizawa, M. A Set of Hox Proteins Interact with the Maf Oncoprotein to Inhibit Its DNA Binding, Transactivation, and Transforming Activities. *Journal of Biological Chemistry* **276,** 819–826 (2001).

131. Hegde, S. P., Kumar, A., Kurschner, C. & Shapiro, L. H. c-Maf Interacts with c-Myb To Regulate Transcription of an Early Myeloid Gene during Differentiation. *Mol Cell Biol* **18,** 2729–2737 (1998).

132. Sieweke, M. H., Tekotte, H., Frampton, J. & Graf, T. MafB represses erythroid genes and differentiation through direct interaction with c-Ets-1. *Leukemia* **11 Suppl 3,** 486–8 (1997).

133. Lawrence, M. C., McGlynn, K., Park, B.-H. & Cobb, M. H. ERK1/2-dependent Activation of Transcription Factors Required for Acute and Chronic Effects of Glucose on the Insulin Gene Promoter. *J Biol Chem* **280,** 26751–26759 (2005).

134. Cvekl, A. & Duncan, M. K. Genetic and epigenetic mechanisms of gene regulation during lens development. *Prog Retin Eye Res* **26,** 555–597 (2007).

135. Rocques, N., Zeid, N., Sii-Felice, K., Lecoin, L., Felder-Schmittbuhl, M.-P., Eychène, A. & Pouponnot, C. GSK-3-Mediated Phosphorylation Enhances Maf-Transforming Activity. *Molecular Cell* **28,** 584–597 (2007).

136. Chen, Q., Dowhan, D. H., Liang, D., Moore, D. D. & Overbeek, P. A. CREB-binding protein/p300 co-activation of crystallin gene expression. *The Journal of biological chemistry* **277,** 24081–9 (2002).

137. Friedman, J. S., Khanna, H., Swain, P. K., DeNicola, R., Cheng, H., Mitton, K. P., Weber, C. H., Hicks, D. & Swaroop, A. The Minimal Transactivation Domain of the Basic Motif-Leucine Zipper Transcription Factor NRL Interacts with TATA-binding Protein. *Journal of Biological Chemistry* **279,** 47233–47241 (2004).

138. Gabryšová, L., Alvarez-Martinez, M., Luisier, R., Cox, L. S., Sodenkamp, J., Hosking, C., Pérez-Mazliah, D., Whicher, C., Kannan, Y., Potempa, K., Wu, X., Bhaw, L., Wende, H., Sieweke, M. H., Elgar, G., Wilson, M., Briscoe, J., Metzis, V., Langhorne, J., Luscombe, N. M. & O'Garra, A. c-Maf controls immune responses by regulating disease-specific gene networks and repressing IL-2 in CD4+ T cells. *Nature Immunology* **19,** 497–507 (2018).

139. Yoshida, H., Lareau, C. A., Ramirez, R. N., Rose, S. A., Maier, B., Wroblewska, A., Desland, F., Chudnovskiy, A., Mortha, A., Dominguez, C., Tellier, J., Kim, E., Dwyer, D., Shinton, S., Nabekura, T., Qi, Y., Yu, B., Robinette, M., Kim, K.-W., Wagers, A., Rhoads, A., Nutt, S. L., Brown, B. D., Mostafavi, S., Buenrostro, J. D., Benoist, C. & Project, I. the. The cis-Regulatory Atlas of the Mouse Immune System. *Cell* **176,** 897-912.e20 (2019).

140. Ochiai, K., Katoh, Y., Ikura, T., Hoshikawa, Y., Noda, T., Karasuyama, H., Tashiro, S., Muto, A. & Igarashi, K. Plasmacytic Transcription Factor Blimp-1 Is Repressed by Bach2 in B Cells. *Journal of Biological Chemistry* **281,** 38226–38234 (2006).

141. Igarashi, K., Ochiai, K., Itoh-Nakadai, A. & Muto, A. Orchestration of plasma cell differentiation by Bach2 and its gene regulatory network. *Immunological Reviews* **261,** 116–125 (2014).

142. Kawai, S., Goto, N., Kataoka, K., Saegusa, T., Shinno-Kohno, H. & Nishizawa, M. Isolation of the avian transforming retrovirus, AS42, carrying the v-maf oncogene and initial characterization of its gene product. *Virology* **188,** 778–784 (1992).

143. Nishizawa, M., Kataoka, K., Goto, N., Fujiwara, K. T. & Kawai, S. v-maf, a viral oncogene that encodes a "leucine zipper" motif. *Proc National Acad Sci* **86,** 7711–7715 (1989).

144. Morito, N., Yoh, K., Fujioka, Y., Nakano, T., Shimohata, H., Hashimoto, Y., Yamada, A., Maeda, A., Matsuno, F., Hata, H., Suzuki, A., Imagawa, S., Mitsuya, H., Esumi, H., Koyama, A., Yamamoto, M., Mori, N. & Takahashi, S. Overexpression of c-Maf Contributes to T-Cell Lymphoma in Both Mice and Human. *Cancer Res* **66,** 812–819 (2006).

145. Annunziata, C. M., Hernandez, L., Davis, E. R., Zingone, A., Lamy, L., Lam, L. T., Hurt, E. M., Shaffer, A. L., Kuehl, M. W. & Staudt, L. M. A mechanistic rationale for MEK inhibitor therapy in myeloma based on blockade of MAF oncogene expression. *Blood* **117,** 2396–2404 (2011).

146. Carrasco, D. R., Sukhdeo, K., Protopopova, M., Sinha, R., Enos, M., Carrasco, D. E., Zheng, M., Mani, M., Henderson, J., Pinkus, G. S., Munshi, N., Horner, J., Ivanova, E. V., Protopopov, A., Anderson, K. C., Tonon, G. & DePinho, R. A. The Differentiation and Stress Response Factor XBP-1 Drives Multiple Myeloma Pathogenesis. *Cancer Cell* **11,** 349–360 (2007).

147. Moreaux, J., Hose, D., Jourdan, M., Reme, T., Hundemer, M., Moos, M., Robert, N., Moine, P., Vos, J., Goldschmidt, H. & Klein, B. TACI expression is associated with a mature bone marrow plasma cell signature and C-MAF overexpression in human myeloma cell lines. *Haematologica* **92,** 803–811 (2007).

148. Nian, F., Zhu, J. & Chang, H. Long non-coding RNA ANGPTL1-3 promotes multiple myeloma bortezomib resistance by sponging miR-30a-3p to activate c-Maf expression. *Biochem Bioph Res Co* **514,** 1140–1146 (2019).

149. White, M. B., Word, C. J., Humphries, C. G., Blattner, F. R. & Tucker, P. W. Immunoglobulin D switching can occur through homologous recombination in human B cells. *Mol Cell Biol* **10,** 3690–3699 (1990).

150. Lo, J.-Y., Chou, Y.-T., Lai, F.-J. & Hsu, L.-J. Regulation of cell signaling and apoptosis by tumor suppressor WWOX. *Experimental Biology and Medicine* **240,** 383–391 (2015).

151. Karras, J. R., Schrock, M. S., Batar, B. & Huebner, K. Fragile Genes That Are Frequently Altered in Cancer: Players Not Passengers. *Cytogenetic and Genome Research* **150,** 208–216 (2017).

152. McBride, K. M., Kil, H., Mu, Y., Plummer, J. B., Lee, J., Zelazowski, M. J., Sebastian, M., Abba, M. C. & Aldaz, M. C. Wwox Deletion in Mouse B Cells Leads to Genomic Instability, Neoplastic Transformation, and Monoclonal Gammopathies. *Frontiers in Oncology* **9,** 517 (2019).

153. Walker, B. A., Mavrommatis, K., Wardell, C. P., Ashby, T., Bauer, M., Davies, F. E., Rosenthal, A., Wang, H., Qu, P., Hoering, A., Samur, M., Towfic, F., Ortiz, M., Flynt, E., Yu, Z., Yang, Z., Rozelle, D., Obenauer, J., Trotter, M., Auclair, D., Keats, J., Bolli, N., Fulciniti, M., Szalat, R., Moreau, P., Durie, B., Stewart, A., Goldschmidt, H., Raab, M. S., Einsele, H., Sonneveld, P., Miguel, J., Lonial, S., Jackson, G. H., Anderson, K. C., Avet-Loiseau, H., Munshi, N., Thakurta, A. & Morgan, G. J. Identification of novel mutational drivers reveals oncogene dependencies in multiple myeloma. *Blood* **132,** 587–597 (2018).

154. Hurt, E. M., Wiestner, A., Rosenwald, A., Shaffer, A. L., Campo, E., Grogan, T., Bergsagel, P. L., Kuehl, W. M. & Staudt, L. M. Overexpression of c-maf is a frequent oncogenic event in multiple myeloma that promotes proliferation and pathological interactions with bone marrow stroma. *Cancer Cell* **5,** 191–199 (2004).

155. Monteiro, P., Gilot, D., Ferrec, E., Lecureur, V., N'diaye, M., Vee, M., Podechard, N., Pouponnot, C. & Fardel, O. AhR- and c-maf-dependent induction of β7-integrin expression in human macrophages in response to environmental polycyclic aromatic hydrocarbons. *Biochemical and Biophysical Research Communications* **358,** 442–448 (2007).

156. Suzuki, A., Iida, S., Kato-Uranishi, M., Tajima, E., Zhan, F., Hanamura, I., Huang, Y., Ogura, T., Takahashi, S., Ueda, R., Barlogie, B., Jr, J. & Esumi, H. ARK5 is transcriptionally regulated by the Large-MAF family and mediates IGF-1-induced cell invasion in multiple myeloma: ARK5 as a new molecular determinant of malignant multiple myeloma. *Oncogene* (2005). doi:10.1038/sj.onc.1208844

157. Cyster, J. G. Homing of antibody secreting cells. *Immunol Rev* **194,** 48–60 (2003).

158. Hynes, R. O. Integrins Bidirectional, Allosteric Signaling Machines. *Cell* **110,** 673–687 (2002).

159. Neri, P., Ren, L., Azab, A. K., Brentnall, M., Gratton, K., Klimowicz, A. C., Lin, C., Duggan, P., Tassone, P., Mansoor, A., Stewart, D. A., Boise, L. H., Ghobrial, I. M. & Bahlis, N. J. Integrin β7-mediated regulation of multiple myeloma cell adhesion, migration, and invasion. *Blood* **117,** 6202–6213 (2011).

160. Stralen, E. van, Wetering, M. van de, Agnelli, L., Neri, A., Clevers, H. C. & Bast, B. Identification of primary MAFB target genes in multiple myeloma. *Experimental Hematology* **37,** 78–86 (2009).

161. Giallongo, C., Tibullo, D., Puglisi, F., Barbato, A., Vicario, N., Cambria, D., Parrinello, N. L., Romano, A., Conticello, C., Forte, S., Parenti, R., Amorini, A. M., Lazzarino, G., Volti, G. L., Palumbo, G. A. & Raimondo, F. D. Inhibition of TLR4 Signaling Affects Mitochondrial Fitness and Overcomes Bortezomib Resistance in Myeloma Plasma Cells. *Cancers* **12,** 1999 (2020).

162. Peterson, T. R., Laplante, M., Thoreen, C. C., Sancak, Y., Kang, S. A., Kuehl, W. M., Gray, N. S. & Sabatini, D. M. DEPTOR Is an mTOR Inhibitor Frequently Overexpressed in Multiple Myeloma Cells and Required for Their Survival. *Cell* **137,** 873–886 (2009).

163. Catena, V., Bruno, T., Nicola, F. D., Goeman, F., Pallocca, M., Iezzi, S., Sorino, C., Cigliana, G., Floridi, A., Blandino, G. & Fanciulli, M. Deptor transcriptionally regulates endoplasmic reticulum homeostasis in multiple myeloma cells. *Oncotarget* **7,** 70546–70558 (2016).

164. Benkhelifa, S., Provot, S., Nabais, E., Eychène, A., Calothy, G. & Felder-Schmittbuhl, M.-P. Phosphorylation of MafA Is Essential for Its Transcriptional and Biological Properties. *Mol Cell Biol* **21,** 4441–4452 (2001).

165. Herath, N., Rocques, N., Garancher, A., Eychène, A. & Pouponnot, C. GSK3-mediated MAF phosphorylation in multiple myeloma as a potential therapeutic target. *Blood Cancer Journal* **4,** e175 (2014).

166. Sii-Felice, K., Pouponnot, C., Gillet, S., Lecoin, L., Girault, J.-A., Eychène, A. & Felder-Schmittbuhl, M.-P. MafA transcription factor is phosphorylated by p38 MAP kinase. *Febs Lett* **579,** 3547–3554 (2005).

167. Qiang, Y.-W., Ye, S., Huang, Y., Chen, Y., Rhee, F. V., Epstein, J., Walker, B. A., Morgan, G. J. & Davies, F. E. MAFb protein confers intrinsic resistance to proteasome inhibitors in multiple myeloma. *Bmc Cancer* **18,** 724 (2018).

168. Chen, G., Xu, X., Tong, J., Han, K., Zhang, Z., Tang, J., Li, S., Yang, C., Li, J., Cao, B., Zhou, H., Wu, D., Moran, M. F. & Mao, X. Ubiquitination of the transcription factor c-MAF is mediated by multiple lysine residues. *The International Journal of Biochemistry & Cell Biology* **57,** 157–166 (2014).

169. Xu, Y., Zhang, Z., Li, J., Tong, J., Cao, B., Taylor, P., Tang, X., Wu, D., Moran, M. F., Zeng, Y. & Mao, X. The ubiquitin-conjugating enzyme UBE2O modulates c-Maf stability and induces myeloma cell apoptosis. *Journal of Hematology & Oncology* **10,** 132 (2017).

170. Zhang, Z., Tong, J., Tang, X., Juan, J., Cao, B., Hurren, R., Chen, G., Taylor, P., Xu, X., Shi, C., Du, J., Hou, J., Wang, G., Wu, D., Stewart, A. K., Schimmer, A. D., Moran, M. F. & Mao, X. The ubiquitin ligase HERC4 mediates c-Maf ubiquitination and delays the growth of multiple myeloma xenografts in nude mice. *Blood* **127,** 1676–1686 (2016).

171. Du, Y., Liu, Y., Xu, Y., Juan, J., Zhang, Z., Xu, Z., Cao, B., Wang, Q., Zeng, Y. & Mao, X. The transmembrane protein TMEPAI induces myeloma cell apoptosis by promoting degradation of the c-Maf transcription factor. *Journal of Biological Chemistry* **293,** 5847–5859 (2018).

172. Wang, S., Juan, J., Zhang, Z., Du, Y., Xu, Y., Tong, J., Cao, B., Moran, M. F., Zeng, Y. & Mao, X. Inhibition of the deubiquitinase USP5 leads to c-Maf protein degradation and myeloma cell apoptosis. *Cell Death Dis* **8,** e3058 (2017).

173. He, Y., Wang, S., Tong, J., Jiang, S., Yang, Y., Zhang, Z., Xu, Y., Zeng, Y., Cao, B., Moran, M. F. & Mao, X. The deubiquitinase USP7 stabilizes Maf proteins to promote myeloma cell survival. *J Biol Chem* **295,** 2084–2096 (2020).

174. Xu, Y., Sun, T., Zeng, K., Xu, M., Chen, J., Xu, X., Zhang, Z., Cao, B., Tang, X., Wu, D., Kong, Y., Zeng, Y. & Mao, X. Anti-bacterial and anti-viral nanchangmycin displays anti-myeloma activity by targeting Otub1 and c-Maf. *Cell Death Dis* **11,** 818 (2020).

175. Xu, Y., Xu, M., Tong, J., Tang, X., Chen, J., Chen, X., Zhang, Z., Cao, B., Stewart, A. K., Moran, M. F., Wu, D. & Mao, X. Targeting the Otub1/c-Maf axis for the treatment of multiple myeloma. *Blood* (2020). doi:10.1182/blood.2020005199

176. Kanai, K., Reza, H. M., Kamitani, A., Hamazaki, Y., Han, S., Yasuda, K. & Kataoka, K. SUMOylation negatively regulates transcriptional and oncogenic activities of MafA. *Genes Cells* **15,** 971–982 (2010).

177. Winkler, W., Díaz, C. F., Blanc, E., Napieczynska, H., Langner, P., Werner, M., Walter, B., Wollert-Wulf, B., Yasuda, T., Heuser, A., Beule, D., Mathas, S., Anagnostopoulos, I., Rosenwald, A., Rajewsky, K. & Janz, M. Mouse models of human multiple myeloma subgroups. *Proc National Acad Sci* **120,** e2219439120 (2023).

178. Winkler, W. Establishment of new multiple myeloma mouse models. Ph.D. thesis, Humboldt-University, Berlin (2018).

179. Hobeika, E., Thiemann, S., Storch, B., Jumaa, H., Nielsen, P. J., Pelanda, R. & Reth, M. Testing gene function early in the B cell lineage in mb1-cre mice. *Proc National Acad Sci* **103,** 13789–13794 (2006).

180. Rickert, R. C., Roes, J. & Rajewsky, K. B Lymphocyte-Specific, Cre-mediated Mutagenesis in Mice. *Nucleic Acids Research* **25,** (1997).

181. Casola, S., Cattoretti, G., Uyttersprot, N., Koralov, S. B., Seagal, J., Segal, J., Hao, Z., Waisman, A., Egert, A., Ghitza, D. & Rajewsky, K. Tracking germinal center B cells expressing germ-line immunoglobulin γ1 transcripts by conditional gene targeting. *Proceedings of the National Academy of Sciences* **103,** 7396–7401 (2006).

182. Sternberg, N., Hamilton, D. & Hoess, R. Bacteriophage P1 site-specific recombination II. Recombination between loxP and the bacterial chromosome. *J Mol Biol* **150,** 487–507 (1981).

183. Hoess, R. H., Ziese, M. & Sternberg, N. P1 site-specific recombination: nucleotide sequence of the recombining sites. *Proc National Acad Sci* **79,** 3398–3402 (1982).

184. Lakso, M., Sauer, B., Mosinger, B., Lee, E. J., Manning, R. W., Yu, S. H., Mulder, K. L. & Westphal, H. Targeted oncogene activation by site-specific recombination in transgenic mice. *Proc National Acad Sci* **89,** 6232–6236 (1992).

185. Kühn, R. & Wurst, W. Gene Knockout Protocols, Second Edition. *Methods Mol Biology* **530,** 1–12 (2009).

186. Indra, A. K., Warot, X., Brocard, J., Bornert, J.-M., Xiao, J.-H., Chambon, P. & Metzger, D. Temporally-controlled site-specific mutagenesis in the basal layer of the epidermis: comparison of the recombinase activity of the tamoxifen-inducible Cre-ERT and Cre-ERT2 recombinases. *Nucleic Acids Res* **27,** 4324–4327 (1999).

187. Calado, D., Sasaki, Y., Godinho, S. A., Pellerin, A., Köchert, K., Sleckman, B. P., Alborán, I. de, Janz, M., Rodig, S. & Rajewsky, K. The cell-cycle regulator c-Myc is essential for the formation and maintenance of germinal centers. *Nat Immunol* **13,** 1092–1100 (2012).

188. Sander, S., Calado, D. P., Srinivasan, L., Köchert, K., Zhang, B., Rosolowski, M., Rodig, S. J., Holzmann, K., Stilgenbauer, S., Siebert, R., Bullinger, L. & Rajewsky, K. Synergy between PI3K Signaling and MYC in Burkitt Lymphomagenesis. *Cancer Cell* **22,** 167–179 (2012).

189. Sommermann, T., Yasuda, T., Ronen, J., Wirtz, T., Weber, T., Sack, U., Caeser, R., Zhang, J., Li, X., Chu, V. T., Jauch, A., Unger, K., Hodson, D. J., Akalin, A. & Rajewsky, K. Functional interplay of Epstein-Barr virus oncoproteins in a mouse model of B cell lymphomagenesis. *Proc National Acad Sci* **117,** 14421–14432 (2020).

190. Weber, T., Seagal, J., Winkler, W., Wirtz, T., Chu, V. T. & Rajewsky, K. A novel allele for inducible Cre expression in germinal center B cells. *Eur J Immunol* **49,** 192–194 (2019).

191. Morita, S., Kojima, T. & Kitamura, T. Plat-E: an efficient and stable system for transient packaging of retroviruses. *Gene Ther* **7,** 1063–1066 (2000).

192. Moore, G. E. & Kitamura, H. Cell line derived from patient with myeloma. *New York State J Med* **68,** 2054–60 (1968).

193. Gong, H., Sun, L., Chen, B., Han, Y., Pang, J., Wu, W., Qi, R. & Zhang, T. Evaluation of candidate reference genes for RT-qPCR studies in three metabolism related tissues of mice after caloric restriction. *Scientific Reports* **6,** srep38513 (2016).

194. Altschul, S. F., Gish, W., Miller, W., Myers, E. W. & Lipman, D. J. Basic local alignment search tool. *J Mol Biol* **215,** 403–410 (1990).

195. Gao, C.-H., Yu, G. & Cai, P. ggVennDiagram: An Intuitive, Easy-to-Use, and Highly Customizable R Package to Generate Venn Diagram. *Frontiers Genetics* **12,** 706907 (2021).

196. Wickham, H. Reshaping Data with the reshape Package. *J Stat Softw* **21,** (2007).

197. Szklarczyk, D., Franceschini, A., Wyder, S., Forslund, K., Heller, D., Huerta-Cepas, J., Simonovic, M., Roth, A., Santos, A., Tsafou, K. P., Kuhn, M., Bork, P., Jensen, L. J. & Mering, C. von. STRING v10: protein–protein interaction networks, integrated over the tree of life. *Nucleic Acids Res* **43,** D447–D452 (2015).

198. Wickham, H., Averick, M., Bryan, J., Chang, W., McGowan, L., François, R., Grolemund, G., Hayes, A., Henry, L., Hester, J., Kuhn, M., Pedersen, T., Miller, E., Bache, S., Müller, K., Ooms, J., Robinson, D., Seidel, D., Spinu, V., Takahashi, K., Vaughan, D., Wilke, C., Woo, K. & Yutani, H. Welcome to the Tidyverse. *J Open Source Softw* **4,** 1686 (2019).

199. Lex, A., Gehlenborg, N., Strobelt, H., Vuillemot, R. & Pfister, H. UpSet: Visualization of Intersecting Sets. *Ieee T Vis Comput Gr* **20,** 1983–1992 (2014).

200. Ramakers, C., Ruijter, J. M., Deprez, R. & Moorman, A. Assumption-free analysis of quantitative real-time polymerase chain reaction (PCR) data. *Neuroscience Letters* **339,** 62–66 (2003).

201. Ruijter, J., Ramakers, C., Hoogaars, W., Karlen, Y., Bakker, O., Hoff, M. van den & Moorman, A. Amplification efficiency: linking baseline and bias in the analysis of quantitative PCR data. *Nucleic Acids Research* **37,** e45–e45 (2009).

202. Vandesompele, J., Preter, K., Pattyn, F., Poppe, B., Roy, N., Paepe, A. & Speleman, F. Accurate normalization of real-time quantitative RT-PCR data by geometric averaging of multiple internal control genes. *Genome Biology* **3,** research0034.1 (2002).

203. Schreiber, E., Matthias, P., Müller, M. M. & Schaffner, W. Rapid detection of octamer binding proteins with "mini-extracts", prepared from a small number of cells. *Nucleic acids research* **17,** 6419 (1989).

204. Fey, E., Wan, K. & Penman, S. Epithelial cytoskeletal framework and nuclear matrix-intermediate filament scaffold: three-dimensional organization and protein composition. *The Journal of Cell Biology* **98,** 1973–1984 (1984).

205. Fey, E., Krochmalnic, G. & Penman, S. The nonchromatin substructures of the nucleus: the ribonucleoprotein (RNP)-containing and RNP-depleted matrices analyzed by sequential fractionation and resinless section electron microscopy. *The Journal of Cell Biology* **102,** 1654–1665 (1986).

206. Herman, R., Weymouth, L. & Penman, S. Heterogeneous nuclear RNA-protein fibers in chromatin-depleted nuclei. *The Journal of Cell Biology* **78,** 663–674 (1978).

207. Shaiken, T. E. & Opekun, A. R. Dissecting the cell to nucleus, perinucleus and cytosol. *Scientific Reports* **4,** srep04923 (2015).

208. Subbotin, R. I. & Chait, B. T. A Pipeline for Determining Protein–Protein Interactions and Proximities in the Cellular Milieu. *Molecular & Cellular Proteomics* **13,** 2824–2835 (2014).

209. Tekaia, F., Yeramian, E. & Dujon, B. Amino acid composition of genomes, lifestyles of organisms, and evolutionary trends: a global picture with correspondence analysis. *Gene* **297,** 51–60 (2002).

210. Fritsche-Guenther, R., Gloaguen, Y., Kirchner, M., Mertins, P., Tunn, P.-U. & Kirwan, J. A. Progression-Dependent Altered Metabolism in Osteosarcoma Resulting in Different Nutrient Source Dependencies. *Cancers* **12,** 1371 (2020).

211. Heesch, S. van, Witte, F., Schneider-Lunitz, V., Schulz, J. F., Adami, E., Faber, A. B., Kirchner, M., Maatz, H., Blachut, S., Sandmann, C.-L., Kanda, M., Worth, C. L., Schafer, S., Calviello, L., Merriott, R., Patone, G., Hummel, O., Wyler, E., Obermayer, B., Mücke, M. B., Lindberg, E. L., Trnka, F., Memczak, S., Schilling, M., Felkin, L. E., Barton, P. J. R., Quaife, N. M., Vanezis, K., Diecke, S., Mukai, M., Mah, N., Oh, S.-J., Kurtz, A., Schramm, C., Schwinge, D., Sebode, M., Harakalova, M., Asselbergs, F. W., Vink, A., Weger, R. A. de, Viswanathan, S., Widjaja, A. A., Gärtner-Rommel, A., Milting, H., Remedios, C. dos, Knosalla, C., Mertins, P., Landthaler, M., Vingron, M., Linke, W. A., Seidman, J. G., Seidman, C. E., Rajewsky, N., Ohler, U., Cook, S. A. & Hubner, N. The Translational Landscape of the Human Heart. *Cell* **178,** 242-260.e29 (2019).

212. Rappsilber, J., Mann, M. & Ishihama, Y. Protocol for micro-purification, enrichment, pre-fractionation and storage of peptides for proteomics using StageTips. *Nat Protoc* **2,** 1896–906 (2007).

213. KRISS, J. P., MARUYAMA, Y., TUNG, L. A., BOND, S. B. & REVESZ, L. The fate of 5-bromodeoxyuridine, 5-bromodeoxycytidine, and 5-iododeoxycytidine in man. *Cancer Res* **23,** 260–8 (1963).

214. Kraal, G., Weissman, I. L. & Butcher, E. C. Germinal centre B cells: antigen specificity and changes in heavy chain class expression. *Nature* **298,** 377–379 (1982).

215. Alvarez-Benayas, J., Trasanidis, N., Katsarou, A., Ponnusamy, K., Chaidos, A., May, P. C., Xiao, X., Bua, M., Atta, M., Roberts, I. A. G., Auner, H. W., Hatjiharissi, E., Papaioannou, M., Caputo, V. S., Sudbery, I. M. & Karadimitris, A. Chromatin-based, in cis and in trans regulatory rewiring underpins distinct oncogenic transcriptomes in multiple myeloma. *Nat Commun* **12,** 5450 (2021).

216. Chaudhuri, A. R. & Nussenzweig, A. The multifaceted roles of PARP1 in DNA repair and chromatin remodelling. *Nat Rev Mol Cell Bio* **18,** 610–621 (2017).

217. Nishikawa, K., Nakashima, T., Takeda, S., Isogai, M., Hamada, M., Kimura, A., Kodama, T., Yamaguchi, A., Owen, M. J., Takahashi, S. & Takayanagi, H. Maf promotes osteoblast differentiation in mice by mediating the age-related switch in mesenchymal cell differentiation. *J Clin Invest* **120,** 3455–3465 (2010).

218. Wiggins, K. J. & Scharer, C. D. Roadmap to a plasma cell: Epigenetic and transcriptional cues that guide B cell differentiation. *Immunol Rev* (2020). doi:10.1111/imr.12934

219. Barwick, B. G., Scharer, C. D., Bally, A. P. R. & Boss, J. M. Plasma cell differentiation is coupled to division-dependent DNA hypomethylation and gene regulation. *Nat Immunol* **17,** 1216–1225 (2016).

220. Caron, G., Hussein, M., Kulis, M., Delaloy, C., Chatonnet, F., Pignarre, A., Avner, S., Lemarié, M., Mahé, E. A., Verdaguer-Dot, N., Queirós, A. C., Tarte, K., Martín-Subero, J. I., Salbert, G. & Fest, T. Cell-Cycle-Dependent Reconfiguration of the DNA Methylome during Terminal Differentiation of Human B Cells into Plasma Cells. *Cell Reports* **13,** 1059–1071 (2015).

221. Scharer, C. D., Barwick, B. G., Guo, M., Bally, A. P. R. & Boss, J. M. Plasma cell differentiation is controlled by multiple cell division-coupled epigenetic programs. *Nat Commun* **9,** 1698 (2018).

222. Allen, C. D. C., Okada, T., Tang, H. L. & Cyster, J. G. Imaging of Germinal Center Selection Events During Affinity Maturation. *Science* **315,** 528–531 (2007).

223. MacLennan, I. C. M. Germinal Centers. *Annu Rev Immunol* **12,** 117–139 (1994).

224. Scharer, C. D., Patterson, D. G., Mi, T., Price, M. J., Hicks, S. L. & Boss, J. M. Antibody-secreting cell destiny emerges during the initial stages of B-cell activation. *Nat Commun* **11,** 3989 (2020).

225. Quah, B. J. C. & Parish, C. R. New and improved methods for measuring lymphocyte proliferation in vitro and in vivo using CFSE-like fluorescent dyes. *J Immunol Methods* **379,** 1–14 (2012).

226. Peng, S., Lalani, S., Leavenworth, J. W., Ho, I. & Pauza, M. E. c-Maf interacts with c-Myb to down-regulate Bcl-2 expression and increase apoptosis in peripheral CD4 cells. *Eur J Immunol* **37,** 2868–2880 (2007).

227. Peng, S., Wu, H., Mo, Y., Watabe, K. & Pauza, M. E. c-Maf increases apoptosis in peripheral CD8 cells by transactivating Caspase 6. *Immunology* **127,** 267–278 (2009).

228. Smith, K. G. C., Light, A., O'Reilly, L. A., Ang, S.-M., Strasser, A. & Tarlinton, D. bcl-2 Transgene Expression Inhibits Apoptosis in the Germinal Center and Reveals Differences in the Selection of Memory B Cells and Bone Marrow Antibody-Forming Cells. *J Exp Medicine* **191,** 475–484 (2000).

229. Strasser, A., Harris, A. W. & Cory, S. E mu-bcl-2 transgene facilitates spontaneous transformation of early pre-B and immunoglobulin-secreting cells but not T cells. *Oncogene* **8,** 1–9 (1993).

230. Stadtfeld, M. & Graf, T. Assessing the role of hematopoietic plasticity for endothelial and hepatocyte development by non-invasive lineage tracing. *Development* **132,** 203–213 (2004).

231. Vinay, D. S., Ryan, E. P., Pawelec, G., Talib, W. H., Stagg, J., Elkord, E., Lichtor, T., Decker, W. K., Whelan, R. L., Kumara, H. M. C., Signori, E., Honoki, K., Georgakilas, A. G., Amin, A., Helferich, W. G., Boosani, C. S., Guha, G., Ciriolo, M., Chen, S., Mohammed, S. I., Azmi, A. S., Keith, N. W., Bilsland, A., Bhakta, D., Halicka, D., Fujii, H., Aquilano, K., Ashraf, S. S., Nowsheen, S., Yang, X., Choi, B. K. & Kwon, B. S. Immune evasion in cancer: Mechanistic basis and therapeutic strategies. *Seminars in Cancer Biology* **35,** S185–S198 (2015).

232. Rigopoulos, T. A. Elucidating the role of c-MAF and its potential co-culprits in multiple myeloma. Master thesis, Charité-University medicine, Berlin (2020).

233. Nojima, T., Haniuda, K., Moutai, T., Matsudaira, M., Mizokawa, S., Shiratori, I., Azuma, T. & Kitamura, D. In-vitro derived germinal centre B cells differentially generate memory B or plasma cells in vivo. *Nature Communications* **2,** 465 (2011).

234. Radbruch, A., Muehlinghaus, G., Luger, E. O., Inamine, A., Smith, K. G. C., Dörner, T. & Hiepe, F. Competence and competition: the challenge of becoming a long-lived plasma cell. *Nat Rev Immunol* **6,** 741–750 (2006).

235. John, S., Rolnick, K., Wilson, L., Wong, S., Gelder, R. N. V. & Pepple, K. L. Bioluminescence for in vivo detection of cell-type-specific inflammation in a mouse model of uveitis. *Sci Rep-uk* **10,** 11377 (2020).

236. Pouponnot, C., Sii-Felice, K., Hmitou, I., Rocques, N., Lecoin, L., Druillennec, S., Felder-Schmittbuhl, M.-P. & Eychène, A. Cell context reveals a dual role for Maf in oncogenesis. *Oncogene* **25,** 1299–1310 (2006).

237. Kienast, J. & Berdel, W. E. c-maf in multiple myeloma An oncogene enhancing tumor-stroma interactions. *Cancer Cell* **5,** 109–110 (2004).

238. Teves, S. S. & Henikoff, S. Chromatin Remodeling, Methods and Protocols. *Methods Mol Biology* **833,** 421–432 (2011).

239. Xu, L., Glass, C. K. & Rosenfeld, M. G. Coactivator and corepressor complexes in nuclear receptor function. *Curr Opin Genet Dev* **9,** 140–147 (1999).

240. Soutoglou, E., Viollet, B., Vaxillaire, M., Yaniv, M., Pontoglio, M. & Talianidis, I. Transcription factor-dependent regulation of CBP and P/CAF histone acetyltransferase activity. *Embo J* **20,** 1984–1992 (2001).

241. Soutoglou, E. & Talianidis, I. Coordination of PIC Assembly and Chromatin Remodeling During Differentiation-Induced Gene Activation. *Science* **295,** 1901–1904 (2002).

242. Ordonez, R., Kulis, M., Russinol, N., Chapaprieta, V., Carrasco-Leon, A., Garcia-Torre, B., Charampopoulou, S., Clot, G., Beekman, R., Meydan, C., Duran-Ferrer, M., Verdaguer-Dot, N., Vilarrasa-Blasi, R., Soler-Vila, P., Garate, L., Miranda, E., Jose-Eneriz, E. S., Rodriguez-Madoz, J. R., Ezponda, T., Martinez-Turrilas, R., Vilas-Zornoza, A., Lara-Astiaso, D., Dupere-Richer, D., Martens, J. H., El-Omri, H., Taha, R. Y., Calasanz, M. J., Paiva, B., Miguel, J. S., Flicek, P. H., Gut, I. G., Melnick, A., Mitsiades, C. S., Licht, J. D., Campo, E., Stunnenberg, H. G., Agirre, X., Prosper, F. & Martin-Subero, I. Chromatin activation as a unifying principle underlying pathogenic mechanisms in multiple myeloma. *Genome Res* **30,** gr.265520.120 (2020).

243. Jin, Y., Chen, K., Paepe, A., Hellqvist, E., Krstic, A. D., Metang, L., Gustafsson, C., Davis, R. E., Levy, Y. M., Surapaneni, R., Wallblom, A., Nahi, H., Mansson, R. & Lin, Y. C. Active enhancer and chromatin accessibility landscapes chart the regulatory network of primary multiple myeloma. *Blood* **131,** 2138–2150 (2018).

244. Mayran, A. & Drouin, J. Pioneer transcription factors shape the epigenetic landscape. *J Biol Chem* **293,** 13795–13804 (2018).

245. Annunziata, C. M., Davis, E. R., Demchenko, Y., Bellamy, W., Gabrea, A., Zhan, F., Lenz, G., Hanamura, I., Wright, G., Xiao, W., Dave, S., Hurt, E. M., Tan, B., Zhao, H., Stephens, O., Santra, M., Williams, D. R., Dang, L., Barlogie, B., Shaughnessy, J. D., Kuehl, M. W. & Staudt, L. M. Frequent Engagement of the Classical and Alternative NF-κB Pathways by Diverse Genetic Abnormalities in Multiple Myeloma. *Cancer Cell* **12,** 115–130 (2007).

246. Keats, J. J., Fonseca, R., Chesi, M., Schop, R., Baker, A., Chng, W.-J., Wier, S., Tiedemann, R., Shi, C.-X., Sebag, M., Braggio, E., Henry, T., Zhu, Y.-X., Fogle, H., Price-Troska, T., Ahmann, G., Mancini, C., Brents, L. A., Kumar, S., Greipp, P., Dispenzieri, A., Bryant, B., Mulligan, G., Bruhn, L., Barrett, M., Valdez, R., Trent, J., Stewart, K. A., Carpten, J. & Bergsagel, L. P. Promiscuous Mutations Activate the Noncanonical NF-κB Pathway in Multiple Myeloma. *Cancer Cell* **12,** 131–144 (2007).

247. Zhou, N., Gutierrez-Uzquiza, A., Zheng, X., Chang, R., Vogl, D. T., Garfall, A. L., Bernabei, L., Saraf, A., Florens, L., Washburn, M. P., Illendula, A., Bushweller, J. H. & Busino, L. RUNX proteins desensitize multiple myeloma to lenalidomide via protecting IKZFs from degradation. *Leukemia* **33,** 2006–2021 (2019).

248. Sasaki, Y., Derudder, E., Hobeika, E., Pelanda, R., Reth, M., Rajewsky, K. & Schmidt-Supprian, M. Canonical NF-κB Activity, Dispensable for B Cell Development, Replaces BAFF-Receptor Signals and Promotes B Cell Proliferation upon Activation. *Immunity* **24,** 729–739 (2006).

249. Sasaki, Y., Calado, D. P., Derudder, E., Zhang, B., Shimizu, Y., Mackay, F., Nishikawa, S., Rajewsky, K. & Schmidt-Supprian, M. NIK overexpression amplifies, whereas ablation of its TRAF3-binding domain replaces BAFF:BAFF-R-mediated survival signals in B cells. *Proc National Acad Sci* **105,** 10883–10888 (2008).

250. Kaya-Okur, H. S., Janssens, D. H., Henikoff, J. G., Ahmad, K. & Henikoff, S. Efficient low-cost chromatin profiling with CUT&Tag. *Nat Protoc* **15,** 3264–3283 (2020).

251. Balani, S., Nguyen, L. V. & Eaves, C. J. Modeling the process of human tumorigenesis. *Nat Commun* **8,** 15422 (2017).

252. Azami, Y., Tsuyama, N., Abe, Y., Sugai-Takahashi, M., Kudo, K., Ota, A., Sivasundaram, K., Muramatsu, M., Shigemura, T., Sasatani, M., Hashimoto, Y., Saji, S., Kamiya, K., Hanamura, I., Ikezoe, T., Onodera, M. & Sakai, A. Chromosomal translocation t(11;14) and p53 deletion induced by the CRISPR/Cas9 system in normal B cell-derived iPS cells. *Sci Rep-uk* **11,** 5216 (2021).

Eidesstattliche Versicherung

„Ich, Marvin Werner, versichere an Eides statt durch meine eigenhändige Unterschrift, dass ich die vorgelegte Dissertation mit dem Thema: „Der Einfluss des Transkriptionsfaktors MAF auf die Physiologie und maligne Transformation in der terminalen B Zell Differenzierung. The impact of the transcription factor MAF on physiology and malignant transformation in terminal B cell differentiation.“ selbstständig und ohne nicht offengelegte Hilfe Dritter verfasst und keine anderen als die angegebenen Quellen und Hilfsmittel genutzt habe.

Alle Stellen, die wörtlich oder dem Sinne nach auf Publikationen oder Vorträgen anderer Autoren/innen beruhen, sind als solche in korrekter Zitierung kenntlich gemacht. Die Abschnitte zu Methodik (insbesondere praktische Arbeiten, Laborbestimmungen, statistische Aufarbeitung) und Resultaten (insbesondere Abbildungen, Graphiken und Tabellen) werden von mir verantwortet.

Ich versichere ferner, dass ich die in Zusammenarbeit mit anderen Personen generierten Daten, Datenauswertungen und Schlussfolgerungen korrekt gekennzeichnet und meinen eigenen Beitrag sowie die Beiträge anderer Personen korrekt kenntlich gemacht habe (siehe Anteilserklärung). Texte oder Textteile, die gemeinsam mit anderen erstellt oder verwendet wurden, habe ich korrekt kenntlich gemacht.

Meine Anteile an etwaigen Publikationen zu dieser Dissertation entsprechen denen, die in der untenstehenden gemeinsamen Erklärung mit dem/der Erstbetreuer/in, angegeben sind. Für sämtliche im Rahmen der Dissertation entstandenen Publikationen wurden die Richtlinien des ICMJE (International Committee of Medical Journal Editors; www.icmje.og) zur Autorenschaft eingehalten. Ich erkläre ferner, dass ich mich zur Einhaltung der Satzung der Charité – Universitätsmedizin Berlin zur Sicherung Guter Wissenschaftlicher Praxis verpflichte.

Weiterhin versichere ich, dass ich diese Dissertation weder in gleicher noch in ähnlicher Form bereits an einer anderen Fakultät eingereicht habe.

Die Bedeutung dieser eidesstattlichen Versicherung und die strafrechtlichen Folgen einer unwahren eidesstattlichen Versicherung (§§156, 161 des Strafgesetzbuches) sind mir bekannt und bewusst.“

_____

Datum, Unterschrift des Doktoranden

Danksagung

Zuallererst möchte ich PD. Dr. Martin Janz danken für die Möglichkeit und Ermutigung zu diesem herausfordernden und spannenden Projekt, das mir den Eintritt in die grundlagenwissenschaftliche Forschung ermöglichte. Seine eindringlichen und konstruktiven inhaltlichen und persönlichen Hinweise inspirierten meine Arbeit und weitere Zukunft. Enorm dankbar bin ich Dr. Wiebke Winkler, die mir mit unerschöpflicher Motivation nahezu alle hier verwendeten Techniken beibrachte, sowie eine konkrete wissenschaftliche Denkweise und mir so ein selbständiges wissenschaftliches Arbeiten ermöglichte. Ohne sie wäre diese Arbeit nicht möglich gewesen. Ich danke Prof. Dr. Stephan Mathas für methodischen Rat und Hilfe.

Weiterhin danke ich Prof. Dr. Klaus Rajewsky für wertvolle Kritik und anerkennende Motivation. Gemeinsame Clubs und Seminare schulten mein kritisches Hinterfragen methodischer Ansätze und wissenschaftlicher Literatur. Mein besonderer Dank gilt dabei Dr. Michela di Virgilio für die Hilfe bei sorgfältiger Planung der Experimente sowie Prof. Dr. Kathrin de la Rosa für persönliche Inspiration und Mut.

Ich bin allen Gruppenmitgliedern dankbar für die warme und unterstützende Arbeitsatmosphäre. Im Besonderen danke ich Dr. Henrike Szakiel und Brigitte Wollert-Wulf für wertvolle technische Unterstützung, Simone Lusatis für ihre humorvolle Herangehensweise, Dr. Maya Constanza und Carlota Farré Díaz für verständnisvolle Diskussionen sowie Angelos Rigopoulos, der sich vertrauensvoll dem Fortgang des Projektes widmete. Weiterer Dank gilt Dr. Marieluise Kirchner und Dr. Philip Mertins der Proteomics Core Facility des MDC für angenehme und konstruktive Zusammenarbeit, sowie Dr. Hans-Peter Rahn und Kirstin Rautenberg der FACS Core Facitily des MDC für technische Unterstützung bei der Durchflusszytometrie. Dr. Daniel Nörenberg danke ich für persönliche Beratung und Empfehlung zu dieser Arbeit.

Meinen Eltern und meinem Bruder danke ich für die liebevolle Unterstützung, Zuversicht und Vertrauen. Mein herzlicher Dank gilt meinen wunderbaren Freunden Gabrielle und Tim für Ihre Teilnahme, herausfordernden Fragen und Nähe, sowie Anna für ihre Liebe.

Lebenslauf

Mein Lebenslauf wird aus datenschutzrechtlichen Gründen in der elektronischen Version meiner Arbeit nicht veröffentlicht.

CHARITÉ

CharitéCentrum für Human- und Gesundheitswissenschaften

Charité | Campus Charité Mitte | 10117 Berlin

Institut für Biometrie und klinische Epidemiologie (iBikE)

Direktor: Prof. Dr. Geraldine Rauch

Postanschrift:
Charitéplatz 1 | 10117 Berlin
Besucheranschrift:
Reinhardtstr. 58 | 10117 Berlin

Tel. +49 (0)30 450 562171
geraldine.rauch@charite.de
https://biometrie.charite.de/

Name, Vorname: Werner, Marvin

Emailadresse: marvin.werner@charite.de

Matrikelnummer: 220793

Promotionsbetreuer: PD Dr. Martin Janz

Promotionsinstitution: ECRC

Bescheinigung

Hiermit bescheinige ich, dass *Herr Marvin Werner* innerhalb der Service Unit Biometrie des Instituts für Biometrie und klinische Epidemiologie (iBikE) bei mir eine statistische Beratung zu einem Promotionsvorhaben wahrgenommen hat. Folgende Beratungstermine wurden wahrgenommen:

- *Termin 1: 20.08.2021*
- *Termin 2: 01.09.2021*

Folgende wesentliche Ratschläge hinsichtlich einer sinnvollen Auswertung und Interpretation der Daten wurden während der Beratung erteilt:

- Teilweise rein deskriptive Analyse möglich aufgrund zu niedriger Fallzahl

Diese Bescheinigung garantiert nicht die richtige Umsetzung der in der Beratung gemachten Vorschläge, die korrekte Durchführung der empfohlenen statistischen Verfahren und die richtige Darstellung und Interpretation der Ergebnisse. Die Verantwortung hierfür obliegt allein dem Promovierenden. Das Institut für Biometrie und klinische Epidemiologie übernimmt hierfür keine Haftung.

Datum:

30.08.2021, Erin Sprünken

Name des Beraters/ der Beraterin:

Erin Spruenken

Digital unterschrieben von Erin Spruenken
Datum: 2021.09.13 09:17:51 +02'00'

Unterschrift BeraterIn, Institutsstempel